

Objective Measures of Tropical Cyclone Intensity and
Formation from Satellite Infrared Imagery

By

MIGUEL FERNANDO PIÑEROS

A Dissertation Submitted to the Faculty of the
DEPARTMENT OF ELECTRICAL AND COMPUTER ENGINEERING

In Partial Fulfillment
For the Degree of

DOCTOR OF PHILOSOPHY

In the Graduate College

THE UNIVERSITY OF ARIZONA

2009

THE UNIVERSITY OF ARIZONA
GRADUATE COLLEGE

As members of the Dissertation Committee, we certify that we have read the dissertation prepared by **Miguel Fernando Piñeros**

entitled **Objective Measures of Tropical Cyclone Intensity and Formation from Satellite Infrared Imagery**

and recommend that it be accepted as fulfilling the dissertation requirement for the Degree of Doctor of Philosophy.

Date: August 12, 2009

Elizabeth A. Ritchie, Ph.D.
Co-Dissertation Director

Date: August 12, 2009

J. Scott Tyo, Ph.D.
Co-Dissertation Director

Date: August 12, 2009

Michael Gehm, Ph.D.

Final approval and acceptance of this dissertation is contingent upon the candidate's submission of the final copies of the dissertation to the Graduate College.

I hereby certify that I have read this dissertation prepared under my direction and recommend that it be accepted as fulfilling the dissertation requirement.

Date: August 12, 2009

Co-Dissertation Director: Elizabeth A. Ritchie, Ph.D.

Date: August 12, 2009

Co-Dissertation Director: J. Scott Tyo, Ph.D.

STATEMENT BY AUTHOR

This dissertation has been submitted in partial fulfillment of requirements for an advanced degree at the University of Arizona and is deposited in the University Library to be made available to borrowers under rules of the Library.

Brief quotations from this dissertation are allowable without special permission, provided that accurate acknowledgment of source is made. Requests for permission for extended quotation from or reproduction of this manuscript in whole or in part may be granted by the head of the major department or the Dean of the Graduate College when in his or her judgment the proposed use of the material is in the interests of scholarship. In all other instances, however, permission must be obtained from the author.

SIGNED: Miguel Fernando Piñeros

ACKNOWLEDGMENTS

The author wishes to thank his advisors Professors Elizabeth A. Ritchie and J. Scott Tyo for their collaboration during this project. He also wants to give thanks to all his fellow graduate students and to the staff of the Departments of Electrical and Computer Engineering and Atmospheric Sciences at the University of Arizona for their interest in this process.

The author also would like to convey thanks to the Office of Naval Research (grant N00014-07-1-0185) and the Technology and Research Initiative Fund Student Fellowship for supporting this project.

The author acknowledges the National Oceanic and Atmospheric Administration NOAA that provided the best track data and QuikSCAT imagery required for this research.

Finally, the author wishes to thank his family for their help and understanding through the duration of his studies.

To my parents and my sister

TABLE OF CONTENTS

| | |
|---|----|
| ABSTRACT..... | 14 |
| 1 INTRODUCTION..... | 16 |
| 2 BACKGROUND..... | 26 |
| 2.1 The Dvorak Technique..... | 26 |
| 2.2 The Objective Dvorak Technique (ODT)..... | 37 |
| 2.3 The Advanced Dvorak technique (ADT)..... | 39 |
| 2.4 Summary..... | 40 |
| 3 DATA AND METHODOLOGY..... | 41 |
| 3.1 Data..... | 41 |
| 3.2 Map projection..... | 43 |
| 3.3 Gradient of the image brightness temperatures..... | 46 |
| 3.4 The Center of the tropical cyclone: the accumulator matrix..... | 48 |
| 3.5 Quantification of the Axisymmetry of a Cloud System..... | 52 |
| 3.6 Summary..... | 58 |
| 4 INTENSITY ESTIMATION RESULTS..... | 61 |
| 4.1 Correlation with tropical cyclone lifecycle..... | 61 |
| 4.2 2005 Seasonal Statistics..... | 65 |
| 4.3 Time series analysis..... | 74 |
| 4.4 Summary..... | 75 |
| 5 TROPICAL CYCLOGENESIS IDENTIFICATION..... | 77 |
| 5.1 Summary..... | 94 |

| | | |
|-----|---|-----|
| 6 | AUTOMATED TROPICAL-CYCLONE CENTER FINDING | 95 |
| 6.1 | Summary | 106 |
| 7 | DISCUSSION, CONCLUSIONS AND FUTURE WORK | 110 |
| | APPENDIX A: TROPICAL CYCLONES IN 2004-2005..... | 116 |
| | APPENDIX B: FALSE ALARMS | 118 |
| | I. African Easterly Waves | 118 |
| | II. Regular Clouds..... | 119 |
| | REFERENCES | 121 |

LIST OF ILLUSTRATIONS

| | |
|---|----|
| Figure 1.1. Intensity trace of the tropical cyclone Philippe (2005) including the estimates from the NHC report. From http://www.nhc.noaa.gov/ | 19 |
| Figure 1.2. Example of a chain code from [16]...... | 23 |
| Figure 1.3. Example of the Hurricane Wilma (2005) Sequence Imagery. | 24 |
| Figure 2.1. Example of the patterns used in the Dvorak technique: a) eye; b) central dense overcast; c) curve band; d) shear. | 28 |
| Figure 2.2. Logarithm spiral example. From Dvorak (1984) [9]...... | 29 |
| Figure 2.3. Shear pattern feature calculation: distance from the center to the dense overcast. From Dvorak (1984) [9]. | 29 |
| Figure 2.4. Banding Features and its BF-numbers. From Dvorak 1984 [9]. | 31 |
| Figure 2.5. Nomogram of Surrounding IR temperature, Eye IR temperature vs T-number. | 32 |
| Figure 2.6. PT-number with respect to predefined patterns. From Dvorak 1984 [9]. | 35 |
| Figure 3.1. QuikSCAT surface winds example of Hurricane Katrina (2325 UTC August 25, 2005), intensity 70 kt, and plotted wind barbs. A full wind barb equals 10 kt and half wind barb equals 5 kt. | 43 |
| Figure 3.2. Infrared image (10.7 μm) of the Gulf of Mexico and western Atlantic Basin. 0315 UTC 29 September 2005. The scene includes Hurricane Rita (left) and Tropical storm Philippe (Right) within the blue section..... | 45 |
| Figure 3.3. Rectified blue section in Figure 3.2. The scene includes Hurricane Rita near 90W and Tropical storm Philippe near 60W. 0315 UTC 29 September 2005. | 45 |
| Figure 3.4. Example of the gradient calculation: a) IR image of Hurricane Beta, 0645 UTC October 2005; b) section represented by the rectangle in a); and c) the gradient of b)..... | 47 |
| Figure 3.5. Example of the gradient line density calculation: a) brightness temperature image of an ideal vortex; b) gradient vectors of the ideal vortex's central section and the projected lines for two of its elements; and c) the resulting accumulator matrix of the projected lines. | 49 |
| Figure 3.6. Infrared channel 4 (10.7 μm) image of Hurricane Beta: a) 1815 UTC October 26, 2005. The current intensity is estimated at 30 kt; and b) the accumulator matrix of the gradient projected lines for a); c) 0615 UTC October 27, 2005. The current intensity is 45 kt.; and d) the accumulator matrix of the gradient projected lines for c). The red dots indicate the corresponding location of the maximum value in accumulator matrix. | 50 |
| Figure 3.7. Infrared channel 4 (10.7 μm) image of Hurricane Beta: a) 0615 UTC October 29, 2005. The current intensity is estimated at 70 kt; and b) the accumulator matrix of the gradient projected lines for a); c) 0645 UTC October 30, 2005. The current intensity is estimated at 100 kt; and d) the accumulator matrix of the gradient | |

| | |
|--|----|
| projected lines for c). The red dots indicate the corresponding location of the maximum value in accumulator matrix. | 51 |
| Figure 3.8. Accumulator matrix of the gradient projected lines for Figure 3.3. This map clearly shows the center locations of Hurricane Rita (left) and Tropical Storm Philippe (right). | 52 |
| Figure 3.9. “Deviation Angle” Calculation. The reference point is the objectively determined center point of each object within the scene. The deviation angle and variance of every gradient vector within 70 pixels (or 350 km) is calculated for that reference point | 53 |
| Figure 3.10. Example of the “deviation angle” for an axisymmetric vortex | 54 |
| Figure 3.11. histogram of deviation angles for the ideal vortex in Figure 3.10. | 54 |
| Figure 3.12. Deviation angle variance calculation for two different atmospheric system of Figure 3.3 and Figure 3.8. | 56 |
| Figure 3.13. Sequence of infrared images and deviation angles histograms for Hurricane Rita (2005): a) 0815 UTC 18 September 2005. Intensity: 25kt, 1009 hPa, variance: 1625 deg ² ; b) 1415 UTC 19 September 2005. Intensity: 55 kt, 997 hPa, variance: 1423 deg ² ; and c) 1415 UTC 21 September 2005. Intensity: 130kt, 932 hPa, variance: 593 deg ² | 57 |
| Figure 3.14. Sequence of infrared images and deviation angles histograms for Tropical Storm Lee (2005): a) 2115 UTC 29 August 2005. Intensity: 20 kt, 1009 hPa, variance: 1910 deg ² ; b) 0015 UTC 31 August 2007. Intensity 25 kt, 1010 hPa, variance: 1678 deg ² ; and c) 1615 UTC 31 August 2007. Intensity 35 kt, 1007 hPa, variance: 1421 deg ² | 59 |
| Figure 3.15. Sequence of infrared images and deviation angles histograms for Hurricane Nate (2005): a) 2245 UTC 5 September 2005. Intensity: 33 kt, 1006 hPa, variance: 1793 deg ² ; b) 0745 UTC 6 September 2005. Intensity: 40 kt, 1002 hPa, variance: 1281 deg ² ; and c) 2245 UTC 8 September 2005. Intensity: 78kt, 9802 hPa, variance: 894 deg ² | 60 |
| Figure 4.1. Time series of the best-track intensity (kt) from the National Hurricane Center best-track data (red), unfiltered angle variance (green; correlation: -0.85), and filtered angle variance (blue: correlation: -0.90) for Hurricane Rita. During the period 15 September to 24 September, midnight local is between 0500 UTC and 0600 UTC. | 63 |
| Figure 4.2. Time series of the best-track intensity (kt) from the National Hurricane Center best-track data (red), unfiltered angle variance (green; correlation: -0.78), and filtered angle variance (blue: correlation: -0.93) for Hurricane Nate. During the period 3 September to 9 September, midnight local 0000 local is between 0300 UTC and 0400 UTC. | 64 |
| Figure 4.3. Time series of the best-track intensity (kt) from the National Hurricane Center best-track data (red), unfiltered angle variance (green; correlation: -0.49), and filtered angle variance (blue: correlation: -0.71) for Tropical Storm Lee. During the period 28 August to 31 August, the midnight local is between 0300 UTC and 0400 UTC. | 65 |

- Figure 4.4. Histogram of the correlation values between the best-track intensity and filtered angle variance for all 26 tropical cyclone cases. The mean correlation magnitude is 0.74, the median is 0.83, with a standard deviation of 0.23. 66
- Figure 4.5. Time series of the best-track intensity (kt) from the National Hurricane Center best-track data (red), unfiltered angle variance (green; correlation: -0.35), and filtered angle variance (blue: correlation: -0.50) for Tropical Storm Alpha. During the period 19 October to 23 October, midnight local is between 0400 UTC and 0500 UTC..... 68
- Figure 4.6. Time series of the best-track intensity (kt) from the National Hurricane Center best-track data (red), unfiltered angle variance (green; correlation: -0.15), and filtered angle variance (blue: correlation: -0.29) for Tropical Storm Gert. During the period 20 July to 25 July, midnight local is between 0600 UTC and 0700 UTC..... 69
- Figure 4.7. Sequence of infrared images and deviation angles histograms for Tropical Storm Alpha (2005): a) 1115 UTC 21 October 2005. Intensity: 25 kt, 1009 hPa, variance: 2124 deg²; b) 1715 UTC 21 October 2005. Intensity: 27 kt, 1009 hPa, variance: 1373 deg²; and c) 2215 UTC 21 October 2005. Intensity: 28 kt, 1009 hPa, variance: 2256 deg²..... 70
- Figure 4.8. Angle variance versus wind speed for all 26 tropical cyclone cases during intensifying periods of 2005 with one standard deviation error bars. Note that there may be more than one time series for any given storm. The number of images going into each wind speed value is indicated at the top of the graph in italics. 72
- Figure 4.9. Angle variance versus wind speed for all 14 tropical cyclone cases during intensifying periods of 2004 with one standard deviation error bars. Note that there may be more than one time series for any given storm. The number of images going into each wind speed value is indicated at the top of the graph in italics. 73
- Figure 4.10. Time series of the best-track intensity (kt) from the National Hurricane Center best-track data (red), unfiltered angle variance (green; correlation: -0.93), and filtered angle variance (blue: correlation: -0.93) for Hurricane Wilma. During the period 12 October to 22 October, midnight local is between 0400 UTC and 0500 UTC..... 74
- Figure 5.1. a) Synthetic brightness temperature image of an ideal vortex; b) example of the map of variances calculation; and c) Map of deviation angle variances [deg²]. 80
- Figure 5.2. Images of Hurricane Wilma at 2015 UTC 13 October 2005: a) Infrared image. Current best-track intensity is not reported at this stage by the NHC; and b) the corresponding map of deviation-angle variances [deg²]. The minimum value in the map of variances is 2173..... 81
- Figure 5.3. Images of Hurricane Wilma at 1345 UTC 15 October 2005: a) Infrared image. Current estimated intensity is 25 kts and 1004 hPa; and b) the corresponding map of deviation-angle variances [deg²]. The minimum value in the map of variances is 1648..... 81
- Figure 5.4. Images of Hurricane Wilma at 0615 UTC 17 October 2005: a) Infrared image. Current best-track intensity is 35 kt and 1000 hPa; and b) the corresponding map of deviation-angle variances [deg²]. The minimum value in the map of variances is 1616..... 82

- Figure 5.5. Images of Hurricane Wilma at 0015 UTC 21 October 2005: a) Infrared image. Current best-track intensity is 130 kt and 924 hPa; and b) the corresponding map of deviation-angle variances [deg^2]. The minimum value in the map of variances is 1189..... 82
- Figure 5.6. Receiver operating characteristics (ROC) curve for storm detections in all IR images during 2004 and 2005 for various deviation-angle variance threshold values. 84
- Figure 5.7. Mean and median time of detection of storms by the technique for various deviation-angle variance threshold values before being classified as Tropical Storms by NHC during 2004 and 2005..... 88
- Figure 5.8. Images of Tropical Storm Hermine at 1215 UTC 29 August 2004: a) Infrared image. Current best-track intensity is 35 kt and 1012 hPa; and b) the corresponding map of deviation-angle variances [deg^2]. The minimum value in the map of variances is 1794..... 89
- Figure 5.9. Images of Hurricanes Karl and Lisa at 1315 UTC 20 September 2004: a) Infrared image: Hurricane Lisa (right), current best-track intensity: 40 kt (1002 hPa), Hurricane Karl (left), current best-track intensity: 110 kt (951 hPa); and b) the corresponding map of deviation-angle variances [deg^2]. The minimum value in the map of variances is 1751 for Lisa, and 1574 for Karl. 89
- Figure 5.10. Images of tropical storm Zeta at 0615 UTC 6 January 2006: a) Infrared image. Current best-track intensity is 35 kt (1007 hPa); and b) the corresponding map of deviation-angle variances [deg^2]. The minimum value in the map of variances is 2036..... 90
- Figure 5.11. Images of an African Easterly Wave 0645 UTC 15 July 2005 that reached winds of at least 50 kt without a defined circulation pattern : a) Infrared image; and b) the corresponding map of deviation-angle variances [deg^2]. The minimum value in the map of variances is 1657; and c) QuikSCAT image from <http://manati.orbit.nesdis.noaa.gov/quikscat/>. 91
- Figure 5.12. Images of a regular cloud at 2115 UTC 30 October 2005 that reached winds of at least 30 kt: a) Infrared image; and b) the corresponding map of deviation-angle variances [deg^2]. The minimum value in the map of variances is 1520; and c) QuikSCAT image from <http://manati.orbit.nesdis.noaa.gov/quikscat/>..... 92
- Figure 5.13. Images of an atmospheric disturbance at 2215 UTC 24 August 2005 that reached winds of at least 35 kt, but was not recorded by the NHC: a) Infrared image; and b) the corresponding map of deviation-angle variances [deg^2]. The minimum value in the map of variances is 1679; and c) QuikSCAT image from <http://manati.orbit.nesdis.noaa.gov/quikscat/>. 93
- Figure 6.1. Image of Hurricane Lisa at 1200 UTC 22 September 2004. Intensity 45 kt, 1000 hPa. a) Infrared image, the black star corresponds to the best-track center position at 14.2°N , 41.1°W , the red star indicates the accumulator matrix center at 13.0°N , 36.5°W , and the blue star indicates the map of variances center at 12.3°N , 37.0°W ; b) Accumulator matrix, the location of the maximum value is indicated by the star; c) Map of variances, the location of the minimum value is indicated by the star..... 98

- Figure 6.2. Image of Hurricane Arlene at 1600 UTC 11 June 2005. Intensity 60 kt, 993 hPa. a) Infrared image, the black star corresponds to the best-track center position at 27.7°N, 86.8°W, the Red star indicates the accumulator matrix center at 31.7°N, 84.7°W, and the blue star indicates the map of variances center at 30.5°N, 85.5°W; b) Accumulator matrix, the location of the maximum value is indicates by the star; c) Map of variances, the location of the minimum value is indicated by the star. ... 99
- Figure 6.3. Image of Hurricane Irene at 1800 UTC 06 August 2005. Intensity 30 kt, 1008 hPa. a) Infrared image, the black star corresponds to the best-track center position at 18.8°N, 42.8°W, the red star indicates the accumulator matrix center at 21.5°N, 38.5°W, the blue star indicates the map of variances center at 17.8°N, 40°W; b) Accumulator matrix, the location of the maximum value is indicates by the star; c) Map of variances, the location of the minimum value is indicated by the star..... 101
- Figure 6.4. Image of Tropical Storm Franklin at 1800 UTC 24 July 2005. Intensity 45 kt, 1000 hPa. a) Infrared image, the black star corresponds to the best-track center position at 31.1°N, 71.2°W, the red star indicates the accumulator matrix center at 29.6°N, 70.3°W, and the blue star indicates the map of variances center at 30.1°N, 70°W; b) Accumulator matrix, the location of the maximum value is indicates by the star; c) Map of variances, the location of the minimum value is indicated by the star. 102
- Figure 6.5. Image of Hurricane Frances at 0000 UTC 01 September 2004. Intensity 120 kt, 941 hPa. a) Infrared image, the black star corresponds to the best-track center position at 20.6°N, 66.4°W, the red star indicates the accumulator matrix center at 20.9°N, 66.3°W, and the blue star indicates the map of variances center at 20.8°N, 66.5°W; b) Accumulator matrix, the location of the maximum value is indicates by the star; c) Map of variances, the location of the minimum value is indicated by the star 104
- Figure 6.6. RMS distance error [km] vs intensity [kt] results of applying the accumulator matrix and the variance map techniques to locate the center of a tropical cyclone, the results are contrasted to the NHC best-track center database. The number of samples is indicated in italics..... 106
- Figure 6.7. Trajectory of Hurricane Rita, 18-26 September 2005. 108

LIST OF TABLES

| | |
|--|-----|
| Table 1.1. Techniques used by the NHC to estimate the wind speed of a tropical cyclone. | 20 |
| Table 2.1. Shear pattern T-number vs distance calculation. | 30 |
| Table 2.2. E-numbers vs Hurricane's Radius. | 31 |
| Table 2.3. Radius vs CF for CDOs | 33 |
| Table 2.4. Dvorak CI, wind speed and pressure relationships..... | 36 |
| Table 5.1. True Positive Rate (TPR), False Positive Rate (FPR), time detection average, time detection median, and deviation-angle variance threshold values. Number of positives cases: 44, number of negatives cases: 131..... | 85 |
| Table 5.2. Three developing cloud cluster that reached tropical storm intensity according to QuikSCAT data, detected by the map of variances technique but not recorded by the NHC. | 88 |
| Table 6.1. RMS distance error vs intensity results of applying the accumulator matrix and the variance map techniques to locate the center of a tropical cyclone, the results are contrasted to the NHC best-track center database. | 107 |
| Table 6.2. Trajectories comparison for Hurricane Rita, 18-26 September 2005..... | 109 |

ABSTRACT

This document proposes an objective technique to estimate the intensity and predict the formation of tropical cyclones using infrared satellite imagery. As the tropical cyclone develops from an unstructured cloud cluster and intensifies the cloud structures become more axisymmetric around an identified reference point or center. This methodology processes the image gradient to measure the level of symmetry of cloud structures, which characterizes the degree of cloud organization of the tropical cyclone.

The center of a cloud system is calculated by projecting and accumulating parallel lines to the gradient vectors. The point where the highest number of line intersections is located pinpoints a common point where the corresponding gradients are directed. This location is used as the center of the system. Next, a procedure that characterizes the departure of the weather system structure from axisymmetry is implemented. The deviation angle of each gradient vector relative to a radial line projected from the center is calculated. The variance of the set of deviation angles enclosed by a circular area around the center describes the axisymmetry of the system, and its behavior through time depicts its dynamics. Results are presented that show the time series of the deviation angle variances is well correlated with the National Hurricane Center best-track estimates.

The formation of tropical cyclones is detected by extending the deviation-angle variance technique, it is calculated using every pixel in the scene as the center of the cloud system. Low angle variances indicate structures with high levels of axisymmetry,

and these values are compared to a set of thresholds to determine whether a cloud structure can be considered as a vortex. The first detection in a sequence indicates a nascent storm. It was found that 86% of the tropical cyclones during 2004 and 2005 were detected 27 h on average before the National Hurricane Center classified them as tropical storms (33kt).

Finally, two procedures to locate the center of a tropical cyclone are compared to the National Hurricane Center best-track center database. Results show that both techniques provide similar accuracy, which increases as the tropical cyclone evolves.

1 INTRODUCTION

A tropical cyclone is an atmospheric vortex characterized by large air masses circulating counterclockwise in the Northern Hemisphere and clockwise in the Southern Hemisphere, a warm and calm center (or eye) of low atmospheric pressure and a ring of intense thunderstorms and heavy rain. The eyewall is the ring immediately surrounding the eye, where the highest wind speeds and heaviest rains are found. The average-sized tropical cyclone measures from 300 to 600 km radius, with a 30 to 60 km diameter eye. Tropical cyclones form during the summer and autumn over large bodies of warm water in tropical oceans, acquiring energy when moist air rises, by releasing heat through condensation of water vapor.

The evolution of a tropical cyclone is a complex process that can involve interactions on many scales. Studies have shown that several environmental factors are required for formation of a cyclone to occur, e.g., ocean waters of at least 26.5° C from the surface to at least 50 m of depth, moist layers around 5 km height, and a minimum distance of at least 500 km from the equator for a non-zero amount of Earth vorticity or the Coriolis parameter [1]. The conditions described by Gray (1979) are necessary but not sufficient, and the processes that cause a tropical cyclone to form are still not fully understood. In the Atlantic Ocean approximately 60% of the tropical cyclones are generated by atmospheric disturbances called African easterly waves, which are formed by a large temperature gradient between the ocean and the Saharan desert during the summer and autumn. Temperature instability creates waves that travel from Africa to the Gulf of

Mexico between April and November, producing cluster of clouds, showers and thunderstorms. These disturbances are not tracked by the National Hurricane Center (NHC) until they exhibit a clear vortex pattern, a time when the genesis stage of a tropical cyclone may have already passed. For this reason, it is essential to track and analyze every possible cloud cluster to detect the formation of tropical cyclones at early stages, even if they do not show evidence of a vortex pattern.

The intensity of a tropical cyclone is measured by the surface maximum sustained wind speed (MSW), defined as the one-minute wind speed average. In the Atlantic and Eastern North Pacific those tropical cyclones whose intensity is less than 34 kt¹ are called Tropical Depressions; from 34 to 63 kt, Tropical Storms; and more than 64 kt, hurricanes. In other ocean basins, for example, the Indian Ocean or Western North Pacific Ocean, the classification includes several subcategories and different intensity thresholds. In addition, the surface maximum sustained wind is measured as a 10-min average everywhere in the world except the United States.

Forecast centers around the world including the National Hurricane Center for the Atlantic basin and the eastern North Pacific basin and the Japanese Meteorological Agency (western North Pacific basin), make use of any available *in situ* measurements and models that predict the intensity and the trajectory of tropical cyclones. These methods typically combine statistical and physical models to simulate the behavior of the storms, which are initialized and periodically corrected with information obtained from direct measurements (buoys, air reconnaissance) or remotely sensed measurements

¹ One knot is equivalent in U.S. to 0.514 m/s , typically this is the unit used to measure the wind speed of tropical cyclones.

(radar, satellite imagery). The intensity estimates based on measurements, models and techniques can have considerable spread, and from these the forecaster must make a final evaluation of the actual current intensity of the tropical cyclone. Figure 1.1 shows an example of the intensity trace of a tropical cyclone with all the estimates from the NHC report summarized in Table 1.1 [2]-[4]. In addition, the techniques that provide intensity estimates generally only are skillful for more developed tropical cyclones that have completed genesis. Although it is possible for a global model to forecast *in situ* developments, the models show little skill in prediction of actual tropical cyclones. Thus, a technique that can provide intensity estimates at very early stages of development, i.e., evolving genesis, would be of considerable use to the forecasting community.

Weather disturbances² have traditionally been described using measurable variables, e.g., atmospheric winds, pressure, temperature, and relative humidity. For tropical cyclones that spend much of their lifetime over the oceans, traditional sources of these measurements are scarce. However, observations that describe characteristics of the dynamics and structure of tropical cyclones can be extracted from satellite-based remote-sensed observations [2], [3], [5]. As shown by the continued success of the Dvorak technique for intensity estimates [2], satellite-based measurements provide a key, reliable source of measurements of tropical cyclones over the data-sparse tropical oceans. These measurements potentially extract important information that can help to identify emerging tropical cyclones.

² Weather disturbances that may develop into tropical cyclones are referred to here as cloud clusters, weather disturbances or cloud systems.

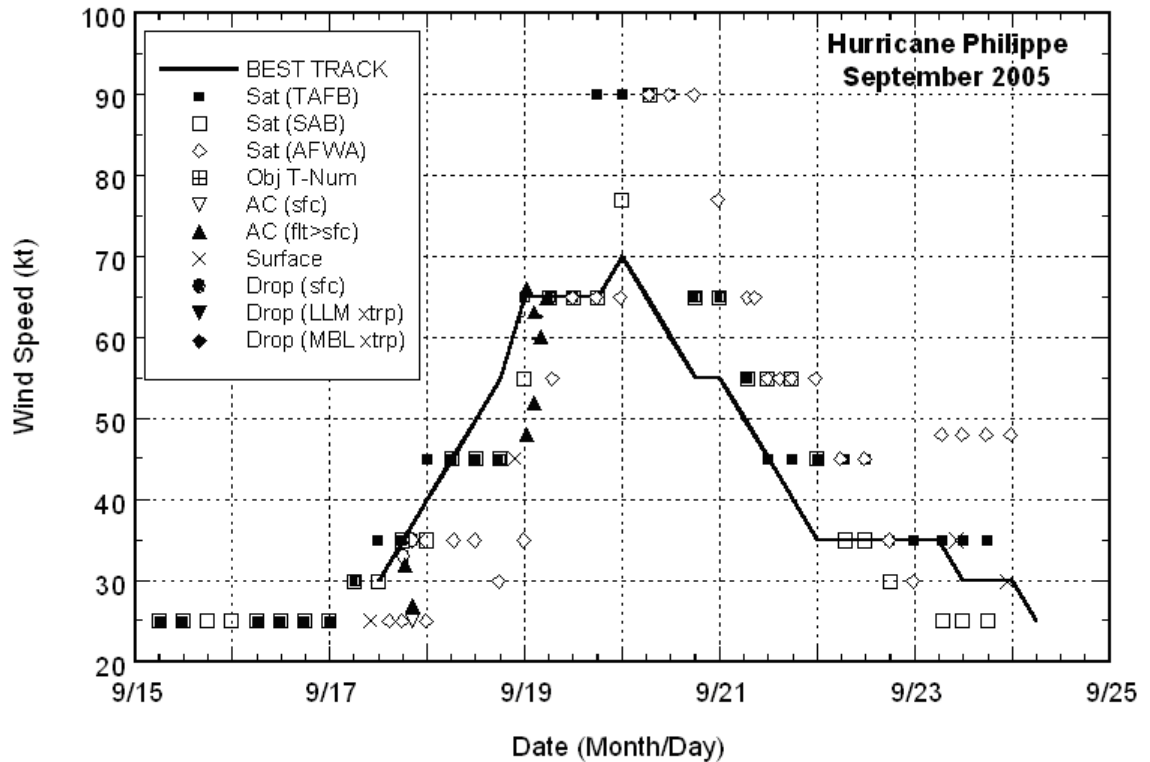


Figure 1.1. Intensity trace of the tropical cyclone Philippe (2005) including the estimates from the NHC report. From <http://www.nhc.noaa.gov/>.

The interpretation of a tropical cyclone's structure from satellite imagery has been an important element for estimating its intensity, from its beginning as a disorganized cloud cluster to its end, whether dissipating over land or cooler oceans, or transforming into an extratropical cyclone [6]-[8]. Since the 1960s satellites have offered the opportunity to observe the tropical atmosphere as never before. Today the suite of satellites provide almost complete coverage of the vast tropical oceans where traditional meteorological observations are scarce.

| Acronym | Description |
|-----------------|--|
| Sat (TAFB) | Satellite-based Dvorak Estimate (Tropical Analysis Forecast Branch) |
| Sat (SAB) | Satellite-based Dvorak Estimate (Satellite Analysis Branch) |
| Sat (AFWA) | Satellite-based Dvorak Estimate (Air Force Weather Agency) |
| Obj T-Num | Objective Dvorak Technique |
| AC (sfc) | Aircraft-Based Estimate (surface estimate) |
| AC (flt>sfc) | Aircraft-Based Estimate (surface estimate from flight level wind measurements) |
| Drop (sfc) | Dropwindsonde (surface estimate) |
| Drop (LLM xtrp) | Dropwindsonde (wind sounding extrapolated) |
| Drop (MLB xtrp) | Dropwindsonde (sounding boundary layer mean extrapolated) |

Table 1.1. Techniques used by the NHC to estimate the wind speed of a tropical cyclone.

Forecast centers rely on satellite observations as the main method to perform the estimation of a tropical cyclone intensity and trajectory. The visible and infrared channels are two of the most used sources of information about the location and structure of atmospheric systems. The visible channels (0.35 – 0.7 μ m) receive reflected and scattered solar radiation from the top of the clouds. Therefore, this information is not available during the night. In contrast, the thermal infrared band (8-16 μ m) receives radiation emitted from the top of the clouds and is always available. Unfortunately, these channels do not provide information about the dynamics of the atmospheric systems in the lower levels of the atmosphere, which are often obscured by clouds. For this reason, some important tasks such as finding the location of the tropical cyclone circulation and the estimation of surface wind speeds have proven to be difficult for many years.

One of the first comprehensive pattern recognition techniques for estimating tropical cyclone intensity from satellite imagery was developed by Vernon Dvorak in the 1970s [2], [9], [10]. The original Dvorak technique is subjective and human-intensive, but is still used as the primary intensity forecasting tool in many tropical cyclone forecasting centers around the world [2], [3]. The Dvorak technique is widely used primarily because it is the only way to estimate intensity of a tropical cyclone in the absence of direct measurements. In particular, for ocean basins where there is no aircraft reconnaissance of tropical cyclones³, the satellite-based technique is the only estimate of tropical cyclone intensity available to tropical cyclone forecasters. The technique is applied by an expert who follows a set of empirically determined rules to quantify features of the clouds seen in the scene. The expert utilizes these measurements to find the final intensity estimation in a lookup table. The classification of the tropical cyclones at their earliest stages is probably the weakest part of the Dvorak technique [2] because the variability in the ways tropical cyclones develop makes it difficult to specify development patterns. Thus, the development of an objective model that can detect the genesis and subsequent evolution of a tropical cyclone throughout its life would enable forecasters to warn on nascent systems with some confidence. Another potential benefit would be to enable better representation of the emerging tropical cyclone in numerical weather prediction models and enhance other methodologies such as the objective Dvorak technique [11], perhaps improving forecasts from an earlier time.

³ U.S. Aircraft reconnaissance is ongoing in the western Atlantic and eastern North Pacific basins. Aircraft reconnaissance was discontinued in the western North Pacific in 1986. No other nation supports a 24-h reconnaissance program for tropical cyclones.

Tropical cyclones exhibit irregular shapes at early stages of their lifecycle. However, curved and circular patterns can be identified as the early formation of vortices and are generated by an initial circulation of winds around a center. When direct measurements of environmental variables such as atmospheric pressure are not available, the detection of typical curved and circular patterns from remote sensed data is a potential method to determine the genesis of tropical cyclones. Another potential method is to estimate the wind vector field from remotely sensed imagery in order to analyze the magnitude and circulation of the wind.

Objective techniques to estimate the wind speed could be based on building a wind vector field from a sequence of images. This information may open new possibilities for the identification of nascent vortices, and the estimation of the tropical cyclone's intensity. The typical approaches to build a vector field from a sequence of images are cross correlations [12] and optical flow [13]. These techniques are two alternatives to detect and quantify the movement of objects, by matching pixels between images of a sequence. However, to be reasonably accurate, these require smooth and small variations between the images. In this particular case of atmospheric scenes, applying these techniques demands large amounts of data to guarantee small changes and cover vast tropical ocean areas. There have been studies to estimate the wind speed by using optical flow, however it is necessary to use images taken as frequently as five to seven minutes apart to have small changes in the images [14]. Unfortunately, imagery with such high time resolution is rarely available. Typically the time resolution varies from 30 min to one hour for stationary satellites to cover large ocean areas, during this time, cloud

clusters can change considerably and the condition of small changes from image to image cannot be assured. It is possible to obtain higher time resolution from a stationary satellite operated in rapid scan mode, but that only is available for short periods and a specific reduced geographic region.

Vortices could be detected by applying several image processing techniques, perhaps the most used one is the Hough Transform [12], [15], which is designed to find simple shapes such as straight lines, circles or ellipses. Fourier descriptors and chain codes are two more examples of techniques to describe and detect shapes, for example [16] describes a procedure to detect vortices from images using chain codes. The technique extracts a binary image of the vortex by applying a threshold, and then calculates the 8-connectivity chain code as shown in Figure 1.2. The vortex is detected by analyzing the code, for example, in order to obtain a loop at least 4 numbers are required in the chain: 6824.

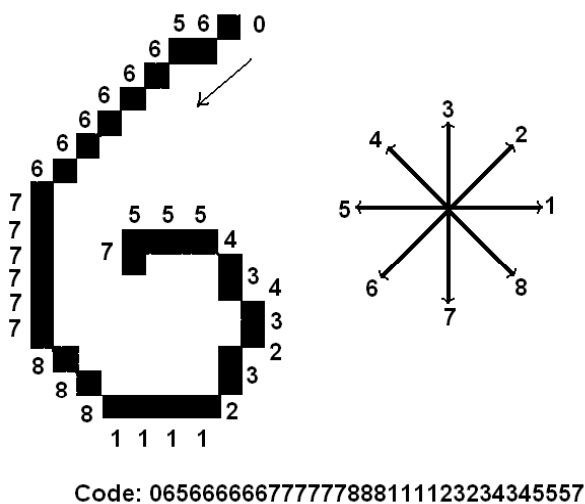


Figure 1.2. Example of a chain code from [16].

Most of the known techniques to recognize vortices require applying an edge detector to obtain contours in binary images. This step is particularly critical when using infrared and visible satellite atmospheric imagery due to the high level of detail, the lack of uniform patterns, and the changes of the intensity of brightness temperature. Figure 1.3 shows two examples of complex cases made of infrared images at early stages of Hurricane Wilma (2005). Note the number of elements of each cloud cluster, the irregularity of their shapes, and the intensity range of brightness temperatures in these images that would make it difficult to apply techniques over binary images consistently.

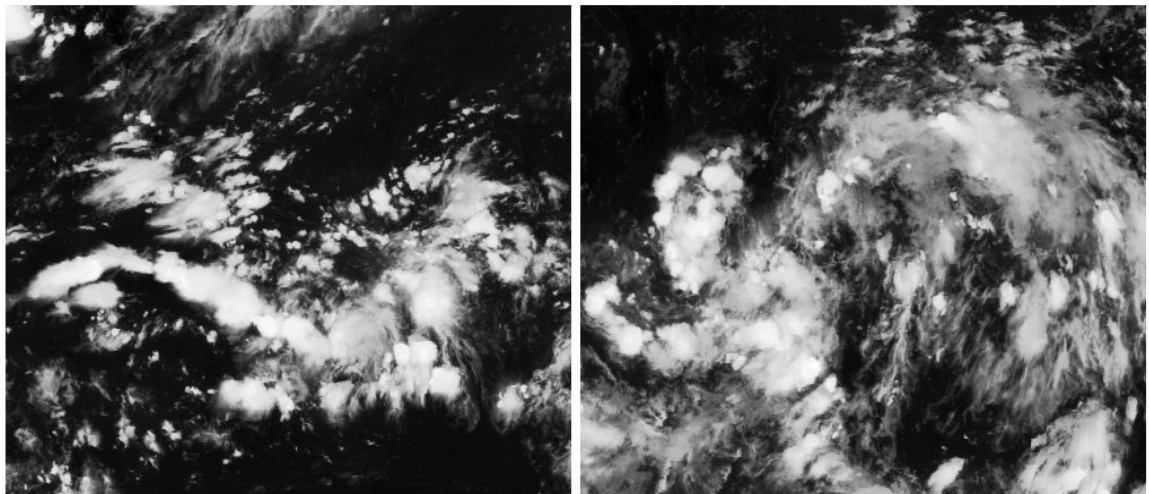


Figure 1.3. Example of the Hurricane Wilma (2005) Sequence Imagery.

This research develops an objective alternative to the Dvorak technique, which describes the dynamics of a storm using only infrared imagery. It is based on the fact that the vorticity structure of tropical cyclones becomes more axisymmetric as they intensify [9], which produces organization in the cloud patterns. This level of axisymmetry or organization is quantified by a variance parameter, which is used to build a signal over the lifetime of the tropical cyclone. This signal is used to separately estimate intensity (Chapter 4), detect the genesis (Chapter 5), and, along with a separate technique, estimate the location of the tropical cyclone (Chapter 6).

Background for this problem will be presented in Chapter 2. The methodology will be described in Chapter 3, results in Chapter 4-6 and final summary, conclusions and future work will be discussed in Chapter 7.

2 BACKGROUND

2.1 The Dvorak Technique

The Dvorak technique [2], [9], [10] is a set of procedures and rules empirically determined to obtain reliable estimates of tropical cyclone intensity from satellite imagery. It combines spatial patterns in the infrared and visible brightness temperatures of clouds to detect rotation, where brightness temperature is the corresponding temperature of a black body that produces the same detected intensity at a given wavelength [17], the coldest brightness temperatures to detect deep thunderstorms in the eyewall, warm brightness temperatures to detect an eye at the center of circulation, and differences between the two to determine intensity when possible.

The technique is applied by an expert who subjectively measures several features of the clouds seen in the images. The methodology is different for the visible and infrared imagery. The major differences between them are that cirrus clouds (high and thin clouds) are not detected by visible imagery, but are seen as smooth gray regions in the infrared. In addition, cloud edges may not be clear in the infrared channel.

The first part of the technique consists of locating the center of the atmospheric disturbance. Dvorak defines the center as “The focal point of all the curved lines or bands of the cloud system. It can also be thought of as the point toward which the curved lines merge or spiral” [9]. To obtain the best possible center position, all the available channels (now including microwave) and previous center locations are used. Unfortunately, locating the center may be difficult because it may not be well defined, particularly at

early stages of the tropical cyclone lifecycle. The center is located at the center of the eye, if this is observed. However, the eye is only visible at very intense stages of the tropical cyclone lifecycle. For curved band clouds, the center is located near the center of curvature of the main cloud band (most dense band). If the center is not visible, there are circles drawn that fit the curved bands, and then the center is located at the center of the common area in the circles. If the center is still unclear, it is extrapolated from past locations. If there is more than one center, then the closest one to the past location is chosen as the current center.

Having located a center, the expert follows a flowchart in order to assign a number known as the “T-number” to the weather disturbance in the scene. T-numbers are in the range of 0 to 8 in increments of 0.5, where the maximum value (8) corresponds to the highest intensity. Generally, T-numbers are composed of two elements: one is related to the features of the central part of the atmospheric system, and the second one is related to the banding features.

Cloud clusters in an image are classified according to the following classes: curved bands, shear, eye, and central dense overcast pattern. Once the expert classifies the cloud, features are measured specifically for each class and these are related to the T-number by empirical relationships. Figure 2.1 illustrates examples of the four patterns used in this technique.

Curved bands are those structures that resemble a spiral; they can be observed and characterized in both visible and infrared images. This pattern is commonly seen when the system is developing, and is typical of a large amount of convection. The expert

locates the center of the atmospheric disturbance and traces a logarithmic curve around the band. The arc length of that curve is the variable related to the T-number, which varies from 1 to 4.5 for this class. Figure 2.2 shows several examples with T-numbers associated.

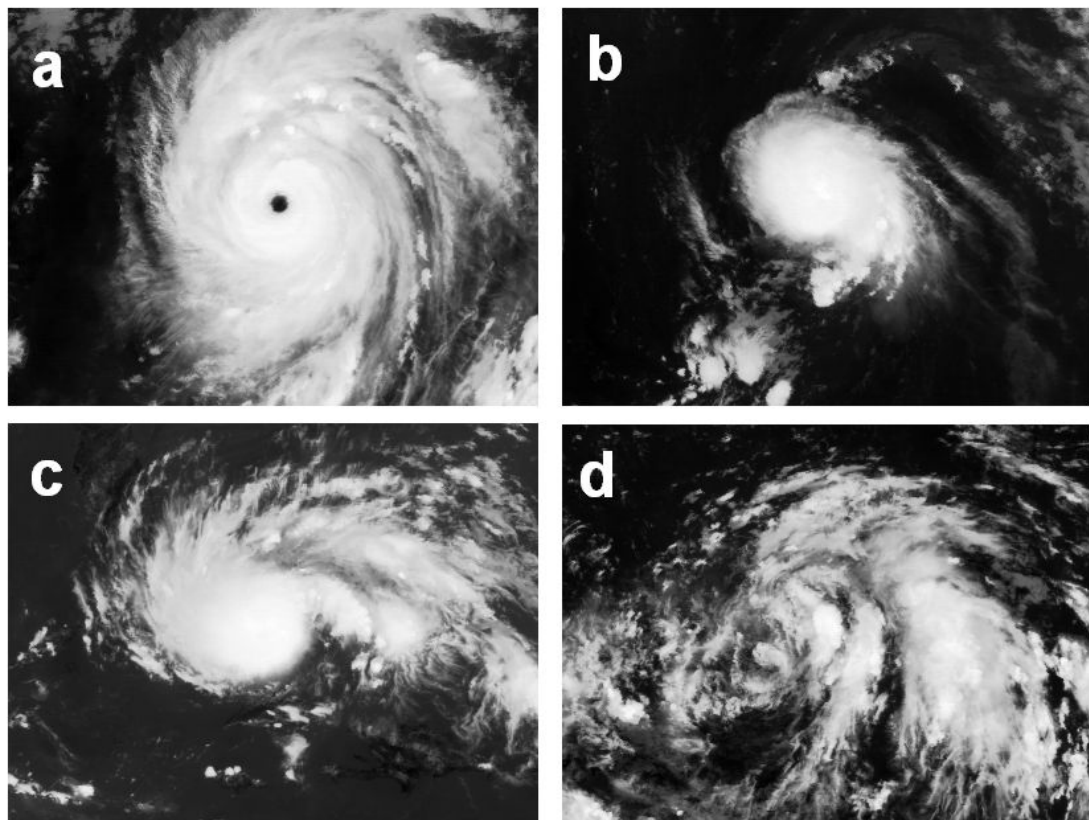


Figure 2.1. Example of the patterns used in the Dvorak technique: a) eye; b) central dense overcast; c) curve band; d) shear.

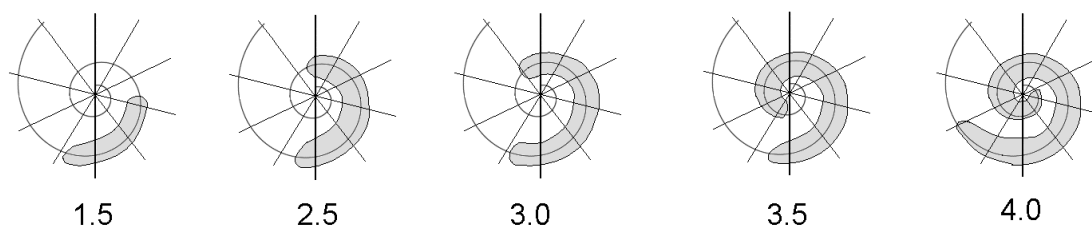


Figure 2.2. Logarithm spiral example. From Dvorak (1984) [9].

Shear patterns are clusters characterized by a smooth circulation surrounded by dense clouds; for both visible and infrared imagery and infrared, T-numbers are obtained by measuring the distance from the center of circulation to the edge of the more dense overcast (see Figure 2.3). The range of number for this class of pattern varies from 1.5 to 3.5 according to the distance d as shown in Table 2.1.

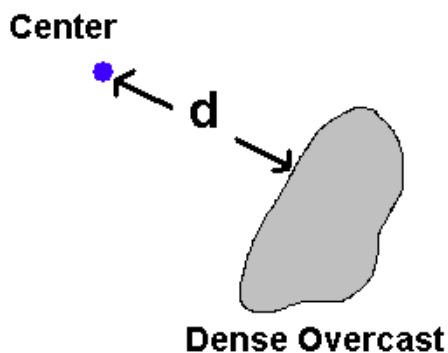


Figure 2.3. Shear pattern feature calculation: distance from the center to the dense overcast. From Dvorak (1984) [9].

| Distance (d) [km] | T-number |
|-------------------------------|----------|
| 130 | 1.5 |
| 85 | 2.5 |
| 55 | 3.0 |
| 37 (center into the overcast) | 3.5 |

Table 2.1. Shear pattern T-number vs distance calculation.

Eye patterns are structures with a well-defined center of circulation typically found in mature tropical cyclones. For visible imagery, the T-number is the summation of two components: central feature (CF) and a banding feature (BF). The central feature is characterized by the “E-number”, which is obtained from the tropical cyclone’s radius in degrees of latitude (See Table 2.2) and an adjustment that depends on the features of the eye. The radius is defined as the nearest distance of the inner wall of the eye to the outside edge of the dense overcast. The adjustment is found by applying the following rules:

- 1) Eye poorly defined: subtract 0.5 from the E-number if this is less or equal than 4.5, and 1 if it is higher or equal than 5.
- 2) Large eye: limit the final T-number to 6 if the eye is well defined, and to 5 for large but not clearly defined eyes.
- 3) Eye well defined, it may be added 0.5 or 1 if the tropical cyclone is rapidly intensifying.

The number BF is calculated by matching the current cloud structure with the patterns described in Figure 2.4. For infrared imagery, it is found by measuring the warmest brightness temperature in the eye and the coldest on the ring surrounding the eye. These temperatures are matched in a nomogram, which is a chart that relates them with the T-Number (Figure 2.5). The range of T-numbers for this class of patterns is from 4.5 to 8.0.

| Radius | E-number |
|-------------|----------|
| $1/4^\circ$ | 3 |
| $1/2^\circ$ | 4 |
| $3/4^\circ$ | 5 |
| 1° | 6 |
| $>1^\circ$ | 7 |

Table 2.2. E-numbers vs Hurricane's Radius.

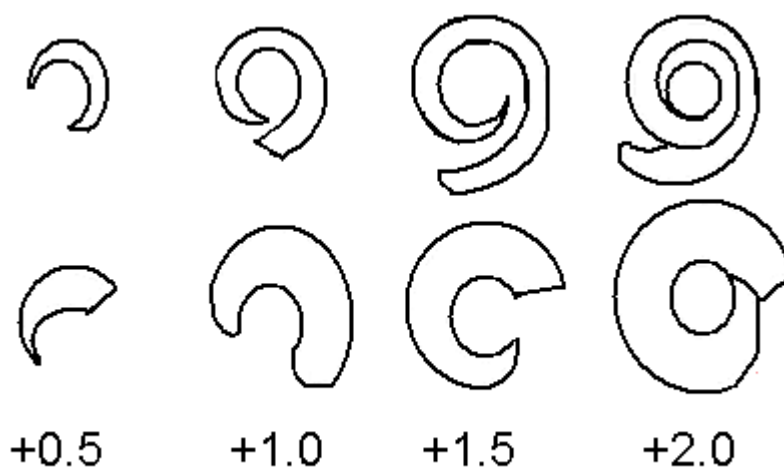


Figure 2.4. Banding Features and its BF-numbers. From Dvorak 1984 [9].

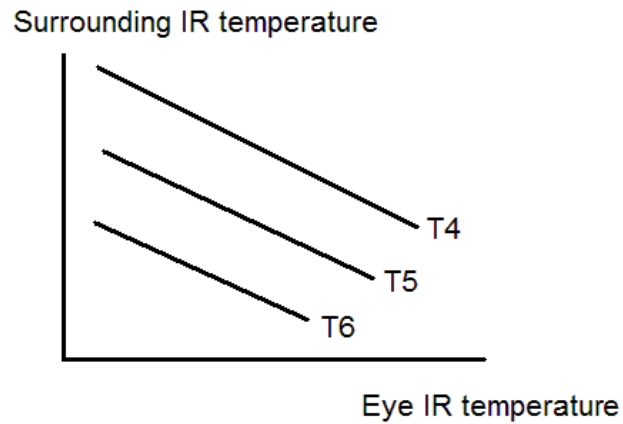


Figure 2.5. Nomogram of Surrounding IR temperature, Eye IR temperature vs T-number.

The central dense overcast (CDO) are clusters defined by a circular structure with some bands around it but without a defined eye. The T-number is obtained by adding two features: the size of the central part of the structure (see Table 2.3); and the number BF obtained from matching the CDO banding feature with the patterns shown in Figure 2.4. The CDO is characterized only with visible imagery because in infrared imagery cirrus clouds increase the size of the overcast. The T-number in this class varies in the range from 2.5 to 5.

| Diameter Size [km] | CF | Cloud Edge |
|--------------------|----|------------|
| 110 - 167 | 2 | Irregular |
| >167 | 3 | |
| 83 | 2 | Regular |
| 139 | 3 | |
| 195 | 4 | |
| >250 | 5 | |

Table 2.3. Radius vs CF for CDOs

Next, the current image is compared with the image taken 24 h ago. The expert determines if the features are qualitatively better defined, which indicates if the storm is intensifying, weakening or maintaining its intensity. If the storm is developing, then curve band patterns increase their curvature, CDOs appear larger in size, shear patterns are better defined (more curved) around the center, and the eye for eye patterns becomes warmer. The opposite characteristics occur for weakening storms. The tropical cyclone maintains its intensity when the features of the clouds do not change significantly or when there are features that indicate both intensifying and weakening trends that approximately offset each other.

After determining the intensity trend of the tropical cyclone, the model expected T-number (MET) is calculated by adding 0.5, 1.0 or 1.5 (slow, normal or rapid changes respectively) to the previous T-number for intensification periods or subtracting 0.5, 1.0 or 1.5 from the previous T-number for weakening periods, and preserving the T-number

when the tropical cyclone maintains its intensity. For rapid rates of intensity change, this process is performed at 6h intervals, however exact time lapses have not been specified to define slow, normal and rapid changes.

Once the MET is determined, the analyst obtains the pattern T-number called “PT-number” by matching the current cloud seen in enhanced infrared imagery (EIR) with the most similar pattern of Figure 2.6. EIR imagery is a lower bit depth representation of infrared images, the relationship between the pixel value and temperature is described in [9].

The final T-number is chosen from the T-number calculated from the cloud features when these are well defined, from the PT-number, when the cloud features are ambiguous and the T-number is not reliable, and finally from the MET, when the T-number and the PT-number are not clear and representative. The final T-number also should follow these constraints: 1) the initial T-number must be 1.0 or 1.5; 2) during the first 48 hours the T-number can not be decreased at night; 3) 24 hours after an initial T-number of 1.0, it must be less or equal to 2.5; and 4) It must be ± 1.0 from MET.

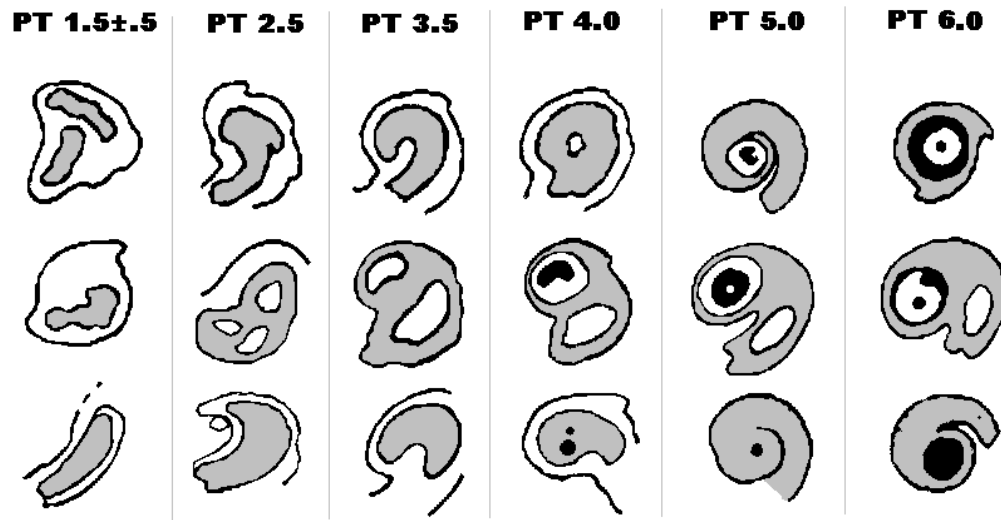


Figure 2.6. PT-number with respect to predefined patterns. From Dvorak 1984 [9].

From the final T-number, the current intensity or “CI” number is obtained, which is equal to the final T-number when the tropical cyclone is developing. However for weakening periods, the CI number cannot decrease with respect to the T-number until at least 12 h have passed. The CI number is converted to an estimate of the maximum sustained surface wind (MSW) through an empirical relationship shown in Table 2.4. Note the difference in minimum sea level pressure (MSLP) from the Atlantic to the Pacific for the same MSW is because of environmental differences in surface pressure, MSW is proportional to the differences of pressure, not the pressure itself. Typically, the accuracy of this technique is within half a T-number or approximately 10 to 15 kt⁴ [18].

⁴ Best-track intensity estimate from the National Hurricane Center is generally used as the reference value.

The process to forecast the intensity (MSW) is performed by extrapolating future values according to the history of the signal already recorded. This value is modified if favorable or unfavorable factors in the environment that can affect the dynamics of the tropical cyclone are detected, e.g. cold waters, land or strong vertical shear of the wind field.

Clearly the Dvorak Technique is a manual, subjective and human-intensive process. Methods to improve the subjectivity of this technique has been developed, the first of which is the “Objective Dvorak technique” described in the next section.

| CI | MSW (kt) | Atlantic MSLP(hPa) | Pacific MSLP (hPa) |
|-----|----------|--------------------|--------------------|
| 1.0 | 25 | | |
| 1.5 | 25 | | |
| 2.0 | 30 | 1009 | 1000 |
| 2.5 | 35 | 1005 | 997 |
| 3.0 | 45 | 1000 | 991 |
| 3.5 | 55 | 994 | 984 |
| 4.0 | 65 | 987 | 976 |
| 4.5 | 77 | 979 | 966 |
| 5.0 | 90 | 970 | 954 |
| 5.5 | 102 | 960 | 941 |
| 6.0 | 115 | 948 | 927 |
| 6.5 | 127 | 935 | 914 |
| 7.0 | 140 | 921 | 898 |
| 7.5 | 155 | 906 | 879 |
| 8.0 | 170 | 890 | 858 |

Table 2.4. Dvorak CI, wind speed and pressure relationships.

2.2 The Objective Dvorak Technique (ODT)

Several modifications have been introduced to the original Dvorak technique by Velden and Olander (1989), who developed an objective technique based on empirical rules similar to those used in the original technique [11]. They utilize infrared imagery to estimate the maximum sustained wind speed and the minimum sea-level pressure. The center of the tropical cyclone is located by either the user, who applies similar procedures of the original Dvorak technique, or by aircraft reconnaissance.

The basis of the technique consists of finding two temperatures from an image. The first corresponds to the highest temperature within a radius of 40 km around the specified center. This selection is rarely reliable when the tropical cyclone does not exhibit a defined eye, e.g. in central dense overcast or shear patterns. In these cases the temperature determined by the pixel corresponding to the center is chosen instead.

Next, the minimum temperature from the pixels that compose concentric rings around the center is found and stored, which vary from 24 to 136 km of radius (one pixel wide). The intensity of the tropical cyclone increases if the difference between the highest temperature (at the center) and the temperature at the surroundings (rings) increases. A lookup table described in [10] and derived from statistical aircraft observations, shows the relationship between the difference of temperatures and the final T-number.

Three more rules are imposed to the final T-number: 1) it cannot be less than 3.5, because the technique is not reliable for weak tropical cyclones; 2) the T-number can not

be more than 5.0 for systems without an defined eye; and 3) if the highest temperature at the center is less than in the surroundings, it is assigned a T-number of 4.5.

The final T-numbers are also averaged to remove large differences in short time periods, generally from 3 to 12h to obtain realistic trends. These fluctuations can be caused by several reasons such as incorrect center location, noise in the image, low spatial resolution, etc.

The accuracy of the objective Dvorak technique is close to the original Dvorak technique [11], however the main limitations are that the center has to be located by the user or by environmental measurements, and it can only be applied to strong storms.

Olander et al. [19] introduced more constraints and rules to the objective Dvorak technique in order to improve the accuracy, analyze weak tropical cyclones and include an automatic center location procedure. This new set of rules is called the Advanced Objective Dvorak Technique. The center of the storm is located by calculating the gradient of the brightness temperature of the image. If the magnitude of these vectors around a point exceeds thresholds empirically determined, the point is considered as the center of the storm [19]. This procedure identifies close regions characterized by high pixel value contrast typically found in the eye of a storm. Unfortunately, non-eye regions can be also incorrectly classified as centers. Recently, two more algorithms were incorporated to locate the center. The first technique finds the best alignment of the image gradient field with a logarithm spiral vector simulating the procedure used in the feature measurement method of curve bands in the original Dvorak technique. The second algorithm consists of finding the best alignment of a ring in the image gradient

field around the center calculated using the first procedure, and then uses a variation of the Hough transform to determine the optimal position and radius of the ring [20]. The performance of these algorithms at locating the center of circulation, independently of the intensity estimation, is not reported in that study.

2.3 The Advanced Dvorak technique (ADT)

This technique focuses on developing new procedures and rules rather than simulating the original Dvorak Technique. New constraints and several modifications have been introduced regarding the allowable intensity rate change during selected periods of time and the existing ODT rules that can apply in certain circumstances. For example, a new adjustment is introduced to the sea level pressure estimation according to the latitude of the storm. One of the most important improvements of this technique over the original Dvorak technique consists of the introduction of regression equations to calculate the tropical cyclone intensity from cloud features such as size, symmetry of the convective region, and temperatures. This technique utilizes not only infrared and visible imagery but also includes water vapor (6-7 μm) and microwave channels (85-92 GHz) to perform the intensity estimation. Although this technique is briefly described in [21] and it has been developed within software libraries [22], a complete description and technical details have not been published yet [23].

2.4 Summary

The original Dvorak technique is a subjective and complex methodology that relies on the expertise of the analyst, who must correctly identify and classify the atmospheric disturbance, locate its center, and measure features from its structure. If these tasks are not precisely accomplished the intensity estimation can be inaccurate. The technique is applied to atmospheric disturbances that exhibit an evident structure of circulation. Unfortunately, tropical cyclones are rarely characterized by common patterns at early stages, making it difficult to estimate their intensity.

The ODT was developed as an alternative to automate the original Dvorak technique, imitating its methodology without human interaction. However, locating the center of the tropical cyclone is still subjective, and estimating the intensity of weak tropical cyclones or at early stages their lifecycle is inaccurate.

For these reasons, new and objective techniques to estimate the tropical cyclone's intensity with a similar accuracy, and predict their formation are being developed as potential methods to replace the original Dvorak technique.

3 DATA AND METHODOLOGY

This dissertation describes an alternative to the Dvorak technique by analyzing infrared imagery. The level of organization or axisymmetry of a tropical cyclone is quantified in order to estimate its intensity and detect its formation. The technique is based on a statistical analysis of the orientation of the image gradient vectors around a reference point or center, which ideally should correspond to the center of the tropical cyclone. This section describes the procedures to calculate the gradient vectors of an image, the center of the tropical cyclone and quantify its organization.

3.1 Data

The data that are used as input to the technique are digital brightness temperatures from longwave infrared (IR) satellite scenes. For the purposes of this study, approximately 9200 half-hourly images of 5km/pixel from the Geostationary Operational Environmental Satellite 12 Imager (GOES-12) [24] comprising three tropical depressions, one subtropical depression, one subtropical storm, 22 tropical storms, and 22 hurricanes from the 004 and 2005 North Atlantic seasons were analyzed. These tropical cyclones include cases that had average intensification rates, cases that had rapid intensification rates, and cases are also included from the end of the record in the 2005 seasons

Best-track intensity and location estimates from the National Hurricane Center (NHC) database [25] are used to verify the results from this technique. The best-track is a smooth

representation of the tropical cyclone intensity at 5 kt intervals, location and minimum sea-level pressure at 6-hourly increments. It depicts the major intensity trends without considering fluctuations and erratic estimations. The best-track is calculated retrospectively after the tropical cyclone decays and includes all the sources of data such as direct measurements, remote-sensed data, and aircraft reconnaissance. Although the best-track intensity is subjectively determined, it is generally utilized as the “truth” intensity to measure the performance of estimation techniques.

The National Hurricane Center tracks tropical cyclones from early stages. However some atmospheric systems reach tropical-storm intensity for only short periods, and are not recorded in the database. QuikSCAT imagery is used here to verify these cases classified as tropical cyclones by the cyclogenesis detection procedure but not reported as tropical cyclones in the best-track archives. QuikSCAT is a polar orbiting satellite that covers a given geographic region twice per day. The NASA/JPL’s SeaWinds Scatterometer aboard the satellite [26] retrieves the sea surface wind magnitude and direction in 25 km x 25 km maps between latitudes 80° N to 80° S and longitudes 180° W to 180° E. Wind barbs are color coded to specify the magnitude of the wind. However, the summation of barbs on each individual element provides a more precise reading (See Figure 3.1).

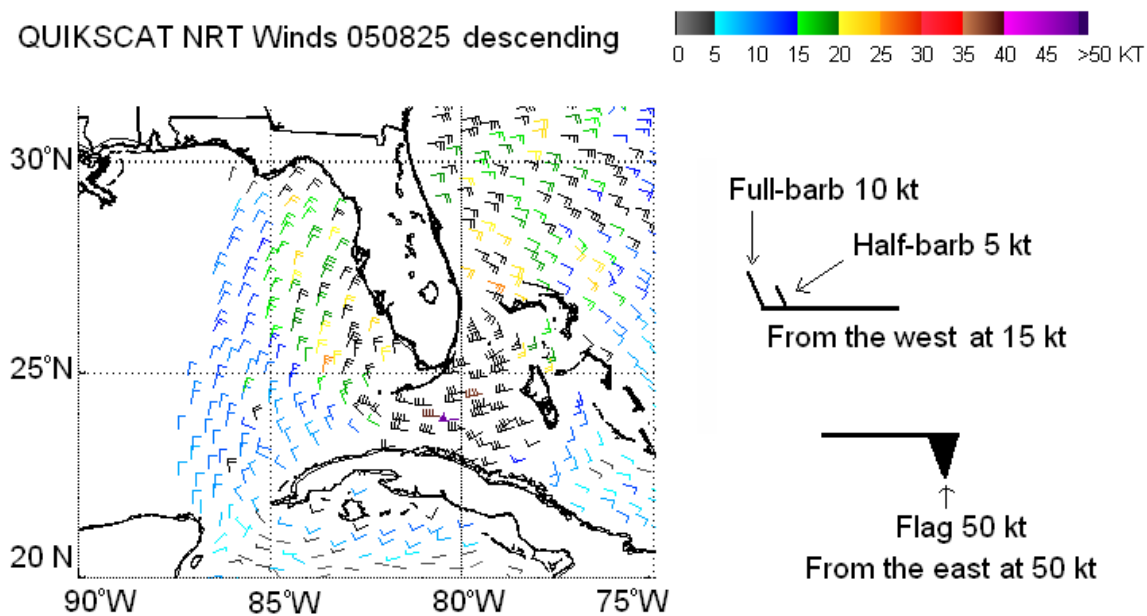


Figure 3.1. QuikSCAT surface winds example of Hurricane Katrina (2325 UTC August 25, 2005), intensity 70 kt, and plotted wind barbs. A full wind barb equals 10 kt and half wind barb equals 5 kt.

3.2 Map projection

Each satellite image is formatted in *Area file format*, which is a binary file format that has at least 256 bytes in the header and the rest of the file contains the image information. The header includes the navigation information and other characteristics of the image and the sensor [27].

The infrared images compress the brightness temperature of each point of the scene and the actual temperature can be retrieved from the value of each pixel by applying (8 bit/pixel) [27]:

$$T = 418 - P \quad (P \geq 176) \quad (1)$$

$$T = 330 - (P/2) \quad (P < 176) \quad (2)$$

where T is the temperature (K) and P is the value of the pixel (0 to 255). Note that a high pixel value (white) indicates low temperatures commonly related to the clouds.

The first step in the process is to convert the imagery from a natural earth coordinate system to a Cartesian projection removing the differences in pixel resolution due to the Earth's curvature. A standard software package developed by the University of Wisconsin-Madison called McIDAS (Man computer Interactive Data Access System) [28] was used to compute the projection change. Because the extreme edges of the satellite footprint contain considerable curvature, they are warped by the map projection change and are not used. Figure 3.2 shows an example of an infrared scene from the Atlantic basin that includes Hurricanes Rita and Philippe. Figure 3.3 shows the rectified section indicated by the blue region in Figure 3.2. After the map projection process, a low pass filter is applied to each image to remove noise. The filter is defined by a Gaussian function of 5×5 and variance one.

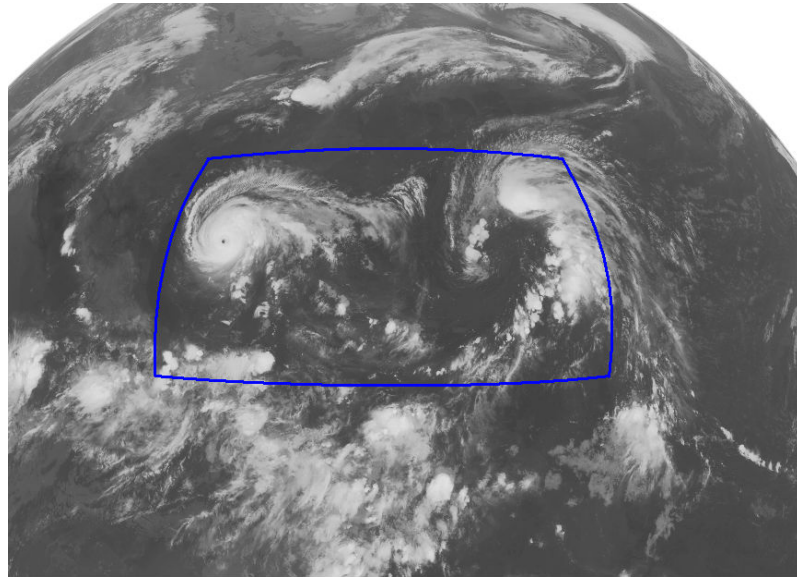


Figure 3.2. Infrared image (10.7 μm) of the Gulf of Mexico and western Atlantic Basin. 0315 UTC 29 September 2005. The scene includes Hurricane Rita (left) and Tropical storm Philippe (Right) within the blue section.

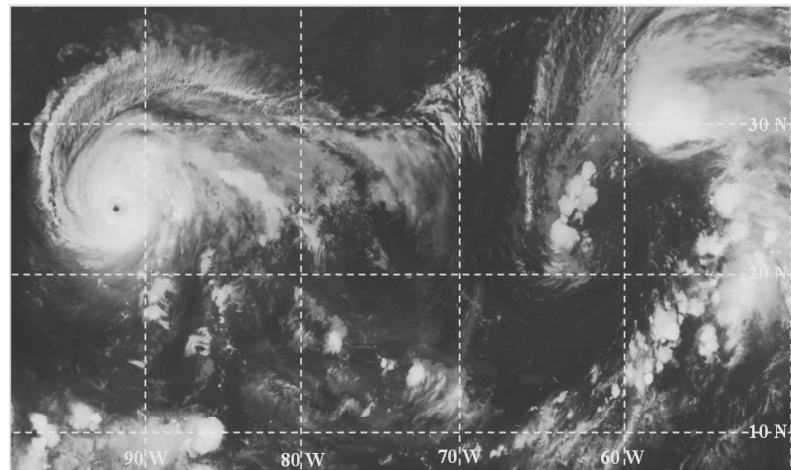


Figure 3.3. Rectified blue section in Figure 3.2. The scene includes Hurricane Rita near 90W and Tropical storm Philippe near 60W. 0315 UTC 29 September 2005.

3.3 Gradient of the image brightness temperatures

The gradient of the brightness temperatures in the image is calculated from the horizontal d_h and the vertical derivative d_v by convolving Sobel or Prewitt templates S_h , S_v , with the image I [12],[15]:

$$d_h = I * S_h \quad (3)$$

$$d_v = I * S_v, \quad (4)$$

where S_h and S_v can be defined by a Prewitt kernel:

$$S_h = \begin{bmatrix} -1 & 0 & 1 \\ -1 & 0 & 1 \\ -1 & 0 & 1 \end{bmatrix} \quad (4)$$

$$S_v = \begin{bmatrix} -1 & -1 & -1 \\ 0 & 0 & 0 \\ 1 & 1 & 1 \end{bmatrix} \quad (5)$$

Figure 3.4c shows an example of the gradient calculation of Figure 3.4b, which corresponds to the blue section of Figure 3.4a.

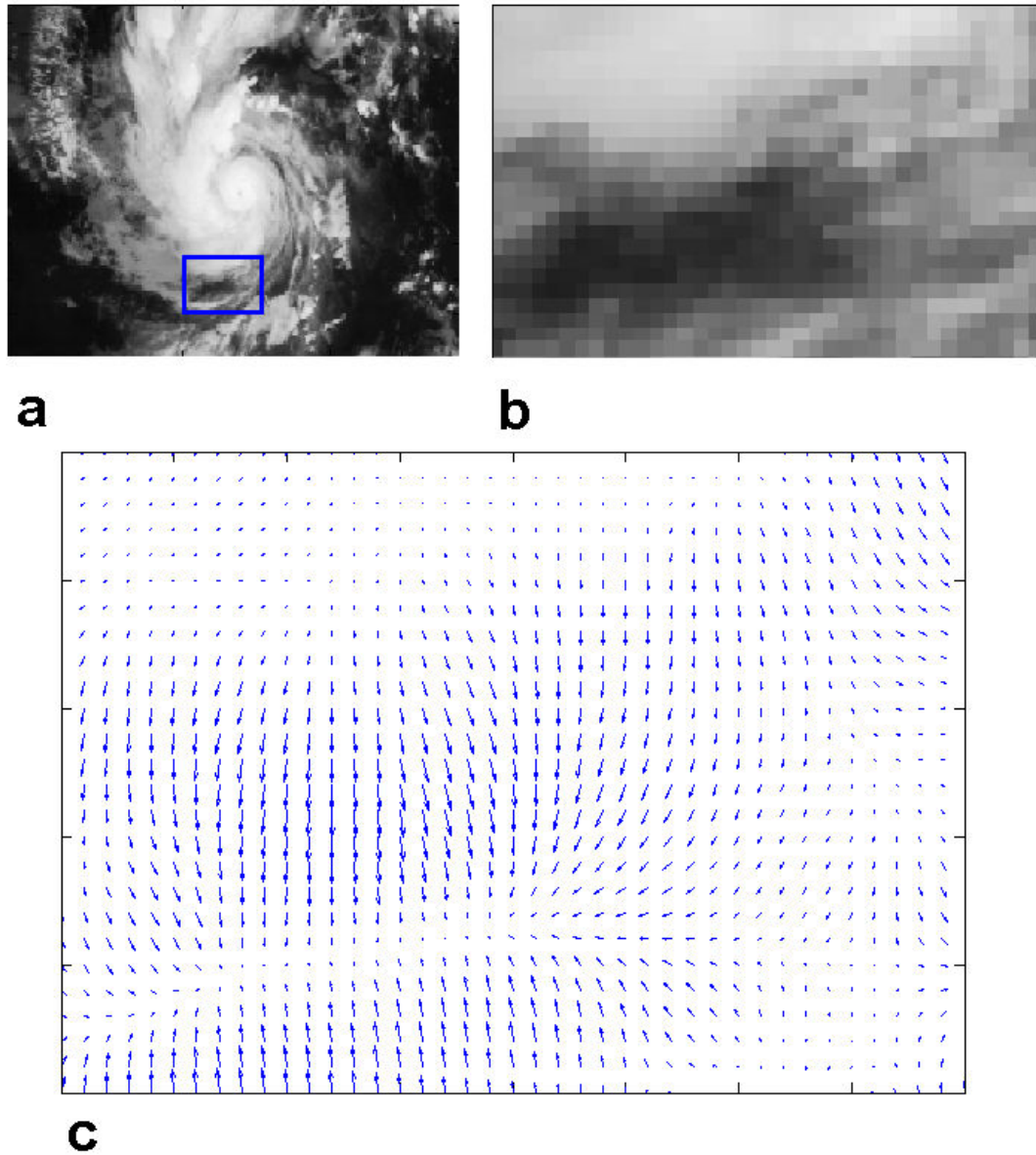


Figure 3.4. Example of the gradient calculation: a) IR image of Hurricane Beta, 0645 UTC October 2005; b) section represented by the rectangle in a); and c) the gradient of b)

3.4 The Center of the tropical cyclone: the accumulator matrix

After calculating the horizontal and vertical derivatives for each image, a line parallel to the gradient vector at each pixel is drawn across the image and the locations where these lines cross are stored in an accumulator (or density) matrix. A high number in the matrix indicates the location where many lines intersect, indicating a common point that the corresponding gradients are directed towards (or away from). The locations of the maxima in the accumulator matrix are considered to be the center locations or reference points of cloud systems of interest.

An idealized representation of the IR image of an axisymmetric tropical cyclone is shown in Figure 3.5a. The white pixels are where the coldest clouds are located in an annulus or eyewall encircling a cloud-free eye. The intensity of the pixels (or clouds) drops off with radius outside the eyewall as $1/r$. In this case, all the gradient vectors are pointing toward or away from the center of the image. Figure 3.5b illustrates the gradient vectors of the central section specified by the square in Figure 3.5a. The technique will produce a high number of intersections of the lines projected in the center of the accumulator matrix. Figure 3.5c shows the accumulator matrix calculation for two vectors (red arrows in Figure 3.5b). Since a tropical cyclone begins as a very disorganized cloud cluster and generally becomes more axisymmetric as it intensifies, the maximum value in the accumulator increases as the tropical cyclone intensifies, increasing the confidence that the central location or reference point of the weather system has been clearly identified.

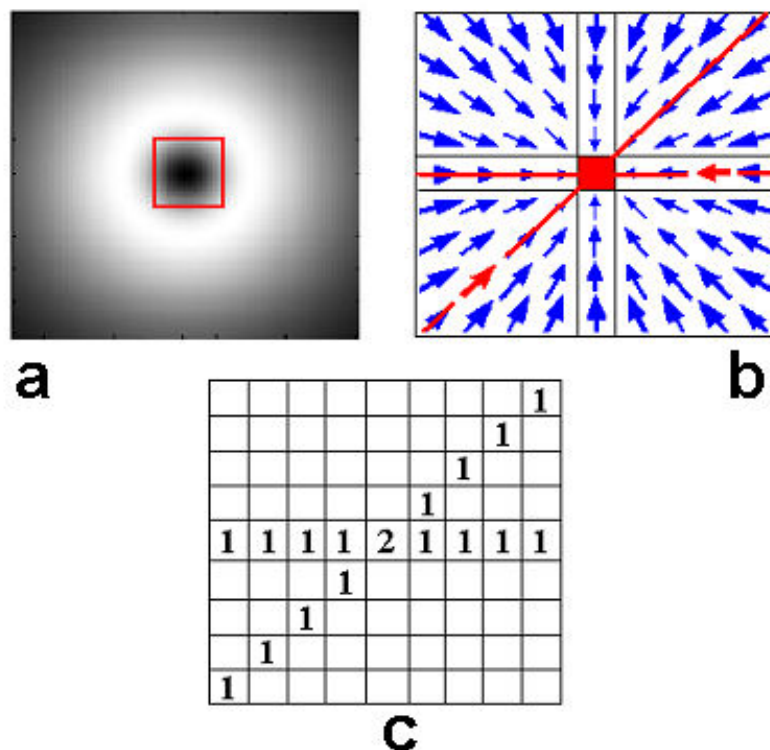


Figure 3.5. Example of the gradient line density calculation: a) brightness temperature image of an ideal vortex; b) gradient vectors of the ideal vortex's central section and the projected lines for two of its elements; and c) the resulting accumulator matrix of the projected lines.

As an example, Figure 3.6 and Figure 3.7 show the accumulator matrix for images of Hurricane Beta (2005) at different intensities. The corresponding location of the maximum accumulator matrix value is indicated on the satellite image (left) by the red dots. Note that the center in Figure 3.6a, when the tropical cyclone has not become a tropical storm, is not well defined. It can be identified with less ambiguity as the storm intensifies, as shown in Figure 3.7c and Figure 3.7d.

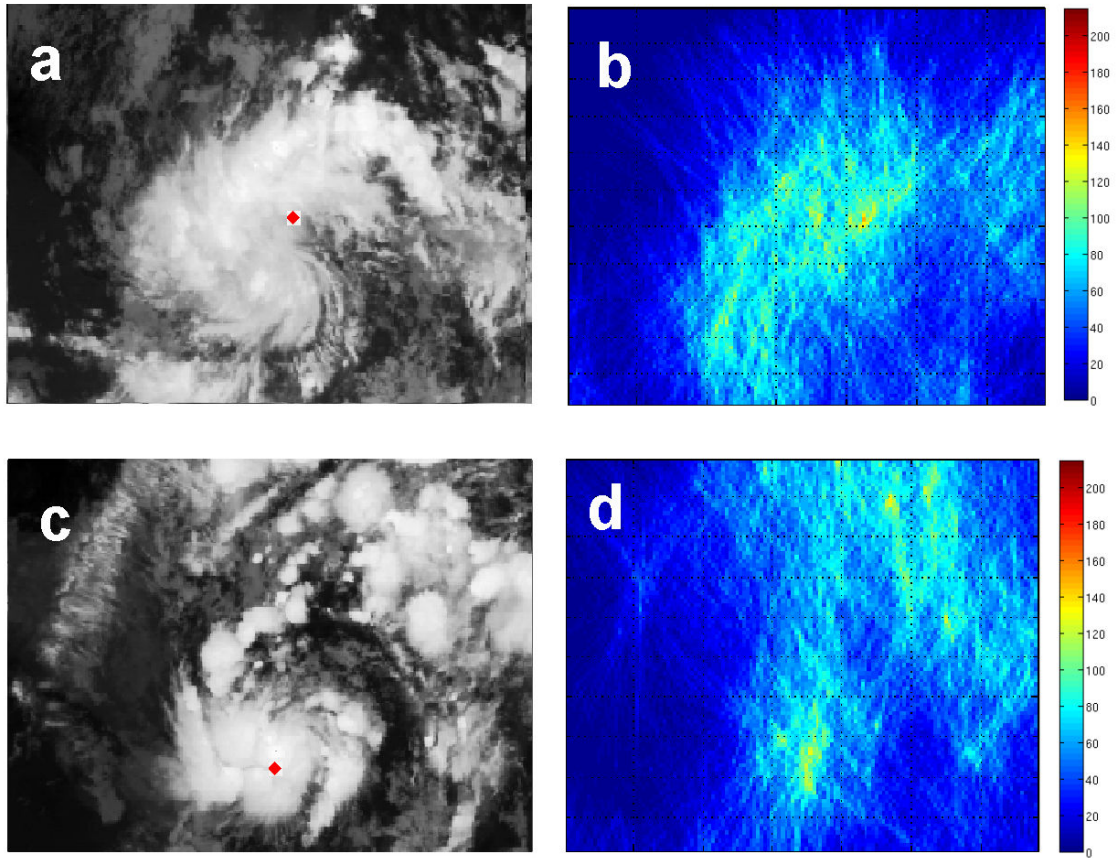


Figure 3.6. Infrared channel 4 ($10.7 \mu\text{m}$) image of Hurricane Beta: a) 1815 UTC October 26, 2005. The current intensity is estimated at 30 kt; and b) the accumulator matrix of the gradient projected lines for a); c) 0615 UTC October 27, 2005. The current intensity is 45 kt.; and d) the accumulator matrix of the gradient projected lines for c). The red dots indicate the corresponding location of the maximum value in accumulator matrix.

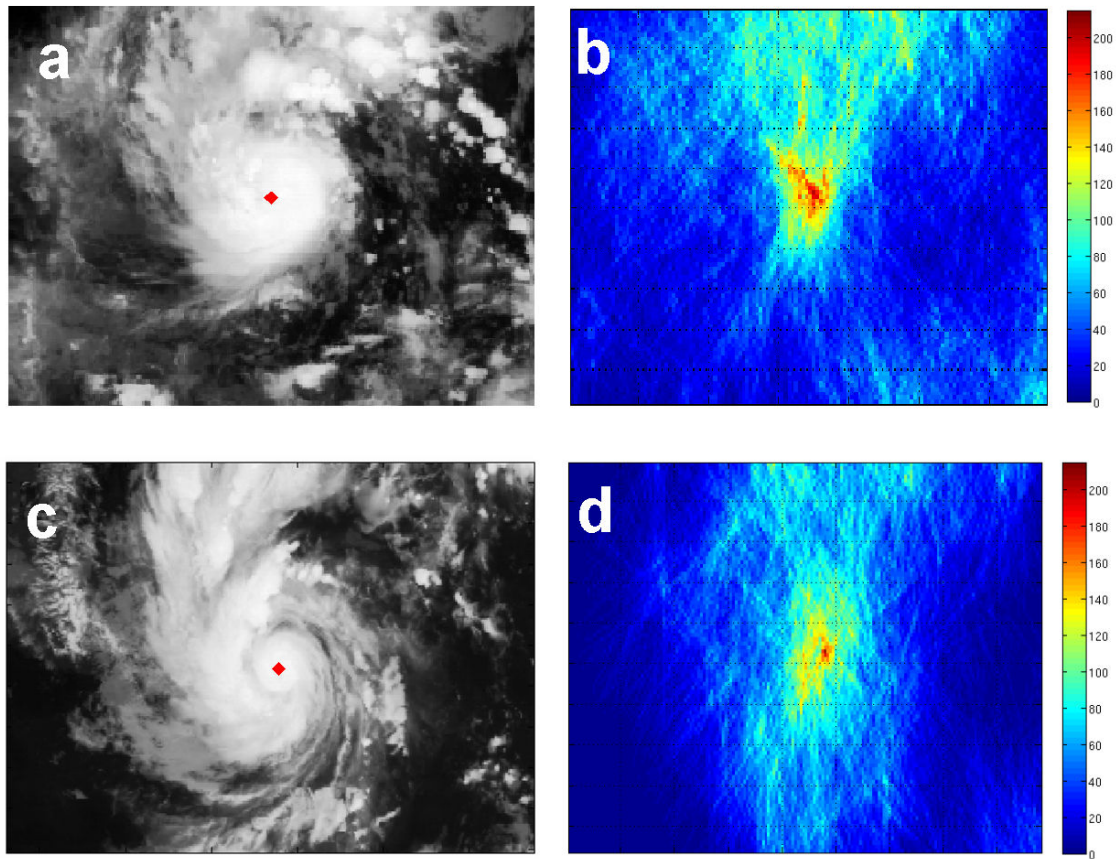


Figure 3.7. Infrared channel 4 ($10.7 \mu\text{m}$) image of Hurricane Beta: a) 0615 UTC October 29, 2005. The current intensity is estimated at 70 kt; and b) the accumulator matrix of the gradient projected lines for a); c) 0645 UTC October 30, 2005. The current intensity is estimated at 100 kt; and d) the accumulator matrix of the gradient projected lines for c). The red dots indicate the corresponding location of the maximum value in accumulator matrix.

An advantage of this system is that generally the number of weather disturbances in the scene does not need to be known in advance in order to identify them and locate their centers. Figure 3.8 shows an example of the accumulator matrix for Figure 3.3, where Hurricane Rita and Tropical Storm Philippe can be clearly identified by their centers located in the red regions. However, for the purposes of this study, each satellite picture

was individually analyzed to ensure that the reference point was consistently located within the atmospheric weather disturbance.

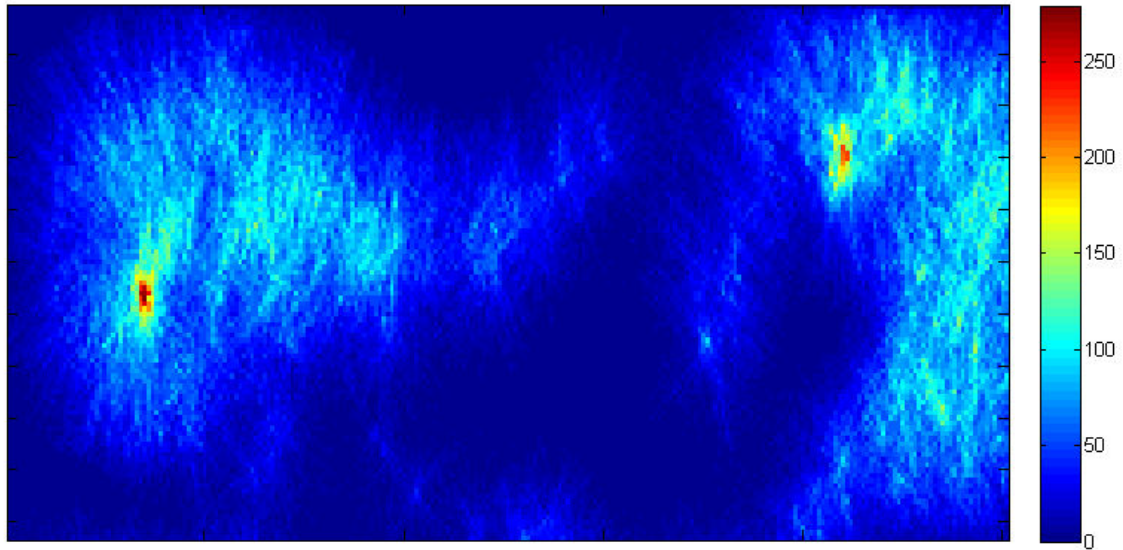


Figure 3.8. Accumulator matrix of the gradient projected lines for Figure 3.3. This map clearly shows the center locations of Hurricane Rita (left) and Tropical Storm Philippe (right).

3.5 Quantification of the Axisymmetry of a Cloud System.

A procedure is implemented that characterizes the departure of the weather system structure from axisymmetry. The deviation angle of each gradient vector relative to a radial line extending from the reference point or center found as described in section 3.4 is calculated as shown in Figure 3.9.

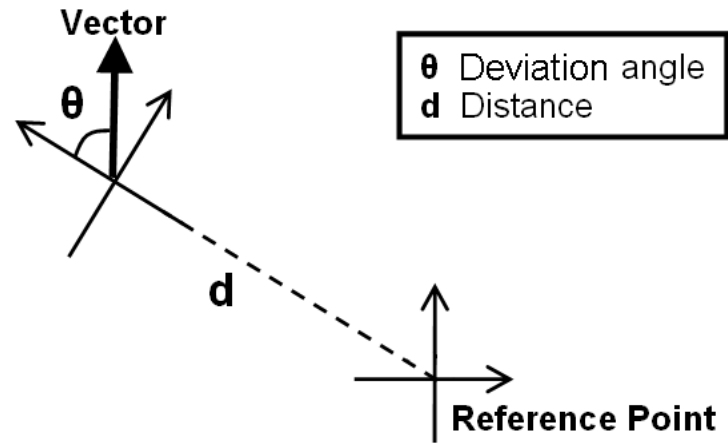


Figure 3.9. “Deviation Angle” Calculation. The reference point is the objectively determined center point of each object within the scene. The deviation angle and variance of every gradient vector within 70 pixels (or 350 km) is calculated for that reference point

Note that if the cloud scene represents an axisymmetric vortex such as that shown in Figure 3.10 then the gradient vector will point directly along the line to the center of the vortex and consequently its deviation angle is zero.

The calculation is repeated for each gradient vector within a radius of 70 pixels (~350 km) of the reference point. The distribution of the departure angles is calculated and a histogram is plotted. An example of the histogram from the ideal vortex in Figure 3.10 is plotted in Figure 3.11.

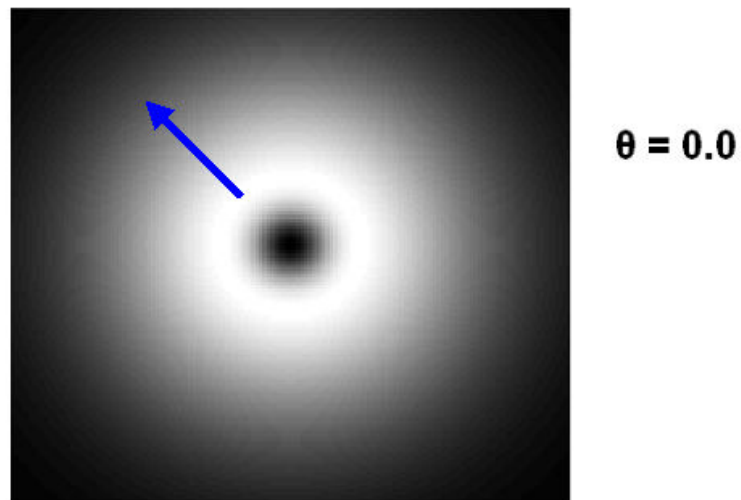


Figure 3.10. Example of the “deviation angle” for an axisymmetric vortex

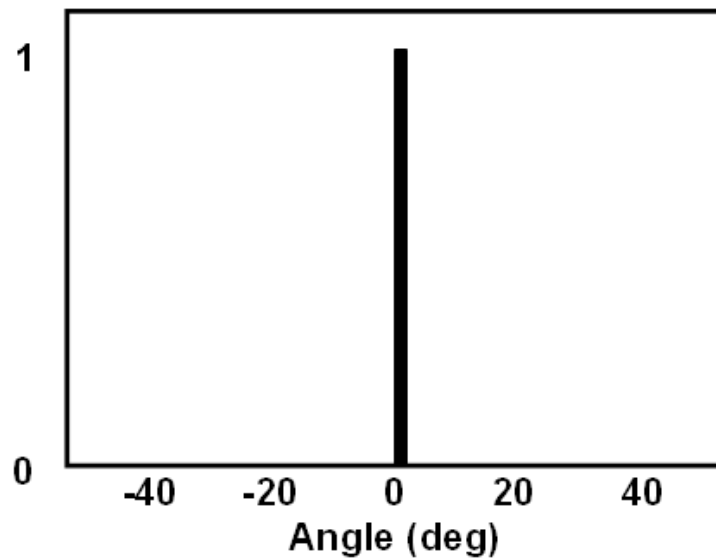


Figure 3.11. histogram of deviation angles for the ideal vortex in Figure 3.10.

The variance of the deviation angles is used as a measure of the “organization” of its surroundings. Whereas for an ideal vortex this variance should be zero, for a regular

cloud there will be a high variance due to the fact that not only is the reference point not well-defined, but also the gradient field is extremely disordered.

A strength of the technique is that only the direction of the vector and not its magnitude is used in the analysis, which makes the technique more robust to variations on the brightness temperatures due to factors such as the calibration of the sensor. Thus, in regions such as central dense overcasts where there may be very small deviations on the brightness temperatures, the technique will still distinguish the cloud structure. However, those pixels with low values in the surroundings of the cloud system that can increase the deviation-angle variance due to their disorganized orientation are removed from the analysis.

The operation is repeated for each reference point (i.e., weather disturbance) in the scene as shown in Figure 3.12 for Hurricane Rita and Tropical Storm Philippe (Figure 3.3 and Figure 3.8).

The time sequence of the deviation-angle variances shows when a cloud object around a reference point is organizing into a vortex. Figure 3.13 is an example of this analysis for three representative stages of the lifecycle of Hurricane Rita (2005). Note the initial large spread of the histogram in Figure 3.13a associated with a large departure in the gradient vectors from an ideal vortex when Rita is a tropical depression. As the storm system increases in intensity, the spread in the histogram reduces (Figure 3.13b) until, by 21 September, Hurricane Rita is a well-structured vortex, and the corresponding histogram (Figure 3.13c) shows a large peak at 0 angle and very little spread. As Rita decays and moves inland, the spread once again increases (not shown).

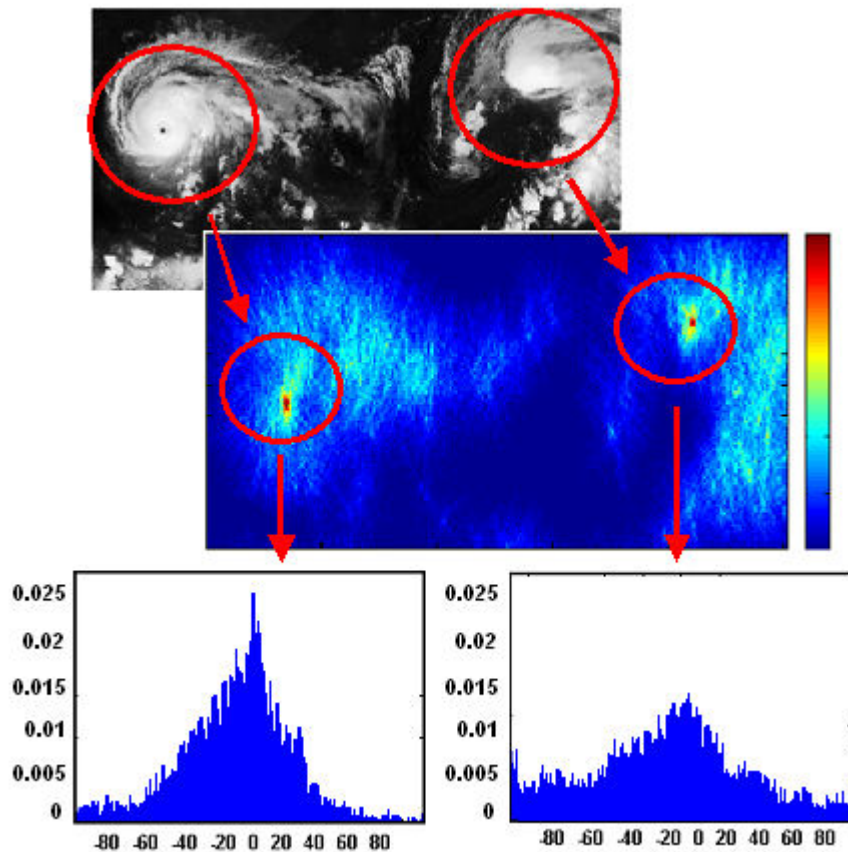


Figure 3.12. Deviation angle variance calculation for two different atmospheric system of Figure 3.3 and Figure 3.8.

A second distribution for Tropical Storm Lee (2005) is shown in Figure 3.14. Lee is of interest because there is considerable disorganization of the cloud structures from Figure 3.14a-c, yet the same organization and sequence of variance reduction with intensity is observed. It is of interest to note that by comparing Figure 3.13 and Figure 3.14, a 25-kt depression can have a range of variance values (1625 and 1678 deg^2 respectively for these two cases).

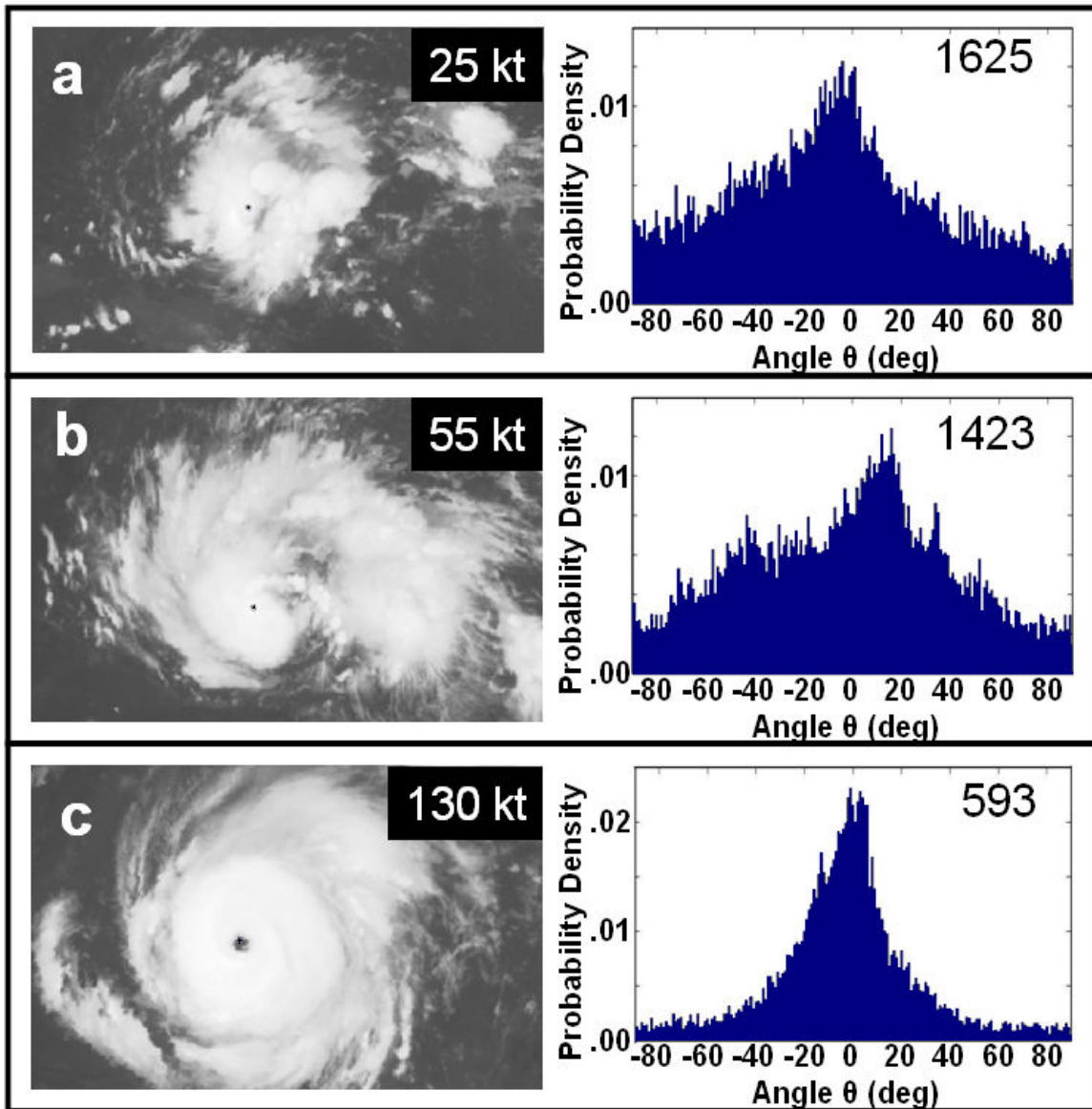


Figure 3.13. Sequence of infrared images and deviation angles histograms for Hurricane Rita (2005): a) 0815 UTC 18 September 2005. Intensity: 25kt, 1009 hPa, variance: 1625 deg²; b) 1415 UTC 19 September 2005. Intensity: 55 kt, 997 hPa, variance: 1423 deg²; and c) 1415 UTC 21 September 2005. Intensity: 130kt, 932 hPa, variance: 593 deg².

Another distribution is shown for Hurricane Nate (2005) in Figure 3.15. When Nate is at tropical depression stage, a large spread in the deviation-angle variance is calculated

(Figure 3.15a). As Nate organizes into first a tropical storm (Figure 3.15b) and then a minimal hurricane (Figure 3.15c), the deviation-angle variance reduces significantly.

In general, the spread in deviation-angle variance values for the same intensity is not large. However, recall that the best-track intensity estimation is a smooth representation of the tropical cyclone intensity. Thus, within the life cycle of an individual storm, there will be fluctuations in the deviation-angle variance value for the same best-track intensity.

3.6 Summary

In this chapter a methodology was described that characterizes the departure of a cloud system from axisymmetry by performing a statistical analysis of the orientation of the brightness-temperature gradient. An objective procedure to locate the center of the cloud system is proposed, in which lines aligned to each gradient vector are projected and accumulated in an auxiliary matrix. The center position corresponds to the location where the highest number of intersections of the lines is found. The variance of the deviation angles, defined by the minimum angle between a line extended from the center position to each gradient vector and the vector itself, describes the axisymmetry of the system. The deviation-angle variance decreases as the axisymmetry of the tropical cyclone increases, which in turn reflects increasing intensity. This technique is simple and objective, compared to the standard Dvorak method of determining intensity from satellite images.

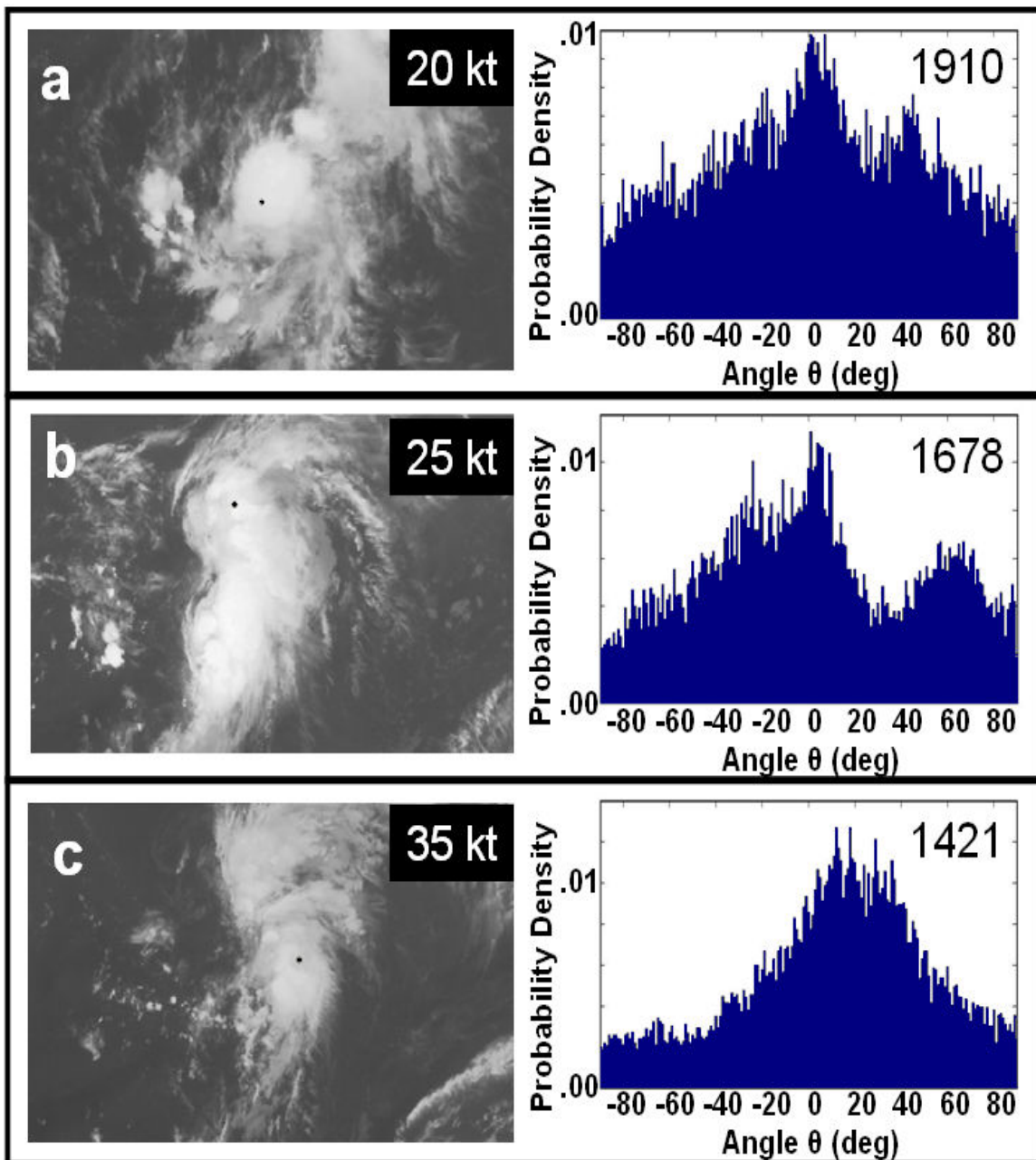


Figure 3.14. Sequence of infrared images and deviation angles histograms for Tropical Storm Lee (2005): a) 2115 UTC 29 August 2005. Intensity: 20 kt, 1009 hPa, variance: 1910 deg²; b) 0015 UTC 31 August 2007. Intensity 25 kt, 1010 hPa, variance: 1678 deg²; and c) 1615 UTC 31 August 2007. Intensity 35 kt, 1007 hPa, variance: 1421 deg².

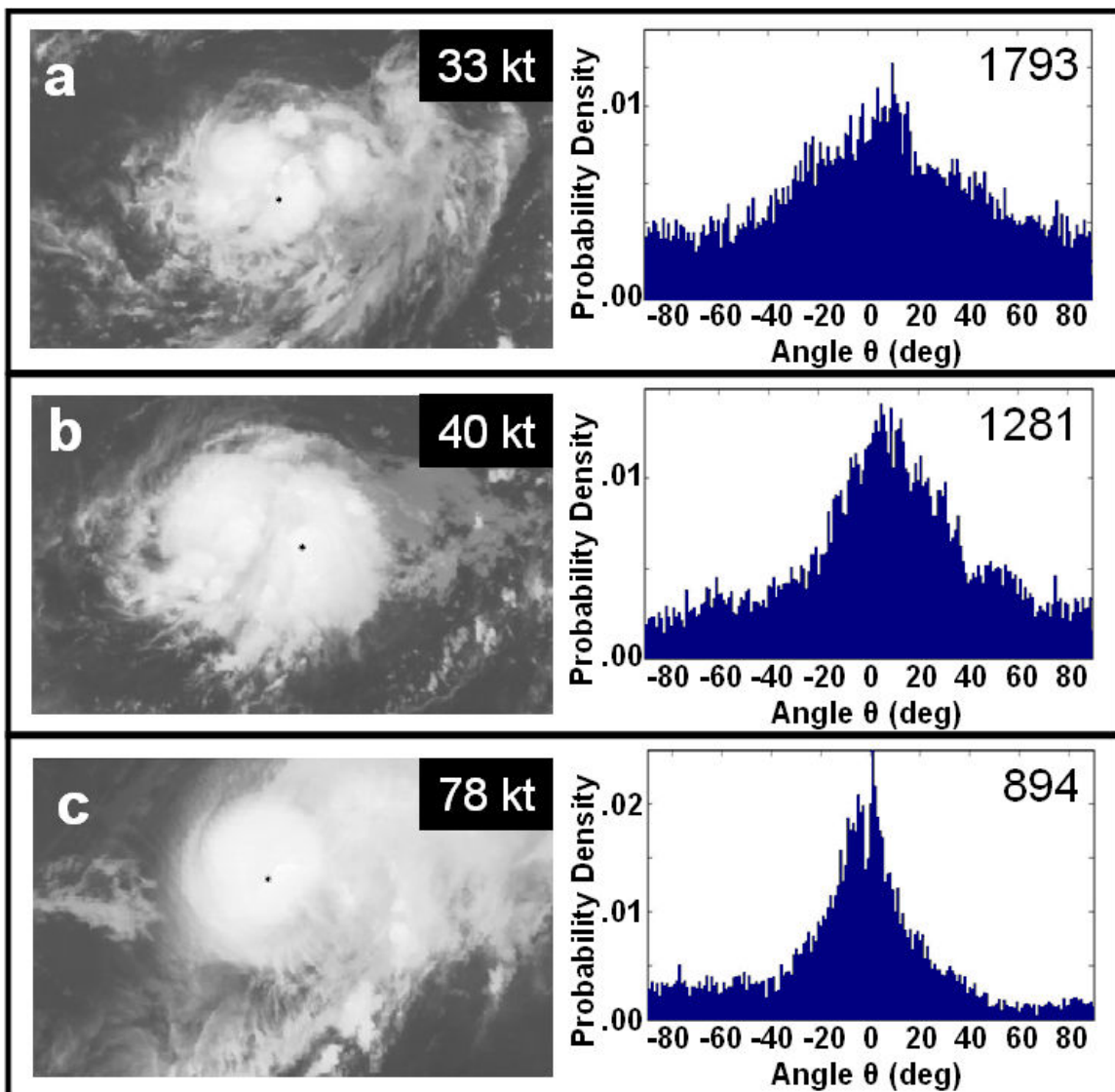


Figure 3.15. Sequence of infrared images and deviation angles histograms for Hurricane Nate (2005): a) 2245 UTC 5 September 2005. Intensity: 33 kt, 1006 hPa, variance: 1793 deg^2 ; b) 0745 UTC 6 September 2005. Intensity: 40 kt, 1002 hPa, variance: 1281 deg^2 ; and c) 2245 UTC 8 September 2005. Intensity: 78kt, 9802 hPa, variance: 894 deg^2 .

4 INTENSITY ESTIMATION RESULTS

4.1 Correlation with tropical cyclone lifecycle

The first test to see if the technique presented in Chapter 3 characterizes tropical cyclone structure is to measure the calculated variance against the simplest measure of tropical cyclone maturity, that is, the intensity as measured by the maximum sustained surface wind speed and recorded in NHC best-track files in 6-hourly increments. From Figure 3.13, Figure 3.14 and Figure 3.15 it can be seen that as the intensity increases, the deviation-angle variance decreases. Thus it may be possible to estimate intensity from the variance value.

There are some obvious limits to comparing these measures. First, the deviation-angle variance is calculated on a different time scale to the recorded best-track intensity values. Second, the deviation-angle variance characterizes structure and not intensity per se and it is not inherently obvious that the two should exactly match. Third, by using images that are high temporal resolution (every 30 minutes), high-frequency signals and noise are introduced into the time-series that are not present in the recorded best-track intensity files, which are at 6-h resolution and have significant subjective components introduced by the expert that have the effect of smoothing the data. The high-frequency signals in the variance data are not necessarily incorrect because they may be identifying times of convective activity within the tropical cyclone circulation and diurnal structure oscillations amongst other possibilities, whereas best-track estimates aim to capture the synoptics of the tropical cyclone.

For example, the development of a thunderstorm within the cloud cluster introduces an asymmetry into the cloud structure that this technique detects as an increase in deviation-angle variance, but would not necessarily reflect as a reduction in intensity in the best-track data. Subsequent merger and axisymmetrization of the thunderstorm into the cloud system results in reduction in the deviation-angle variance and possibly an increase in the actual recorded intensity.

Figure 4.1 shows a time series of the raw deviation-angle variance (green), a low-pass filtered deviation-angle variance (blue), and NHC wind speed estimates (red) for Hurricane Rita (2005) using half-hourly imagery. A first order low-pass filter with cutoff frequency of 0.025π rad/sample [29] is used to reduce the high-frequency oscillations in the variance in order to compare more readily with the 6-h resolution of the NHC best-track intensity estimates. The filter utilized only has one pole in order to capture the primary trend in the deviation-angle variance, reduce some frequency components (e.g. the component at 0.025π rad/sample is attenuated 70.7%) and produce a short transient response for a future real-time application.

For purposes of comparison, the NHC best-track intensity estimates are linearly interpolated to half-hourly temporal resolution. Recall that as the tropical cyclone exhibits a more axisymmetric structure the calculated deviation-angle variance in the gradient decreases. This behavior is well illustrated in Figure 4.1, both by the original time series and the filtered series. The correlation magnitude calculated between the intensity and variance in Figure 4.1 is 0.85 for the unfiltered deviation-angle variance and 0.90 for the filtered deviation-angle variance.

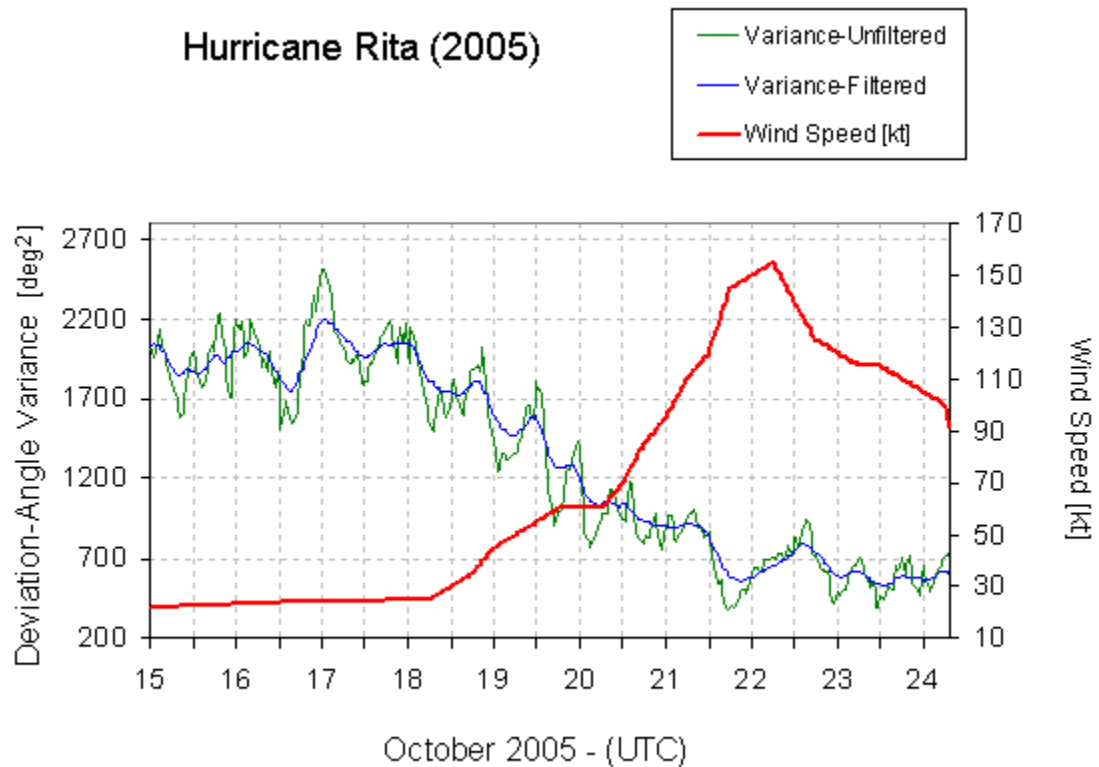


Figure 4.1. Time series of the best-track intensity (kt) from the National Hurricane Center best-track data (red), unfiltered angle variance (green; correlation: -0.85), and filtered angle variance (blue; correlation: -0.90) for Hurricane Rita. During the period 15 September to 24 September, midnight local is between 0500 UTC and 0600 UTC.

Figure 4.2 and Figure 4.3 show two examples of weaker tropical cyclones. Hurricane Nate reached a maximum intensity of 80 kt, and the magnitude of the correlation for the filtered variance was 0.93 and 0.77 for the unfiltered deviation-angle variance. Tropical Storm Lee reached only 35 kt, and the correlation magnitude was 0.5 for the unfiltered deviation-angle variance and 0.72 for the filtered variance. Note in the time series for Tropical Storm Lee, the amplitude of the semi-diurnal oscillations that are present in the

deviation-angle variance time series but not in the best-track intensity overwhelm the low-frequency intensity signal. In addition, these oscillations between 28 August at 1200 UTC and 30 August 00 UTC do not show an evident increasing or decreasing average trend, but the wind speed remains constant in two time intervals. This is the reason why the correlations are so much lower for this case.

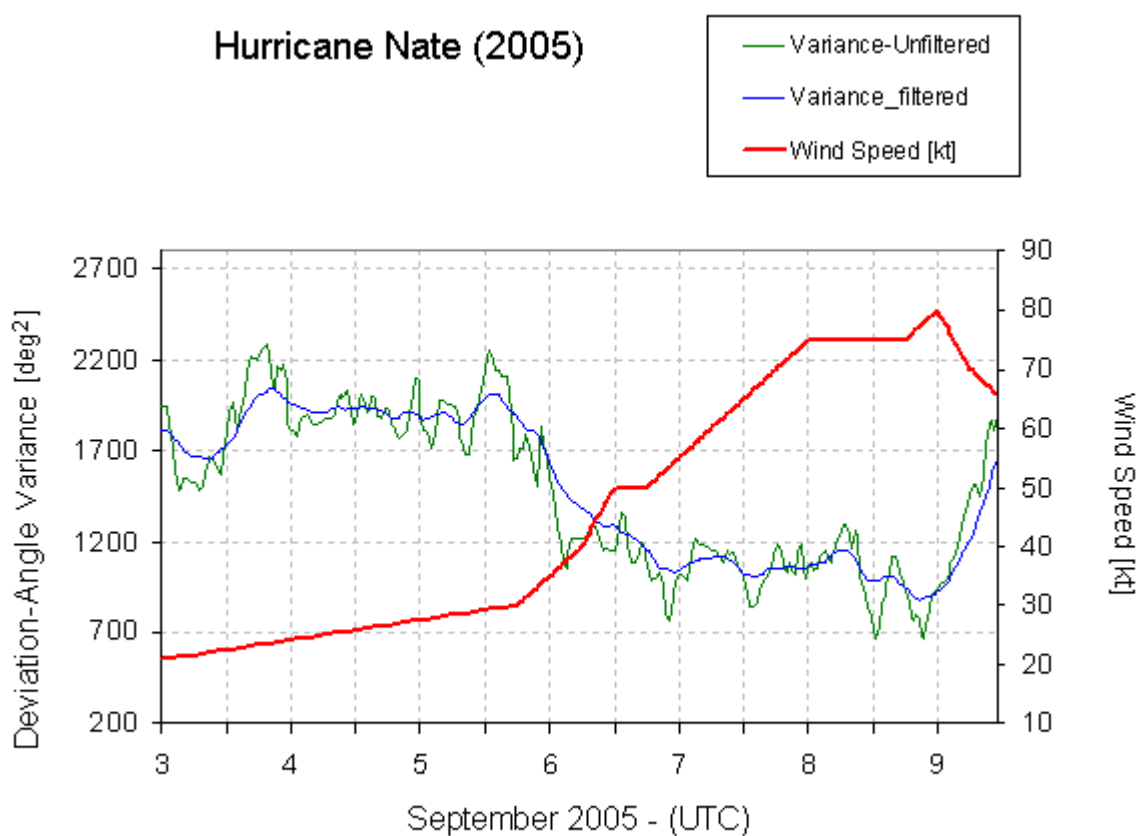


Figure 4.2. Time series of the best-track intensity (kt) from the National Hurricane Center best-track data (red), unfiltered angle variance (green; correlation: -0.78), and filtered angle variance (blue; correlation: -0.93) for Hurricane Nate. During the period 3 September to 9 September, midnight local 0000 local is between 0300 UTC and 0400 UTC.

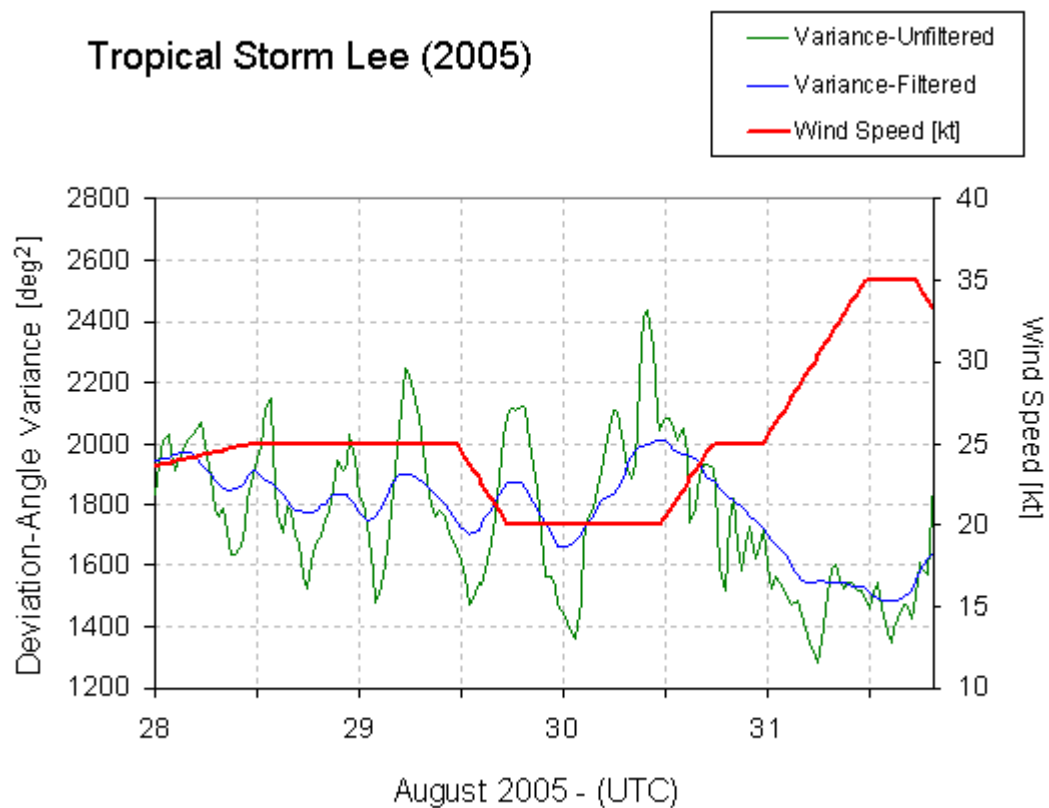


Figure 4.3. Time series of the best-track intensity (kt) from the National Hurricane Center best-track data (red), unfiltered angle variance (green; correlation: -0.49), and filtered angle variance (blue; correlation: -0.71) for Tropical Storm Lee. During the period 28 August to 31 August, the midnight local is between 0300 UTC and 0400 UTC.

4.2 2005 Seasonal Statistics

To test the variance technique for intensity estimation, GOES imagery of 26 tropical cyclones from the Atlantic basin during 2005 were examined from their earliest beginnings to their demise. Half-hourly images were processed as described above, the

deviation-angle variance calculated relative to the reference point, and time series of both unfiltered and filtered deviation-angle variances were constructed for each case.

The correlations calculated between the NHC best-track intensity and deviation-angle variance for all 26 tropical cyclone cases are shown in Figure 4.4. Note that the correlations are negative; intensity increases as the angle variance decreases. Overall there is an average correlation magnitude of 0.74 for the filtered deviation-angle variance and over half of the cases (57%) have magnitudes of 0.8 or higher, resulting in a median correlation of 0.83. Correlations are the highest overall for the thirteen systems that reach hurricane strength (average magnitude 0.86).

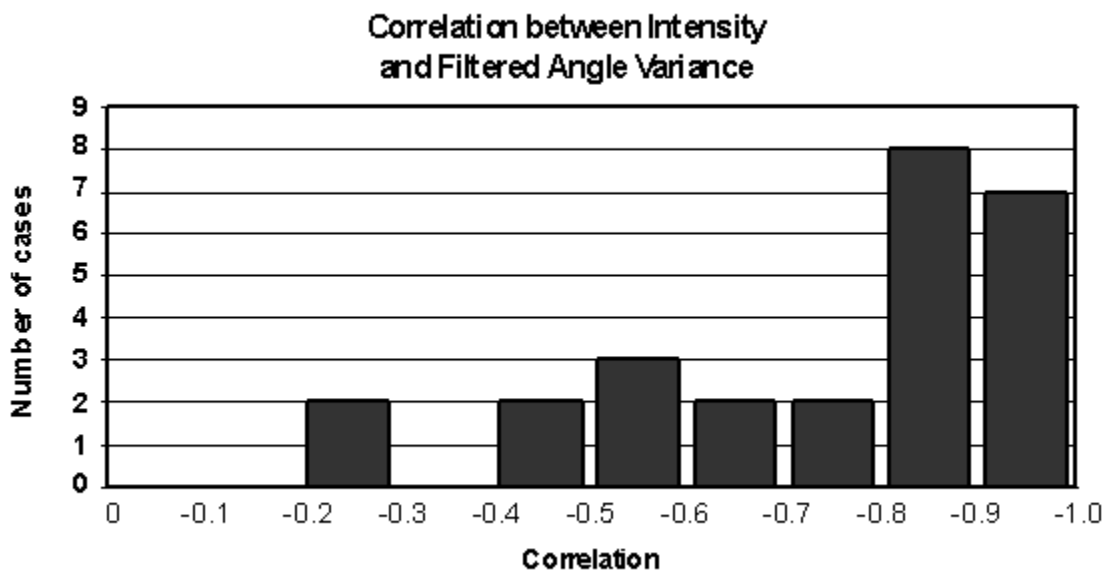


Figure 4.4. Histogram of the correlation values between the best-track intensity and filtered angle variance for all 26 tropical cyclone cases. The mean correlation magnitude is 0.74, the median is 0.83, with a standard deviation of 0.23.

In four cases, Tropical Storms Gert, Harvey, Jose, and Alpha, the magnitude of the correlation with the best-track intensity estimate is less than 0.5. Figure 4.5 and Figure 4.6 show two examples of these cases: Tropical Storm Alpha, which had a correlation magnitude of 0.35 on the unfiltered deviation-angle variance, and 0.50 on the filtered signal, and Tropical Storm Gert, which had a correlation magnitude of 0.15 for the unfiltered deviation-angle variance and 0.29 for the filtered deviation-angle variance. In all four cases the time series of deviation-angle variance is dominated by high-amplitude oscillations that overwhelm the intensity signal. The correlations for all cases are somewhat reduced because of the presence of these oscillations. In addition, these storms are characterized by slow or no variations in the reported intensity. However, their organization can change considerably over a period of just hours. Figure 4.7 shows an example of this behavior, three frames of the Tropical Storm Alpha sequence indicated by black dots in Figure 4.5. Although the intensity varies only 3 kt in the best-track data at these three moments, it is evident that there is considerable structural change in the satellite imagery (Figure 4.7). Note that during this period, the estimates being used by the NHC for intensity were from the Dvorak technique estimates, which, as described in section 2, are considerably constrained particularly at the lowest T-numbers.

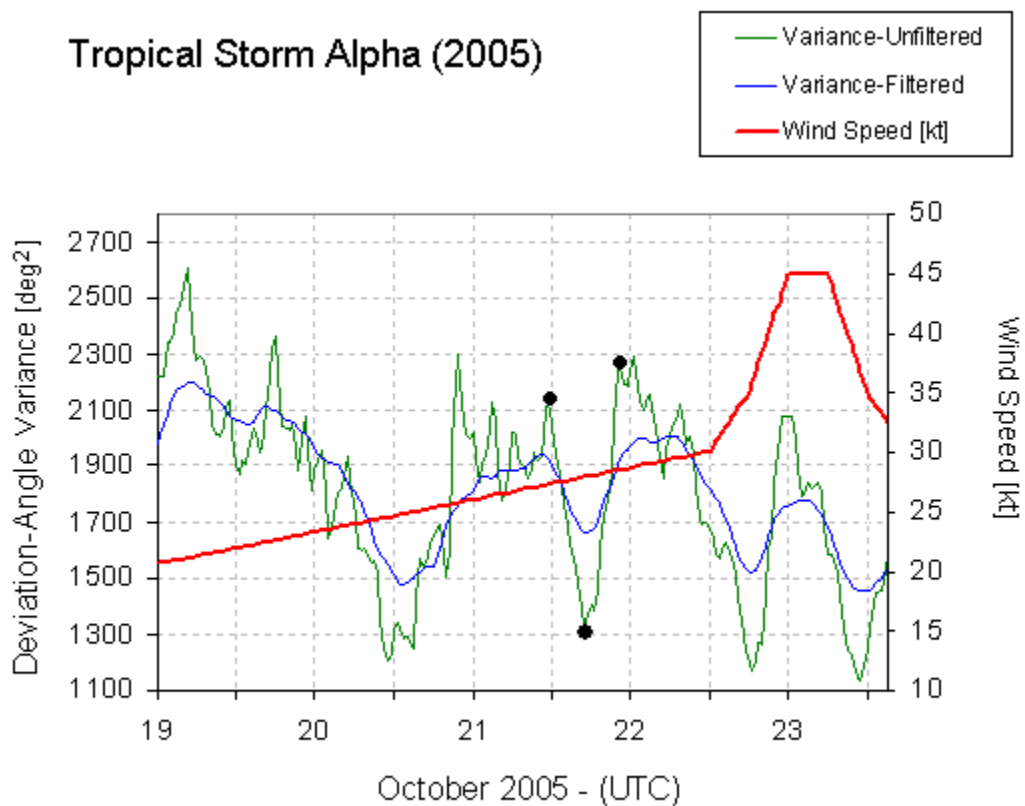


Figure 4.5. Time series of the best-track intensity (kt) from the National Hurricane Center best-track data (red), unfiltered angle variance (green; correlation: -0.35), and filtered angle variance (blue; correlation: -0.50) for Tropical Storm Alpha. During the period 19 October to 23 October, midnight local is between 0400 UTC and 0500 UTC.

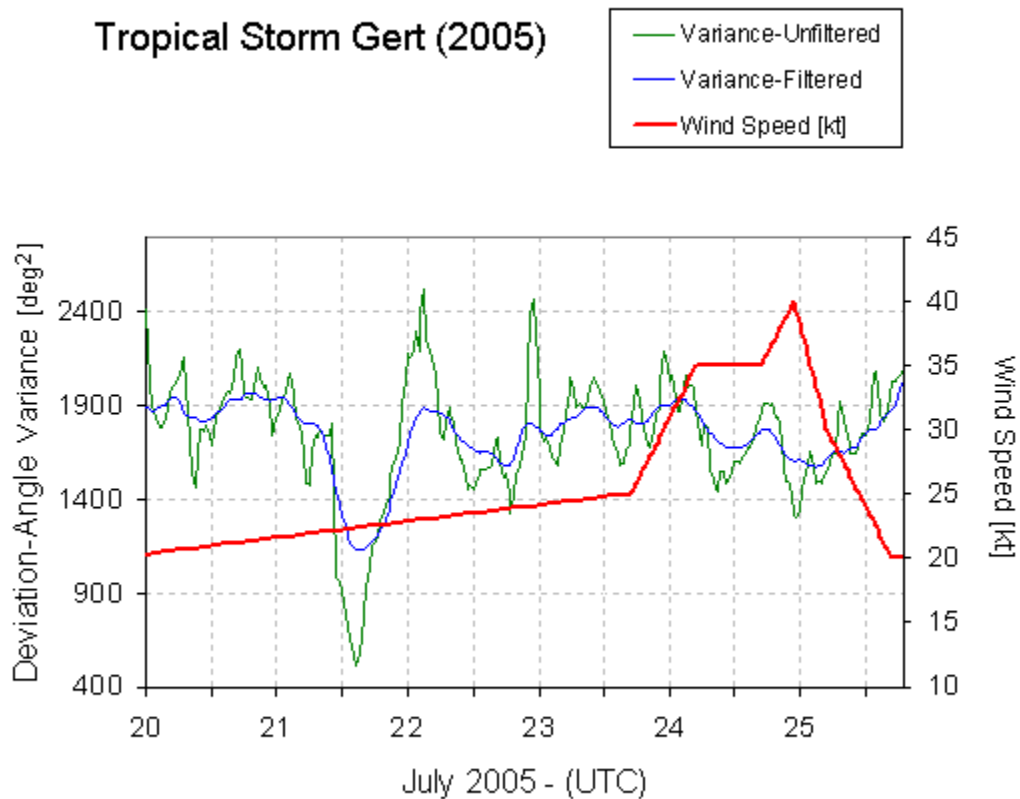


Figure 4.6. Time series of the best-track intensity (kt) from the National Hurricane Center best-track data (red), unfiltered angle variance (green; correlation: -0.15), and filtered angle variance (blue; correlation: -0.29) for Tropical Storm Gert. During the period 20 July to 25 July, midnight local is between 0600 UTC and 0700 UTC.

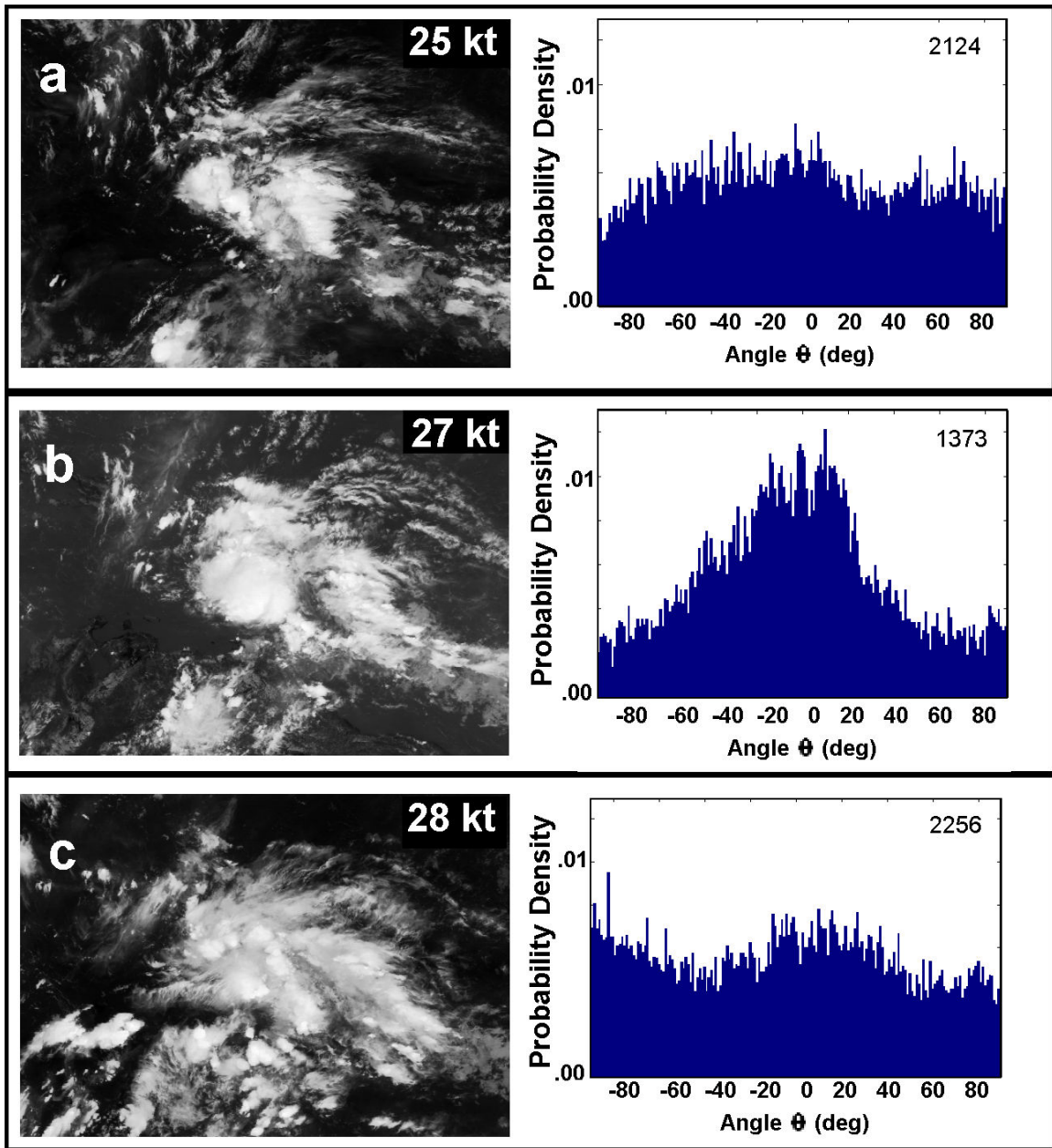


Figure 4.7. Sequence of infrared images and deviation angles histograms for Tropical Storm Alpha (2005): a) 1115 UTC 21 October 2005. Intensity: 25 kt, 1009 hPa, variance: 2124 deg²; b) 1715 UTC 21 October 2005. Intensity: 27 kt, 1009 hPa, variance: 1373 deg²; and c) 2215 UTC 21 October 2005. Intensity: 28 kt, 1009 hPa, variance: 2256 deg².

The best-fit curve of the deviation-angle variances for tropical cyclones in 2005 and 2004 for periods when the storms are intensifying plotted against the NHC best-track wind speeds are shown in Figure 4.8 and Figure 4.9 respectively. While there is some variation in the raw deviation-angle variance values calculated at these different values of intensity, the agreement is remarkably good. The exceptions are at higher wind speeds when the number of tropical cyclones contributing to the average drops. In these cases, disproportionately high deviation-angle variance values from Hurricane Wilma, which intensified at record rates, skew the statistics. Although the deviation-angle variances correlated with the wind speed is -0.93 when this storm reached its maximum intensity value, the deviation-angle variance were considerably higher (~850) than other similar cases such as Katrina and Rita (~650) (see Figure 4.10). These time series supports the notion that not only does the trend of the satellite-derived variance values indicate the intensification of the tropical cyclone but the absolute value also provides an estimate of the actual intensity of the tropical cyclone.

For intensification periods, the RMS wind speed error after applying the results shown in Figure 4.8 to the angle-deviation variances for the 2005 dataset is approximately 18.2 kt. However, for 90% of the samples the RMS wind speed error is 11.3 kt, 80% of the samples had an error of 8.97 kt and for 50% of the samples the error is only 3.84 kt. To test the technique, the procedure is applied to the 2004 dataset that comprises 14 tropical cyclones. The RMS wind speed error is 19.45 kt for deviation-angle variance samples during intensification periods, the error is 14.1 kt, 11.3 kt and 5.2 kt for 90%, 80% and 50% of the samples respectively. Recall that the error of the Dvorak technique is from 10

to 15 kt. Although the accuracy of this technique is a little less than the Dvorak technique, it is objective and easy to implement. In addition, diurnal and semidiurnal fluctuations in the intensity are not shown in the best-track estimates, and the reason why the error increases.

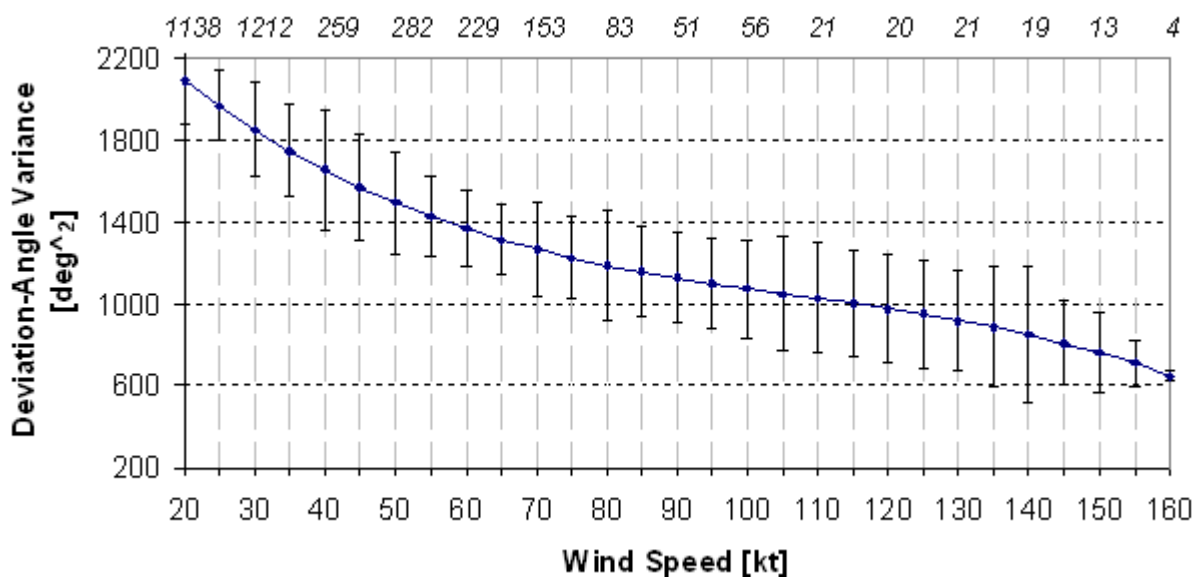


Figure 4.8. Angle variance versus wind speed for all 26 tropical cyclone cases during intensifying periods of 2005 with one standard deviation error bars. Note that there may be more than one time series for any given storm. The number of images going into each wind speed value is indicated at the top of the graph in italics.

One potential method to increase the accuracy of this technique is to reduce the error in the center position of the tropical cyclone that is defined by the accumulator matrix. Incorrect locations of the center can generate higher deviation-angle variances, decreasing the correlation with the wind speed and increasing the spread around each deviation-angle variance value in Figure 4.8.

The presence of oscillations in the deviation-angle variance time series and a low spread of variances for low wind speeds suggest the potential of this technique to detect the genesis of a tropical cyclone. This technique is extended for this purpose in Chapter 5.

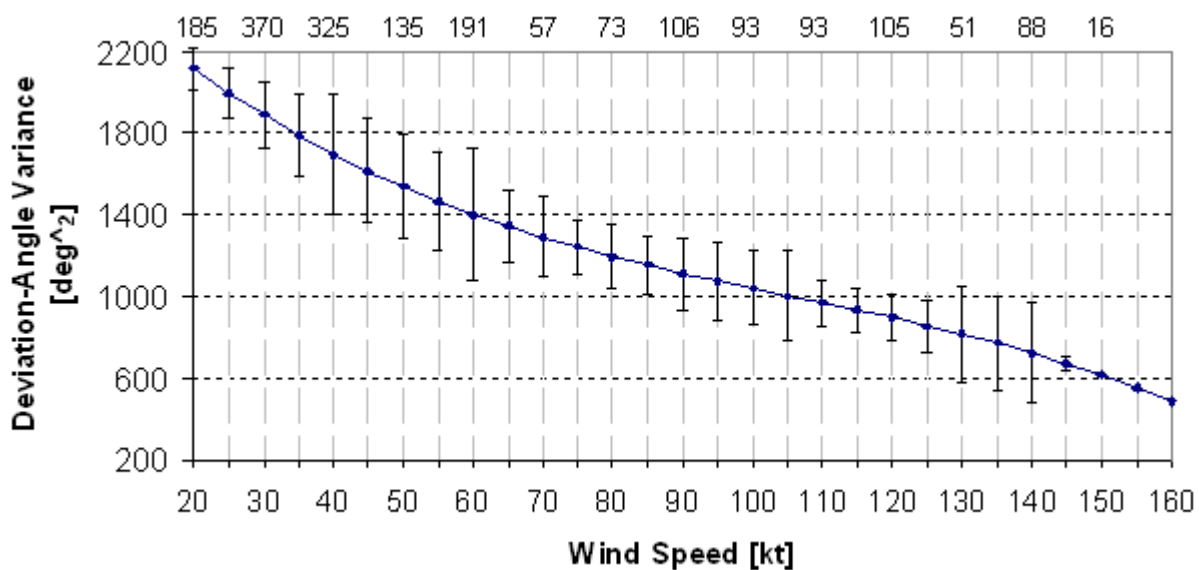


Figure 4.9. Angle variance versus wind speed for all 14 tropical cyclone cases during intensifying periods of 2004 with one standard deviation error bars. Note that there may be more than one time series for any given storm. The number of images going into each wind speed value is indicated at the top of the graph in italics.

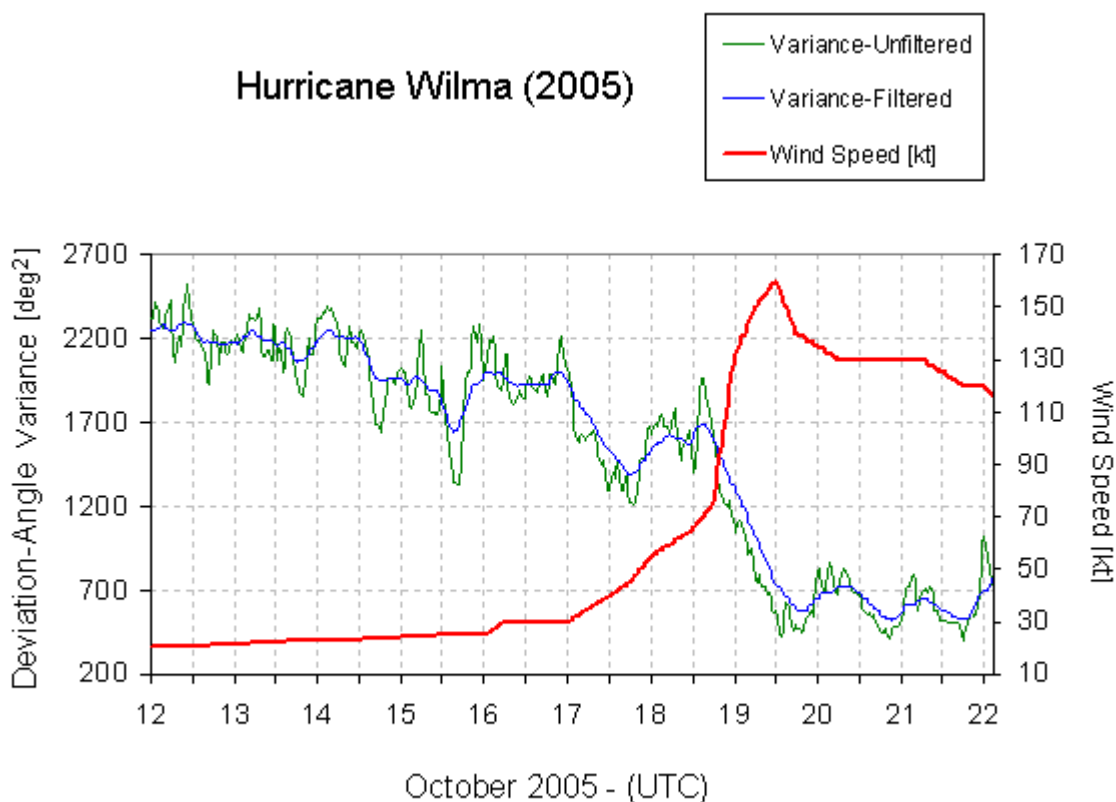


Figure 4.10. Time series of the best-track intensity (kt) from the National Hurricane Center best-track data (red), unfiltered angle variance (green; correlation: -0.93), and filtered angle variance (blue; correlation: -0.93) for Hurricane Wilma. During the period 12 October to 22 October, midnight local is between 0400 UTC and 0500 UTC.

4.3 Time series analysis

Analysis of the time series of deviation-angle variance reveals a number of oscillations of differing scales. Of importance is the approximately 24-h or diurnal oscillation in the time series shown in Figure 4.1 for Hurricane Rita, with a maximum in variance (or minimum in organization) at around 12 UTC. A period of reorganization and axisymmetrization then follows over a period of approximately 12 hours during the first

four days (15 September – 18 September) of the sequence, and the variance again drops. However, diurnal and semidiurnal frequencies are only observed in approximately half of the cases analyzed, particularly at early stages of their lifecycle when the convection of the tropical cyclones is forced by the atmospheric tide [30], [31], [32]. In addition to these oscillations, some higher-frequency (1-3h) oscillations are evident in the unfiltered angle variance time series for many cases including that of Rita in Figure 4.1. This may be caused by noise in the technique because of slight inconsistencies in the reference point location, the resolution of the original scene, which is 5 km/pixel, and some stretching caused by the re-mapping of the natural-coordinate system to the regular Cartesian system employed by the technique.

4.4 Summary

This section presents the results of the methodology described in Chapter 3, time series of the deviation-angle variances of each tropical cyclone are built and correlated to the NHC best-track intensities estimates of 2005. Results show an average correlation magnitude of 0.74, and higher correlations for intense tropical cyclones [33]. These results (Figure 4.8) are applied to the deviation-angle variance dataset of 2004 to obtain wind speed estimates that are compared with the best-track records. The RMS wind speed error calculated is approximately 19 kt for intensification periods. The error increases due to some factors such as incorrect tropical cyclone center location, and large diurnal and/or semidiurnal oscillations in the deviation-angle variance time series of some tropical cyclones. These oscillations reduce the correlation of these time series with the best-track

intensity estimates, which does not reflect intensity changes due to convective activity within the tropical cyclone circulation and diurnal structure oscillations.

5 TROPICAL CYCLOGENESIS IDENTIFICATION

The genesis of a tropical cyclone has been a subject of study for many years. However, the physical processes that initiate these atmospheric events are not totally understood. The actual forecasting models and methodologies (e.g. Dvorak technique) do not discriminate developing from non-developing cloud clusters, and are applied when the cloud structures show an evident circulation pattern. The development of a technique to detect the formation of a tropical cyclone would allow forecasters to start tracking atmospheric disturbances and run actual models with some confidence.

In Chapters 3 and 4 a new methodology to estimate the intensity of a tropical cyclone by quantifying its axisymmetry is described. The time series of the deviation-angle variances is well correlated to the time series of tropical cyclone best-track intensity. This parameter describes the development of tropical cyclone in terms of its organization. Interestingly, the signals obtained with that technique showed some frequency components that suggest the presence of organized structures even when the storms are in very early stages of development. However, locating the center of a storm is a difficult task, particularly at early stage of its lifecycle. One potential solution to this problem is to extend the deviation-angle variance technique in order to detect the genesis of a tropical cyclone without an initial center calculation.

Each image is processed as described in Chapter 3 to calculate the gradient of brightness temperature. Then, using every pixel in the image sequentially as a central reference point, the deviation angle from a perfect radial for each gradient vector

extending from that central point for a radius of 70 pixels is calculated and a histogram of deviation angles is constructed similar to Chapter 3. The variance of the histogram of deviation angles is the signal that determines the axisymmetry of any particular cloud cluster in the image. The main difference from Chapter 3 is that instead of isolating every disturbance and individually locating a center point, then calculating the deviation angles and variance around that point, the deviation angles and variance are now calculated for every pixel in the entire scene. In addition, every pixel is included in the analysis. Disregarding pixels with low brightness temperature values may produce low deviation-angle variances particularly in warm (dark) regions in the scene, which are generated by low number of gradient vector samples when calculating the variance instead of indicating axisymmetric structures. The output is a frame or map of deviation-angle variances, in which low values of variance indicate that the clouds exhibit high levels of axisymmetry in the neighborhood of that pixel, as generally observed in vortices. Conversely, high levels of deviation-angle variance indicate low levels of axisymmetry or “organization”, typically found in regular cloud clusters.

Consider the ideal synthetic vortex shown in Figure 5.1a. The process to build the map of variances is shown in Figure 5.1b. The corresponding deviation map of variances in Figure 5.1c pinpoints both the location of, and highly axisymmetric behavior of the vortex with zero deviation-angle variance at the very center of the vortex. For pixels away from the center of the ideal vortex, the deviation angle calculation results in higher levels of variance.

Figure 5.2a shows the calculation of the map of variances for a real case, a disorganized cloud cluster at the very early stage of Hurricane Wilma sequence (2005). The minimum value in the map of variances in Figure 5.2b is 2173, at this time this cloud system was not tracked by the National Hurricane Center. Figure 5.3a shows a more developed stage of Hurricane Wilma with an approximate intensity of 25 kt (1004 hPa), in which an initial vortex structure is evident. The minimum value in the map of variances in Figure 5.3b is 1648. Wilma reached tropical storm intensity approximately 40 hours later. Figure 5.4 shows the minimal tropical-storm strength Wilma, which had an approximate intensity of 35 kt (1000 hPa). The minimum value in the map of variances in Figure 5.4b is 1616. Following the expected increment in axisymmetry as the storm develops, the minimum value in the map of variances for a mature stage of Hurricane Wilma (130-kt, 924hPa) is 1189 (Figure 5.5), and the location of that variance value corresponds to the eye of Wilma.

The map of deviation-angle variances is calculated for all 9200 images from the 2004-2005 Atlantic hurricane seasons. A threshold variance value is set that determines whether a cloud has reached a level of symmetry to be considered a vortex. All pixels in the image are checked for threshold values and the first time that pixels in a disturbance reach this threshold value is considered the detection time. This process is repeated for every image and all detected systems are recorded and checked against: 1) the NHC best-track database; and 2) QuikSCAT imagery, which is a satellite-based ocean surface winds product produced by measuring the backscatter from the ocean, for verification.

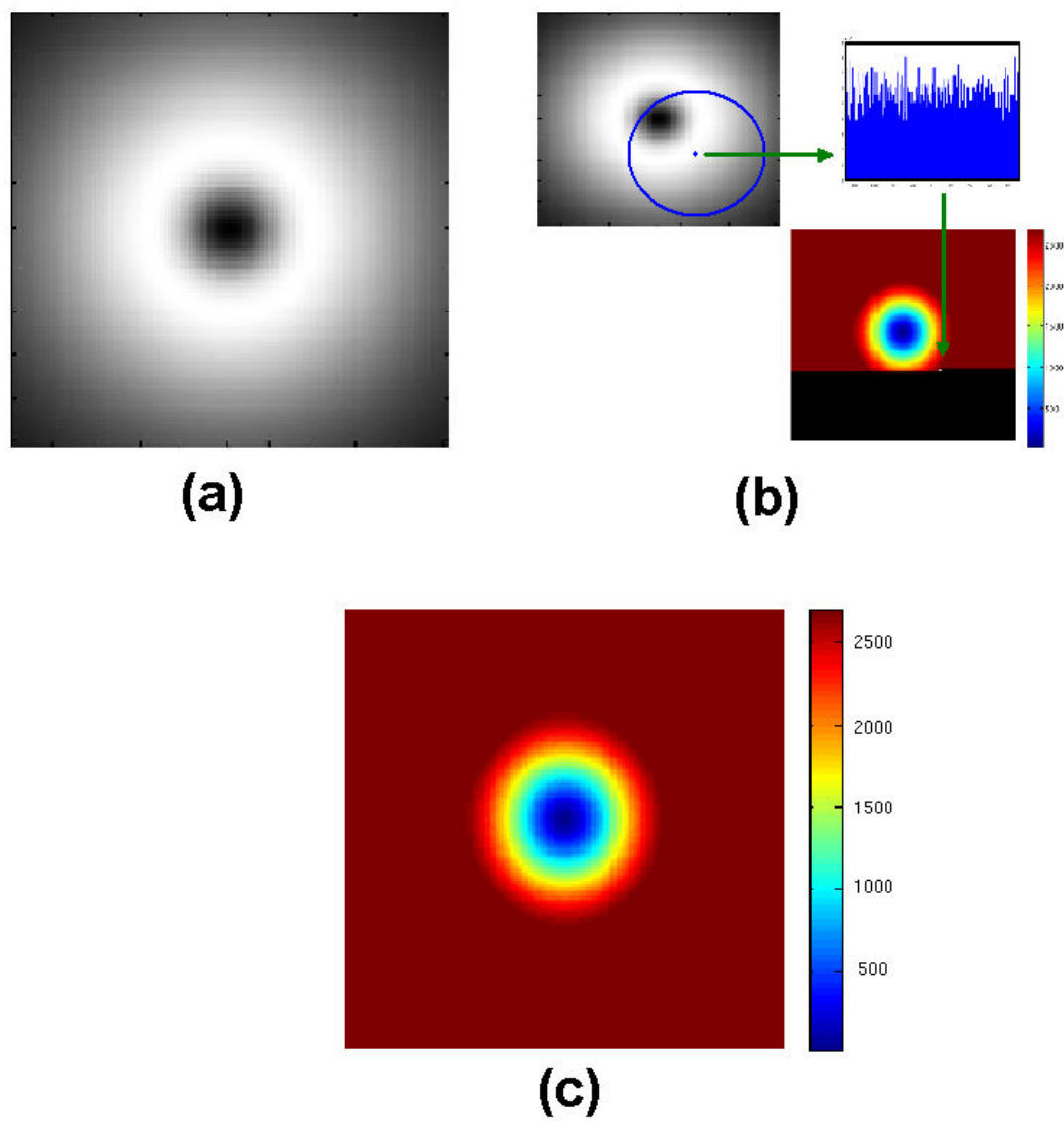


Figure 5.1. a) Synthetic brightness temperature image of an ideal vortex; b) example of the map of variances calculation; and c) Map of deviation angle variances [deg^2].

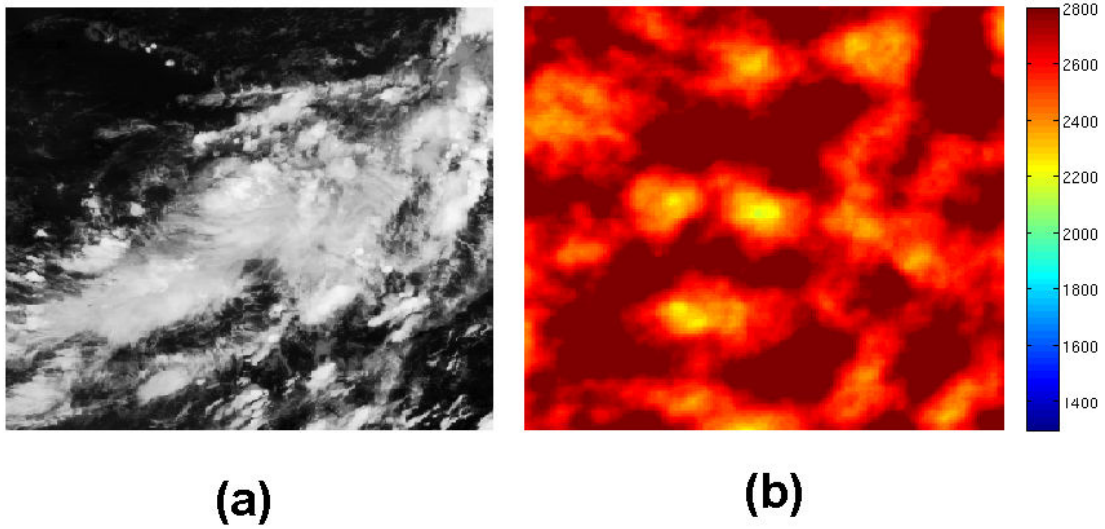


Figure 5.2. Images of Hurricane Wilma at 15 UTC 13 October 2005: a) Infrared image. Current best-track intensity is not reported at this stage by the NHC; and b) the corresponding map of deviation-angle variances [deg^2]. The minimum value in the map of variances is 2173.

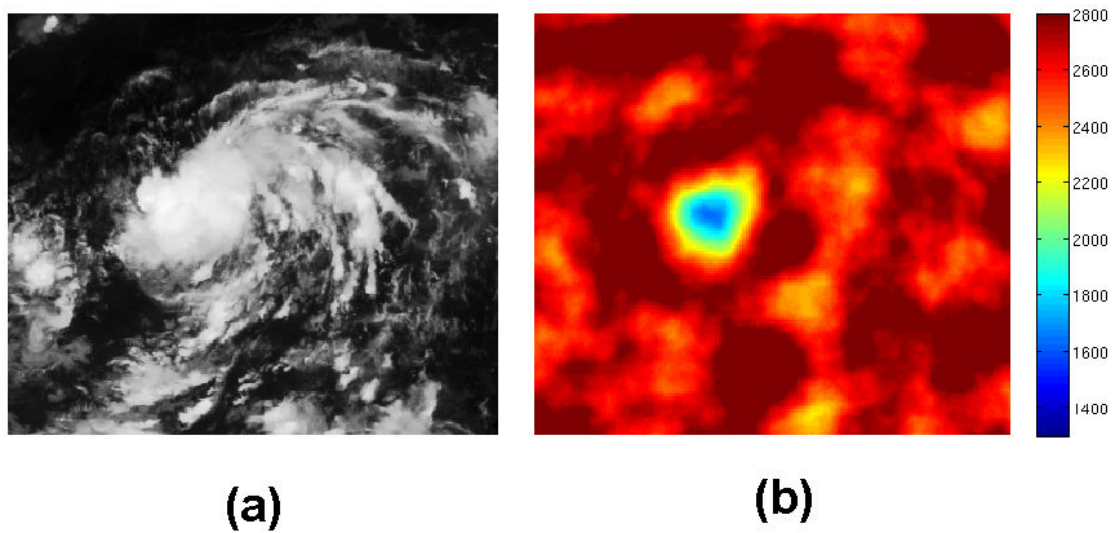


Figure 5.3. Images of Hurricane Wilma at 1345 UTC 15 October 2005: a) Infrared image. Current estimated intensity is 25 kts and 1004 hPa; and b) the corresponding map of deviation-angle variances [deg^2]. The minimum value in the map of variances is 1648.

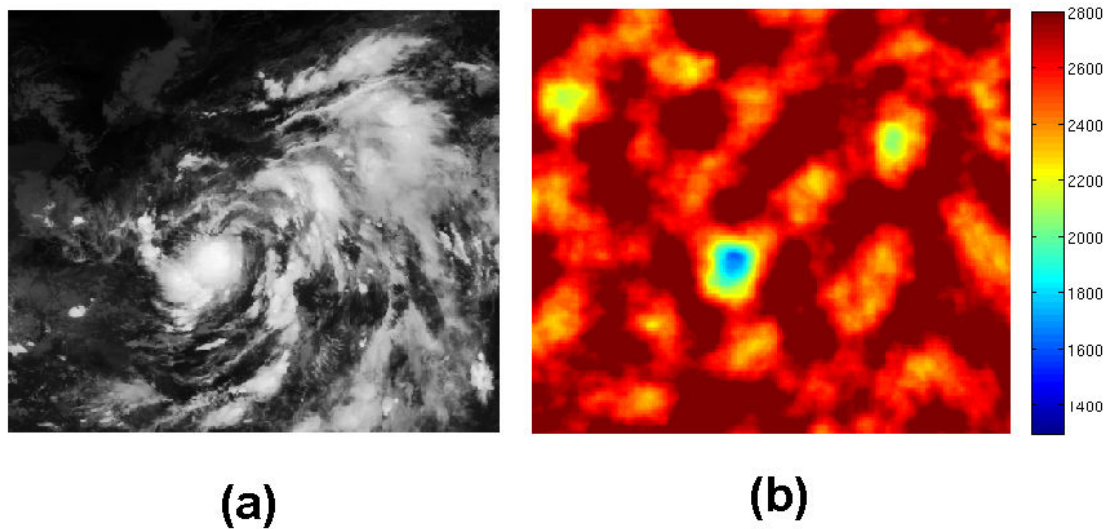


Figure 5.4. Images of Hurricane Wilma at 0615 UTC 17 October 2005: a) Infrared image. Current best-track intensity is 35 kt and 1000 hPa; and b) the corresponding map of deviation-angle variances [deg^2]. The minimum value in the map of variances is 1616.

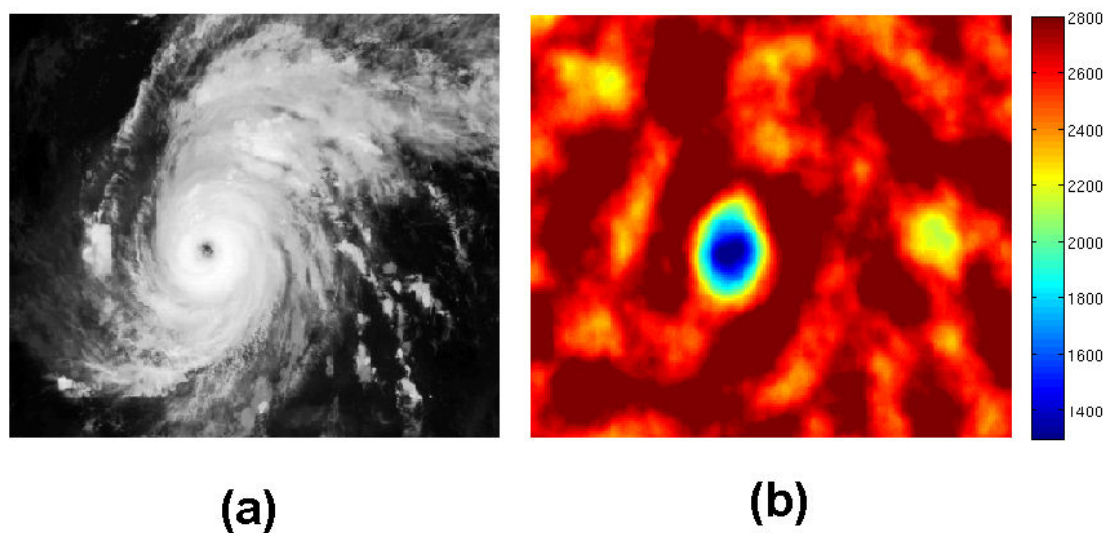


Figure 5.5. Images of Hurricane Wilma at 0015 UTC 21 October 2005: a) Infrared image. Current best-track intensity is 130 kt and 924 hPa; and b) the corresponding map of deviation-angle variances [deg^2]. The minimum value in the map of variances is 1189.

The performance of this technique was measured by applying threshold variance values of axisymmetry from 1350 to 2000 (in steps of 50) in the vortex detection process. Note that for this range of variances, Wilma in Figure 5.3 would have already been detected as a developing tropical cyclone. These results were contrasted to the NHC best-track files to obtain the number of true detections (true positives), the time duration from the first vortex detection to the time when the atmospheric system reached the tropical storm stage (33-kt), and the number of detections of non-developing cloud clusters (false alarms). Necessary climatological conditions for formation of a tropical cyclone are described in [1] and include a requirement for a non-zero amount of Earth vorticity or Coriolis to exist. For this reason all cloud clusters equator-ward of 5 degrees latitude were removed from the analysis. In addition, all cloud clusters over land and cloud clusters with low average brightness temperatures were also removed from the analysis. The final results are summarized in a receiver operating characteristic (ROC) curve in Figure 5.6 and Table 5.1. In addition, a plot of the mean detection time versus threshold value is shown in Figure 5.7.

From Figure 5.6 it can be determined that a high value of the detection threshold is a poor criterion to discriminate an axisymmetric structure from a disorganized cloud. When the highest threshold value of 2000 was applied all cloud clusters met the genesis criteria. This is because a threshold level of 2000 indicates a very disorganized system, and this threshold often fails to discriminate those systems that truly go on to develop into tropical cyclones. Conversely, when the lowest threshold value of 1350 was applied, only five of the tropical cyclones (11.4%) were detected 14 h after they reached tropical cyclone

storm intensity (Figure 5.7). The best performance in terms of the detection time, false positive rate and true positive rate is obtained with the threshold value of 1700, a total of 38 of the tropical cyclones (86%) were successfully detected an average 27 h before they reached tropical storm intensity. These cases are summarized in Appendix A.

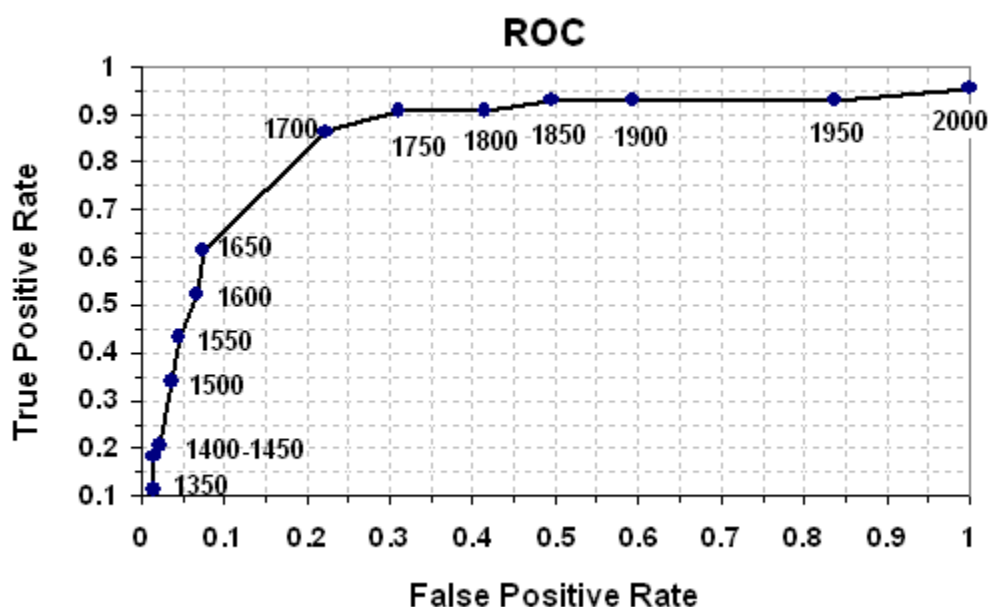


Figure 5.6. Receiver operating characteristics (ROC) curve for storm detections in all IR images during 2004 and 2005 for various deviation-angle variance threshold values.

The best cases corresponded to Hurricane Cindy (2005) and Tropical Storm Gamma (2005), which were detected approximately 100 h before developing into tropical storms. These cases evolved from cloud clusters that lasted around four days. In contrast, the worst case was Hurricane Charlie (2004), characterized by a small area of associated deep convection at early stages. This system was identified as a vortex almost 19 h after

reaching 33-kt, due to its insufficient level of axisymmetry when evolving. Furthermore, four tropical storms Hermine and Nicole (2004), Bret and Zeta (2005), the subtropical depression twenty-two that reached an intensity of 35 kt, and Hurricane Lisa (2004), were not detected at all due to their high degree of disorganization and small area of associated deep convection during their lifecycle. From these six cases, subtropical depression twenty-two, tropical storms Hermine and Nicole occurred close to 30° N latitude where the Coriolis effect makes more elongated the cloud structures, decreasing the axisymmetry.

| Variance threshold | True Positive Rate | False Positive Rate | Time Detection Average [h] | Time Detection Median [h] |
|--------------------|--------------------|---------------------|----------------------------|---------------------------|
| 1350 | 0.11 | 0.01 | 14.08 | 12.75 |
| 1400 | 0.18 | 0.01 | 10.39 | 12.75 |
| 1450 | 0.20 | 0.02 | 8.19 | 10.75 |
| 1500 | 0.34 | 0.04 | -1.04 | 3.75 |
| 1550 | 0.43 | 0.04 | -2.25 | 1.25 |
| 1600 | 0.52 | 0.07 | -11.21 | 0.75 |
| 1650 | 0.61 | 0.07 | -15.15 | -4.25 |
| 1700 | 0.86 | 0.22 | -27.02 | -13.25 |
| 1750 | 0.91 | 0.31 | -31.70 | -20.75 |
| 1800 | 0.91 | 0.41 | -37.17 | -30.75 |
| 1850 | 0.93 | 0.50 | -40.96 | -41.00 |
| 1900 | 0.93 | 0.59 | -47.18 | -45.00 |
| 1950 | 0.93 | 0.84 | -49.24 | -49.00 |
| 2000 | 0.95 | 1 | -53.57 | -51.75 |

Table 5.1. True Positive Rate (TPR), False Positive Rate (FPR), time detection average, time detection median, and deviation-angle variance threshold values. Number of positives cases: 44, number of negatives cases: 131.

Figure 5.8 shows an example of a case that was not detected. Tropical storm Hermine reached an intensity of 35 kt (1012 hPa). The minimum value in the map of variances in Figure 5.8b is 1794, which does not meet the threshold values of 1700 and 1750. Tropical storm Bret was a weak system that lasted approximately two days, but only one over the ocean before making landfall in Mexico. During this short time it did not show sufficient organization to be detected with this technique. Hurricane Lisa was a small system, characterized by several intensification and weakening periods, reaching 40 kt on September 20 at 12UTC. This small tropical cyclone did not develop enough axisymmetry to meet the variance threshold value of 1700. Figure 5.9a shows an image of Hurricane Lisa after reaching 40 kt (right) close to Hurricane Karl (left) at 110 kt. Note the small area of Lisa, in which the minimum value found in the map of variances is only 1751, whereas Karl at this developed stage has a minimum variance value of 1574 (Figure 5.9b). Tropical storm Zeta was an unusual case that occurred between December 30 of 2005 and January 6 of 2006. It was characterized by an elongated area of convection at early stages and disorganized spatial patterns, making it difficult to obtain low deviation-angles variances. Figure 5.10 shows an example of the disorganized pattern of Zeta at 35 kt, the minimum value in the map of variances is 2036.

Only 29 false alarms out of 131 non-developing cloud clusters (22%) occurred when using the threshold value (1700). Clearly, the threshold value of 1700 reaches good performance at discriminating developing from non-developing cloud clusters. In addition, 13 African easterly waves were detected as developing tropical cyclones that did not evolve into tropical cyclones. Although these atmospheric disturbances can have

winds higher than 35 kt and axisymmetric structures, they do not show a complete circulation. Figure 5.11a-b show an example of an African easterly wave that has enough level of axisymmetry to be detected in the map of variances with the threshold of 1700. Figure 5.11c shows the QuikSCAT image for this system. Note that the wind circulation pattern is not completely well defined. The rest of the false alarms are regular clouds that do not have any circulation associated but are detected by the technique because of their organized structure. Figure 5.12 shows an example of a regular cloud that detected by the technique without any circulation associated. False alarms found with the threshold value of 1700 are summarized in Appendix B.

In addition, three developing cloud clusters were detected that were not included in the NHC best-track database, but were confirmed using QuikSCAT imagery to have developed circulation with winds exceeding 30 kt for at least 12 hours (See Table 5.2). Figure 5.13a shows an example of an atmospheric disturbance that was not reported by the NHC, located between 45° to 40°W, and 15° and 20°N. Figure 5.13b shows the map of variances for this system, the minimum value is 1684 that is detected when using the variance threshold value (1700). Figure 5.13c shows the QuikSCAT image for this disturbance that makes evident the circulation pattern. Note that the wind barbs indicate wind speeds of at least 35 kt. Also note in the QuikSCAT imagery that a wind barb in black indicates that the return was attenuated by rain. Signal attenuation usually results in a wind speed vector that is lower than the actual wind speed. That is, a rain-flagged 30 kt observation may be 35 or 40 kt.

| Date (MM-DD-YY) /Time (UTC) | Latitude (°N) | Longitude (°W) |
|--------------------------------|---------------|----------------|
| 08-02-2005/0615 | 40 | 60 |
| 08-23-2005/0915 | 15 | 36 |
| 10-13-2005/0145 | 32 | 65 |

Table 5.2. Three developing cloud cluster that reached tropical storm intensity according to QuikSCAT data, detected by the map of variances technique but not recorded by the NHC.

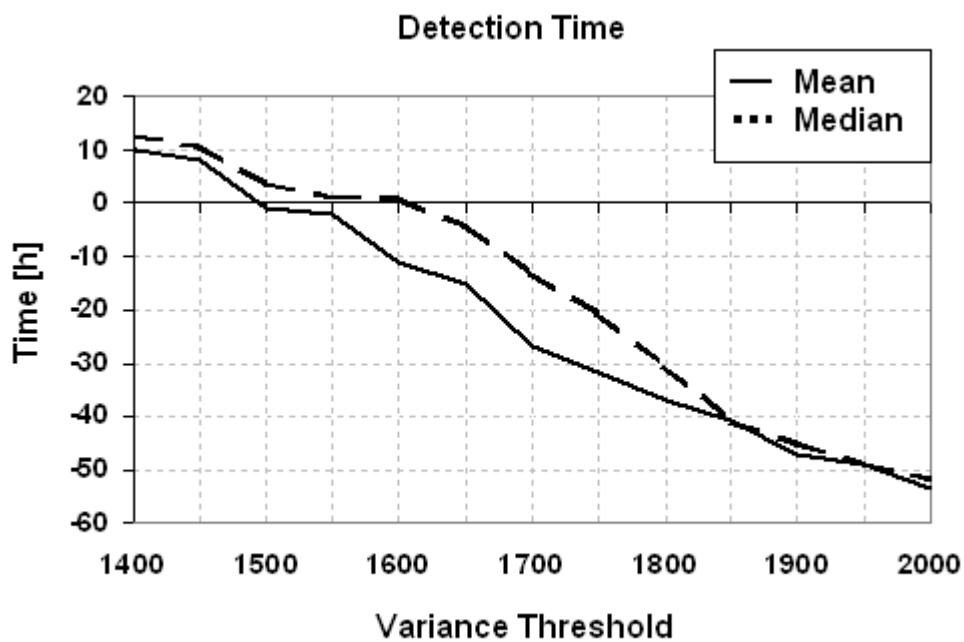


Figure 5.7. Mean and median time of detection of storms by the technique for various deviation-angle variance threshold values before being classified as Tropical Storms by NHC during 2004 and 2005.

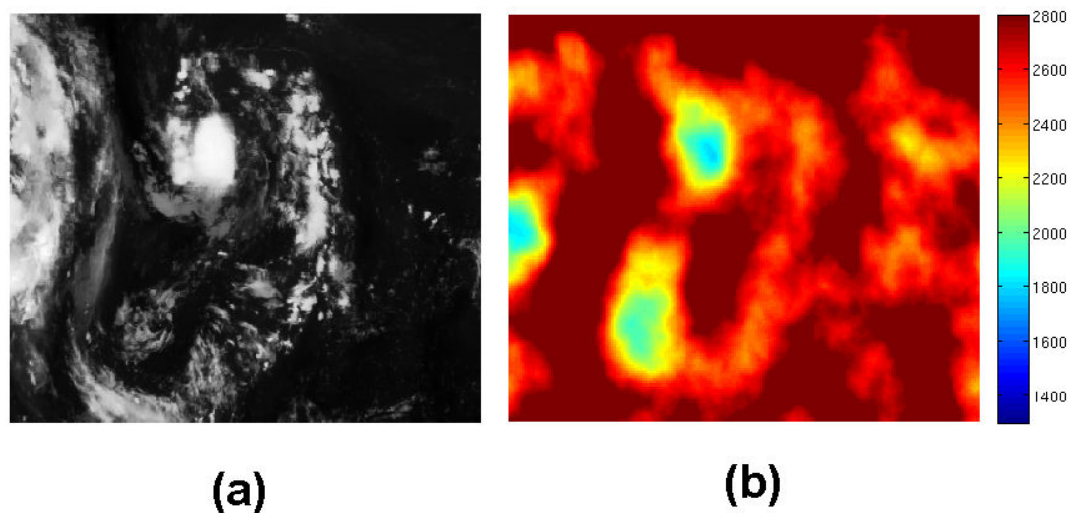


Figure 5.8. Images of Tropical Storm Hermine at 1215 UTC 29 August 2004: a) Infrared image. Current best-track intensity is 35 kt and 1012 hPa; and b) the corresponding map of deviation-angle variances [deg^2]. The minimum value in the map of variances is 1794.

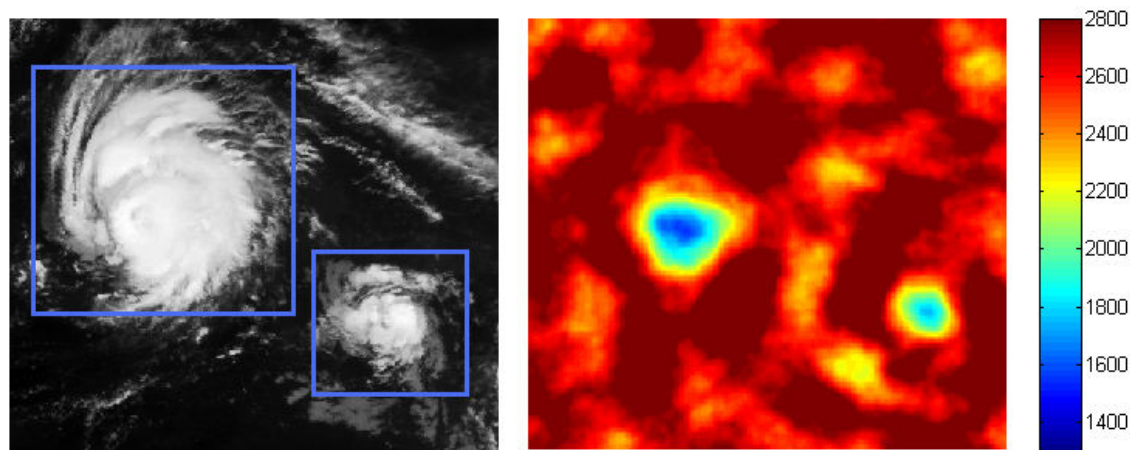


Figure 5.9. Images of Hurricanes Karl and Lisa at 1315 UTC 20 September 2004: a) Infrared image: Hurricane Lisa (right), current best-track intensity: 40 kt (1002 hPa), Hurricane Karl (left), current best-track intensity: 110 kt (951 hPa); and b) the corresponding map of deviation-angle variances [deg^2]. The minimum value in the map of variances is 1751 for Lisa, and 1574 for Karl.

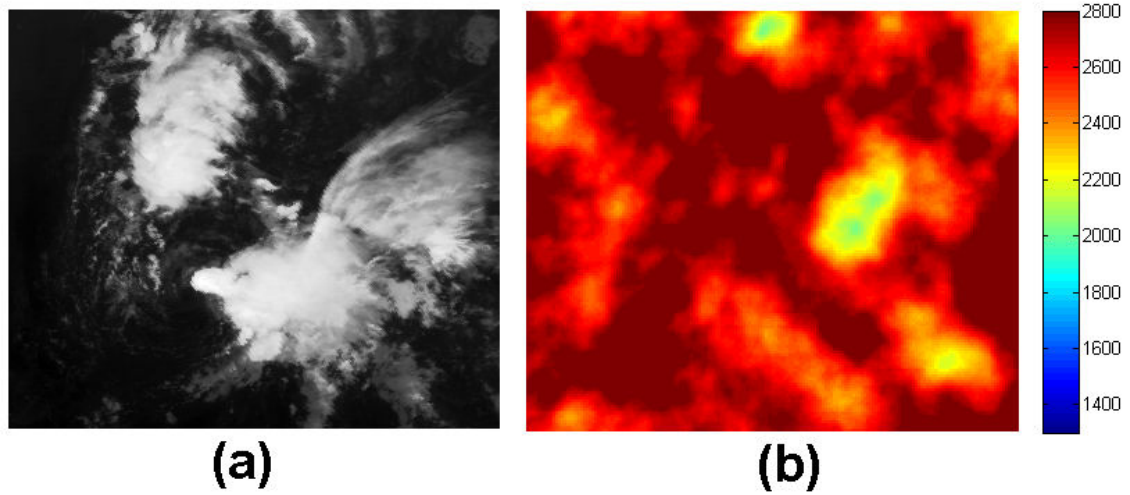


Figure 5.10. Images of tropical storm Zeta at 0615 UTC 6 January 2006: a) Infrared image. Current best-track intensity is 35 kt (1007 hPa); and b) the corresponding map of deviation-angle variances [deg²]. The minimum value in the map of variances is 2036.

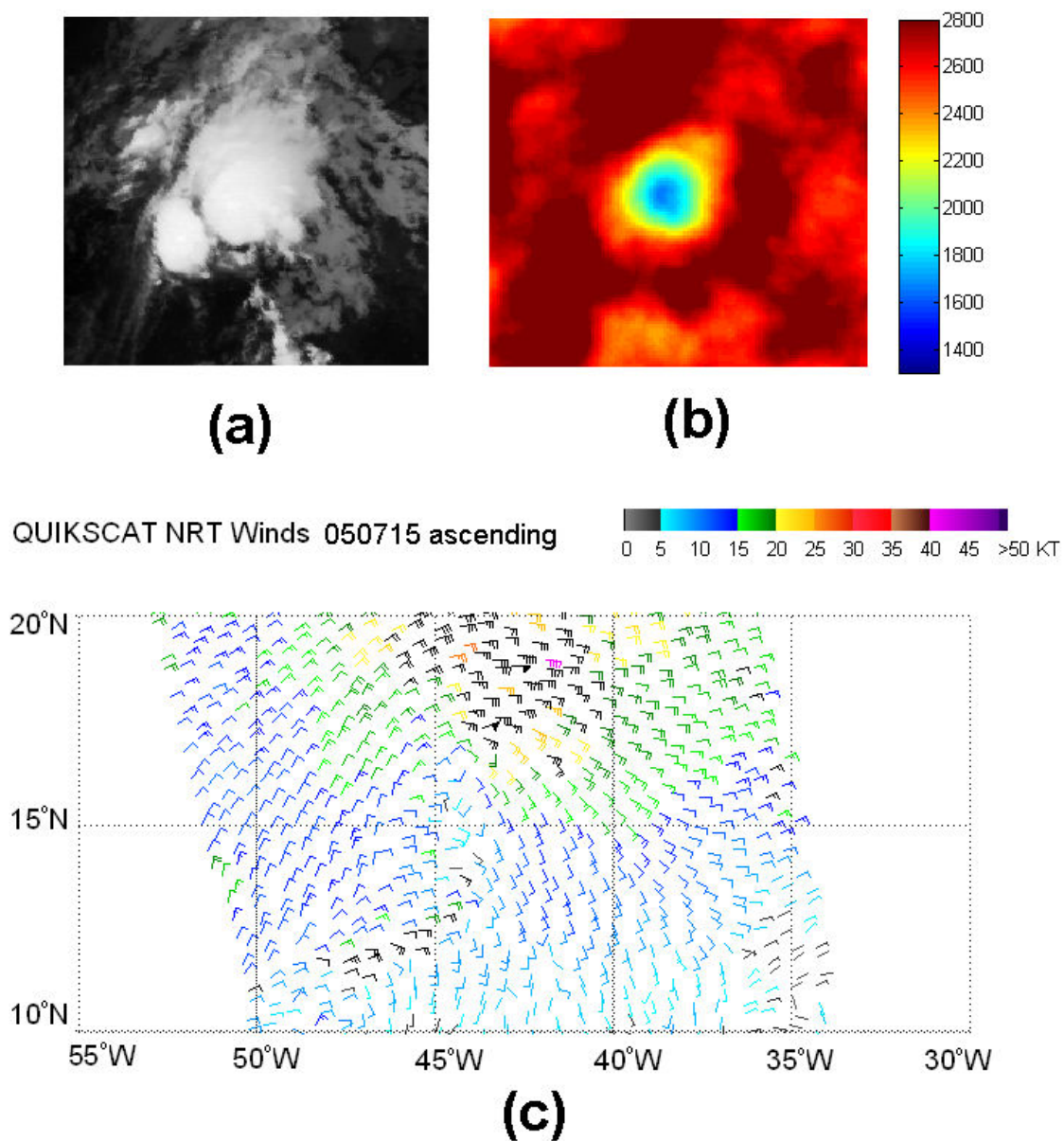


Figure 5.11. Images of an African Easterly Wave 0645 UTC 15 July 2005 that reached winds of at least 50 kt without a defined circulation pattern : a) Infrared image; and b) the corresponding map of deviation-angle variances [deg^2]. The minimum value in the map of variances is 1657; and c) QuikSCAT image from <http://manati.orbit.nesdis.noaa.gov/quikscat/>.

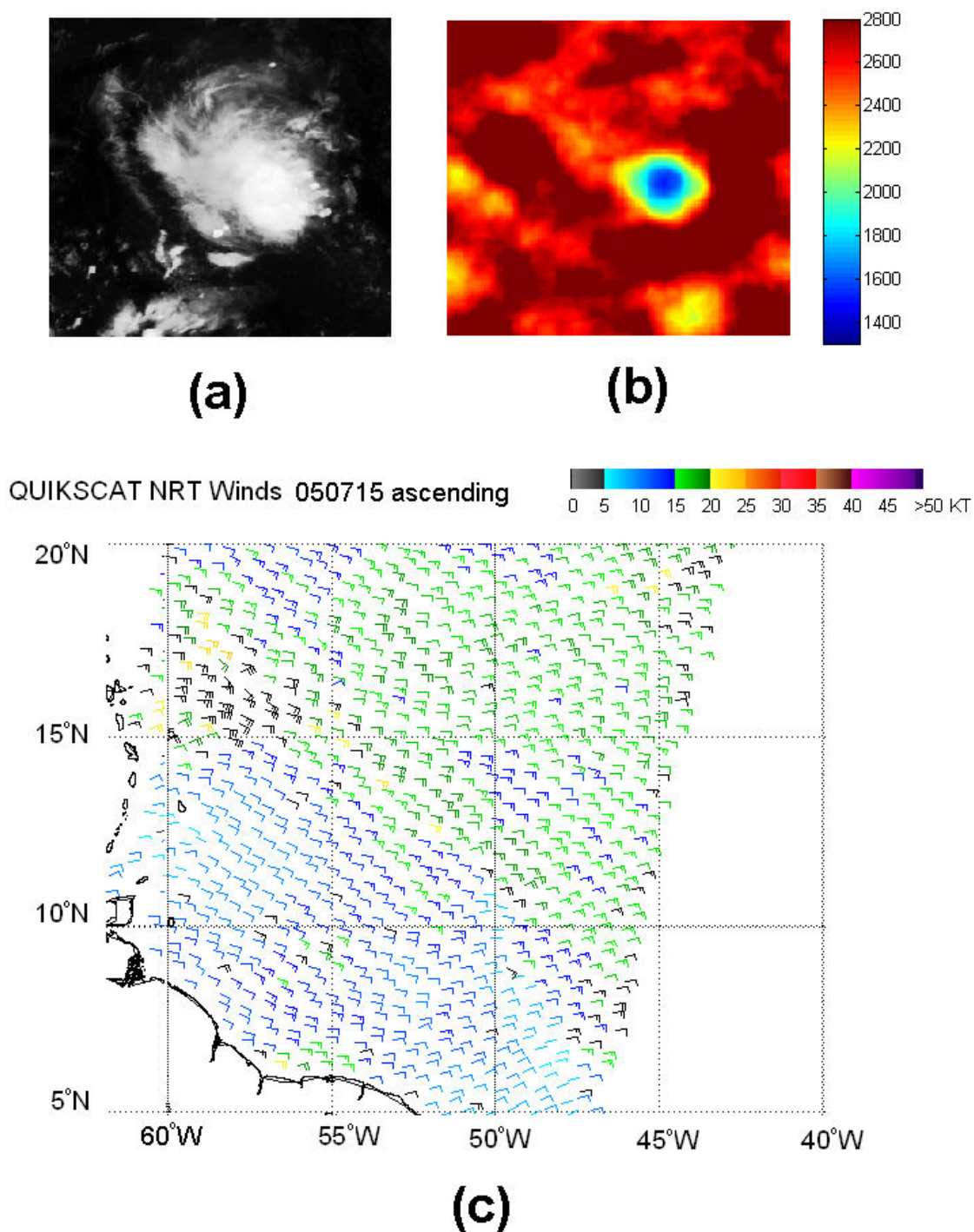


Figure 5.12. Images of a regular cloud at 2115 UTC 30 October 2005 that reached winds of at least 30 kt: a) Infrared image; and b) the corresponding map of deviation-angle variances [deg^2]. The minimum value in the map of variances is 1520; and c) QuikSCAT image from <http://manati.orbit.nesdis.noaa.gov/quikscat/>.

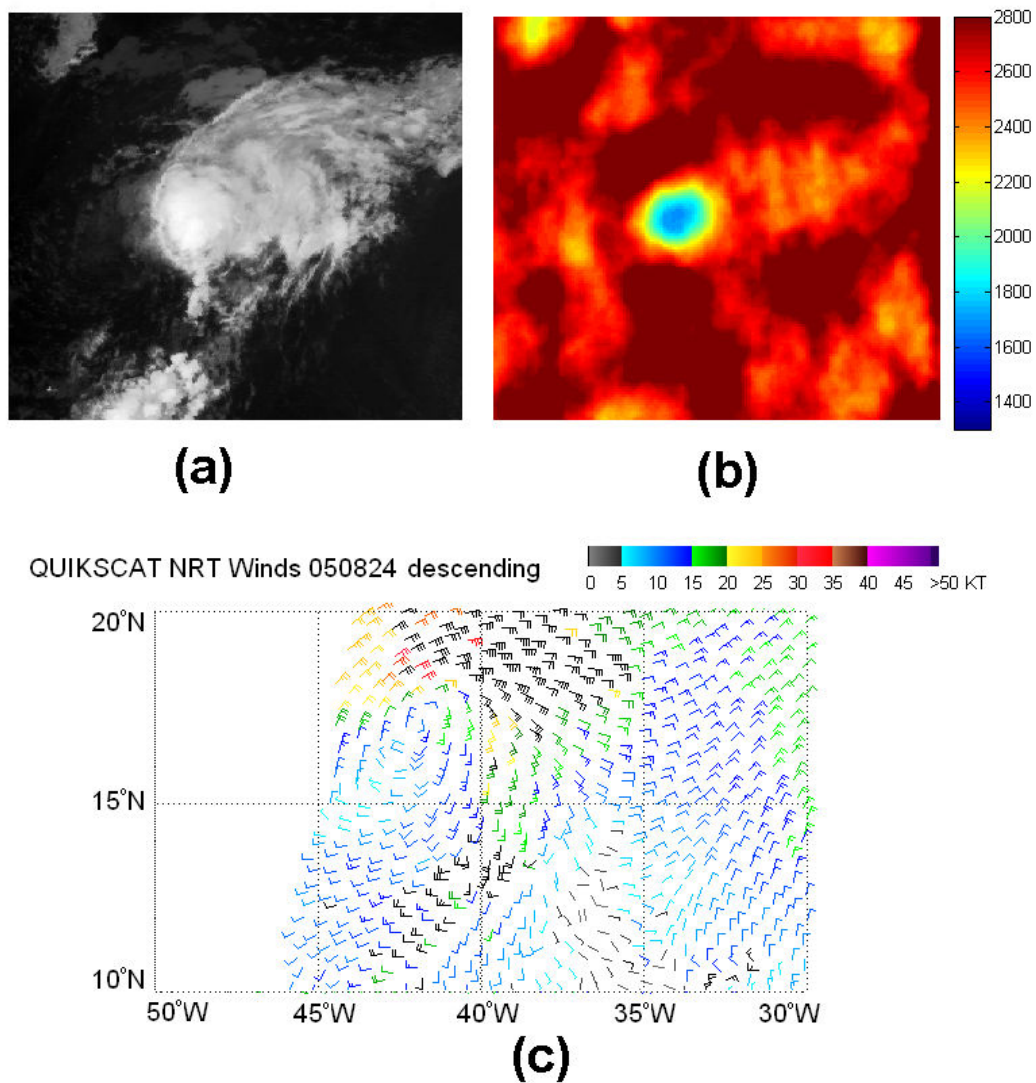


Figure 5.13. Images of an atmospheric disturbance at 2215 UTC 24 August 2005 that reached winds of at least 35 kt, but was not recorded by the NHC: a) Infrared image; and b) the corresponding map of deviation-angle variances [deg^2]. The minimum value in the map of variances is 1679; and c) QuikSCAT image from <http://manati.orbit.nesdis.noaa.gov/quikscat/>.

5.1 Summary

The technique described in Chapter 3 is extended in order to detect developing from non-developing cloud clusters. The deviation-angle variance is calculated using every pixel in the scene as the reference point, these results are stored in an auxiliary matrix called map of variances. Low values in the map pinpoint axisymmetric structures, which in turn, identify potential vortices embedded in cloud clusters. The early detection of axisymmetric structures is used to distinguish nascent tropical cyclones from non-developing system. The vortex detection procedure is adjusted by applying threshold variance values of axisymmetry to the map of variances, those cloud structures with deviation-angle variances below to a threshold are considered vortices. The results show that 86% of the tropical cyclones are detected on average 27 h before they reached tropical storm intensity, while 22% of non-developing systems are incorrectly classified as nascent tropical cyclones.

6 AUTOMATED TROPICAL-CYCLONE CENTER FINDING

The accuracy of forecasting techniques based on satellite imagery relies on the correct location of the tropical cyclone center, such as the original Dvorak technique and its objective versions. These techniques utilize features of cloud clusters in the images to estimate the center position. In the original Dvorak technique, the expert classifies the cloud clusters before locating the center, the features that define the center vary according to the type of cluster. When the cluster cannot be classified into several predefined categories, the expert extrapolates it from past locations. The Objective and the Advance Dvorak Techniques incorporate aircraft reconnaissance observations of the circulation center, and two additional procedures to find the best alignment of predefined curves into the image gradient field. However, the large variety of spatial patterns, particularly at early stages of a tropical cyclone's lifecycle, makes it difficult to define classes and features from cloud clusters. In addition, infrared and visible satellite imagery show the clouds from the top, hiding the lower layers that tend to show circulation patterns better. The actual center of a tropical cyclone typically is defined by the point of minimum surface winds or minimum sea-level atmospheric pressure. Unfortunately, this point may be difficult to locate in absence of direct measurements. The best-track records from the NHC uses all the available data from direct measurements and models to find the center trajectory after the tropical cyclone decays. For this reason, the best-track center record is used as the "truth" in spite of the fact that it is subjectively obtained.

The development of an automated algorithm to locate the center of a tropical has been a difficult problem for years, but it may enhance the accuracy of the real-time techniques employed by forecasting centers around the world.

In this chapter, the results of two new procedures to locate the center of circulation of a tropical cyclone are compared to the best-track center database. The first technique was described in section 3.4, and finds the center position of the disturbance by accumulating the projected lines parallel to each gradient vector of the image in a density matrix. High values in the density matrix indicate centers of cloud systems in the original infrared scene. Recall that warm (black) pixels are not included in the analysis because those gradient vectors in the warm surroundings of a cloud system can significantly influence the location of the center even though they are not part of the cloud cluster. The second technique was described in Chapter 5 and was developed to detect vortices at early stages of the lifecycle of a tropical cyclone. The technique creates a map of deviation-angle variances in which low values pinpoint axisymmetric structures. The location of the local minimum value is then used as the center of the cloud cluster. Because the variance map includes every pixel in the scene regardless of its intensity value, all cloud clusters in the image are automatically detected as minima, and the values of the minimum indicates the intensity of each cloud cluster.

The accumulator matrix and the map of variances techniques were compared with a subset of 645 images from 2004 and 2005, which correspond to the 6 h best-track database of the NHC. Recall that the spatial resolution of each image is 5 km/pixel and the best-track intensity estimate varies at increments of 5 kt.

Although the map of variances and the accumulator matrix technique produce good results for the majority of the cases, cloud systems characterized by complex, elongated or compound patterns can generate inaccurate center locations. Typically in these cases there is not a point of evident axisymmetry. Figure 6.1 and Figure 6.2 show examples of elongated and complex patterns. The centers calculated by the accumulator matrix (red star) and the map of variances (blue star) are consistently shifted away from the best-track center (black star). Two nearby cloud clusters, which both have associated vortices will merge with the western (left) system becoming dominant center (Figure 6.1).

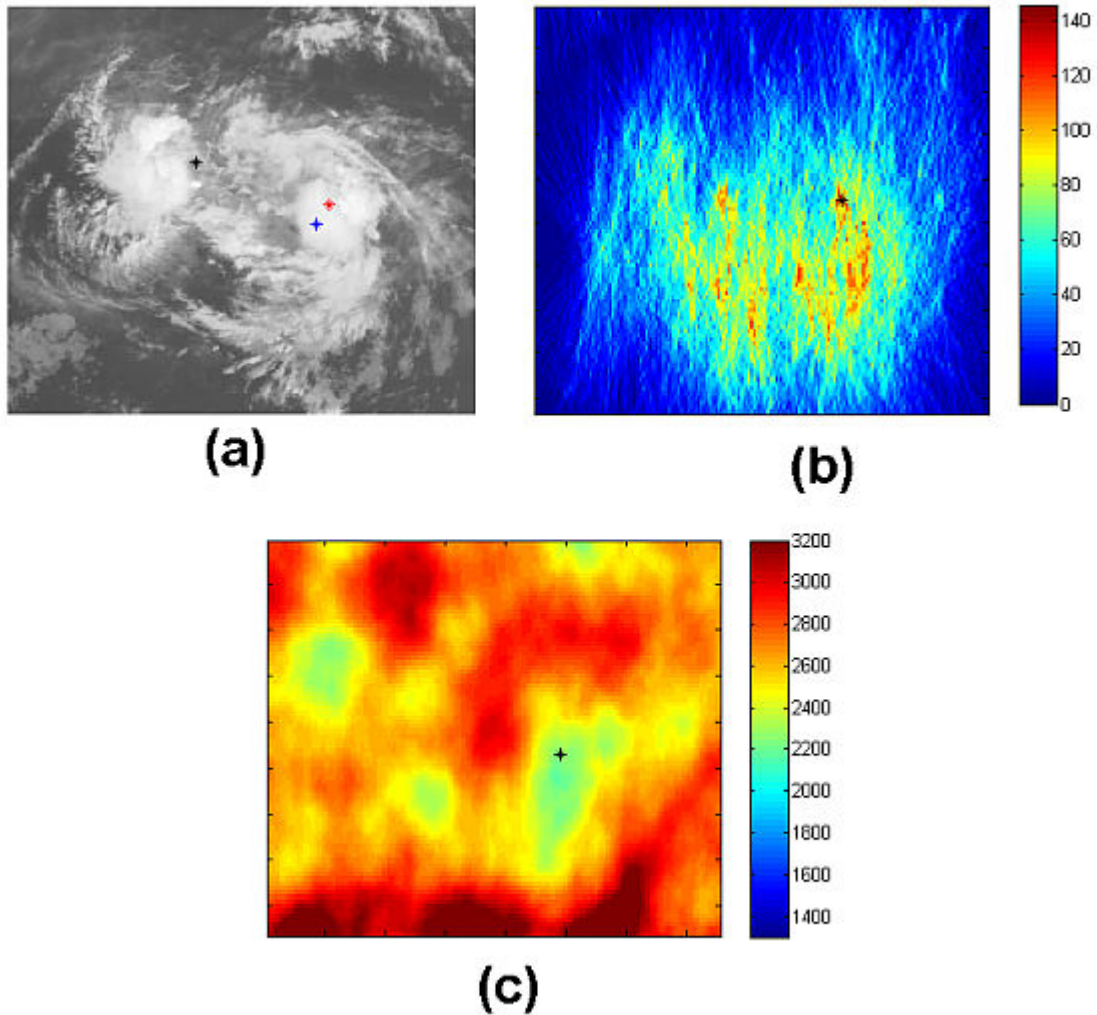


Figure 6.1. Image of Hurricane Lisa at 1200 UTC 22 September 2004. Intensity 45 kt, 1000 hPa. a) Infrared image, the black star corresponds to the best-track center position at 14.2°N , 41.1°W , the red star indicates the accumulator matrix center at 13.0°N , 36.5°W , and the blue star indicates the map of variances center at 12.3°N , 37.0°W ; b) Accumulator matrix, the location of the maximum value is indicated by the star; c) Map of variances, the location of the minimum value is indicated by the star.

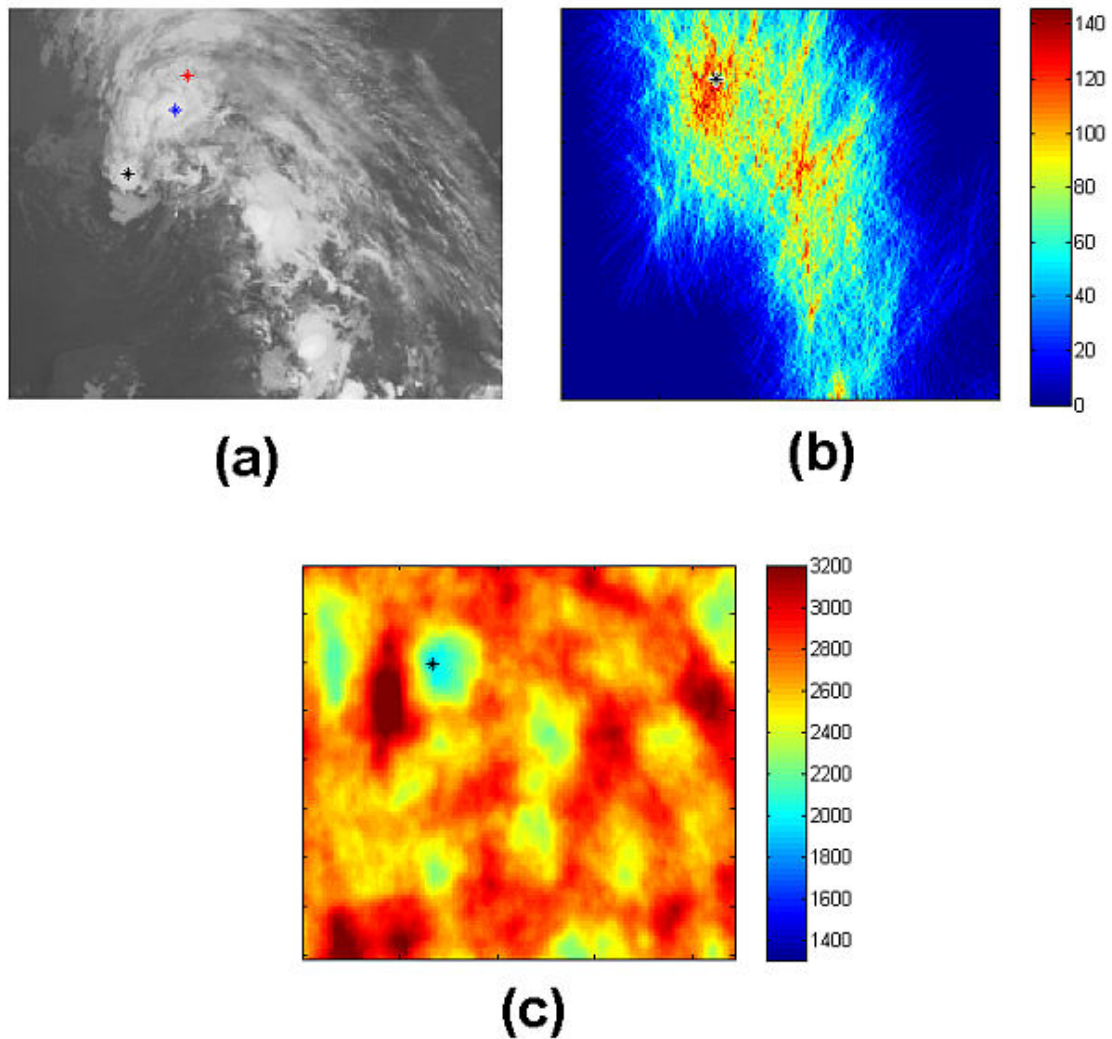


Figure 6.2. Image of Hurricane Arlene at 1600 UTC 11 June 2005. Intensity 60 kt, 993 hPa. a) Infrared image, the black star corresponds to the best-track center position at 27.7°N , 86.8°W , the Red star indicates the accumulator matrix center at 31.7°N , 84.7°W , and the blue star indicates the map of variances center at 30.5°N , 85.5°W ; b) Accumulator matrix, the location of the maximum value is indicated by the star; c) Map of variances, the location of the minimum value is indicated by the star.

Both techniques utilize the axisymmetry of a cloud system to locate its center, therefore those centers out of the cloud cluster or at the border of it, are not correctly

calculated. Figure 6.3 shows an example of an early stage of Hurricane Irene (2005), in which the best-track center is located out of the cloud cluster (black star). Note that the accumulator matrix (red star) and the variance map technique (blue star) track two different sections of the cloud cluster. There are many reasons why these asymmetric patterns that are so distorted the actual center of circulation is located on the edge of, or even outside the cloudy areas. Environmental circulation patterns that include strong vertical wind shear will tend to advect the clouds away from the circulation center (Figure 6.2 and Figure 6.3) [34]. Figure 6.4 shows an image of tropical storm Franklin (2005), in this example the centers calculated are within cloud system but the best-track center is located at the edge of it. Again because environmental vertical wind shear has shifted the convection to the edge of the circulation.

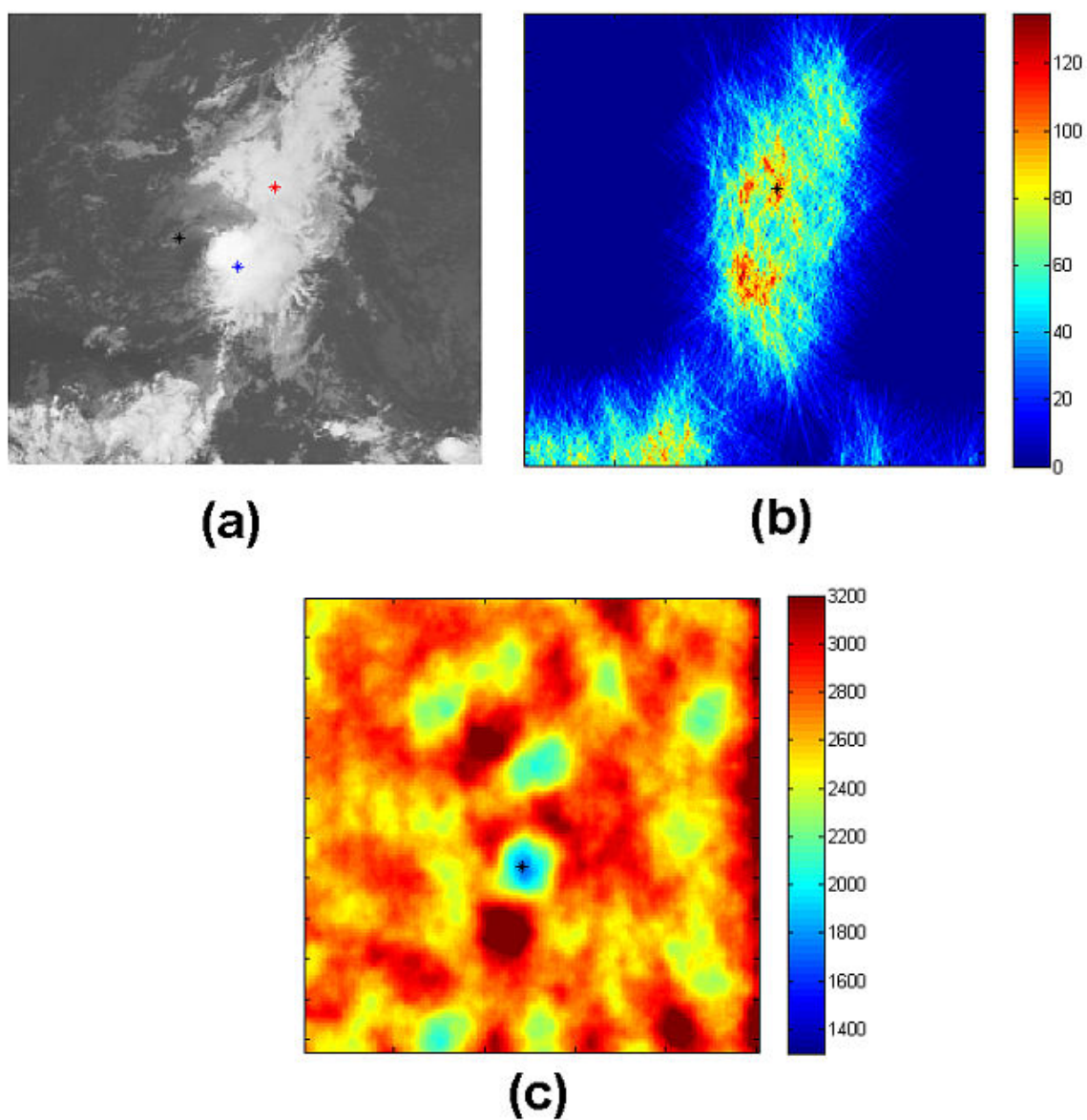


Figure 6.3. Image of Hurricane Irene at 1800 UTC 06 August 2005. Intensity 30 kt, 1008 hPa. a) Infrared image, the black star corresponds to the best-track center position at 18.8°N , 42.8°W , the red star indicates the accumulator matrix center at 21.5°N , 38.5°W , the blue star indicates the map of variances center at 17.8°N , 40°W ; b) Accumulator matrix, the location of the maximum value is indicated by the star; c) Map of variances, the location of the minimum value is indicated by the star.

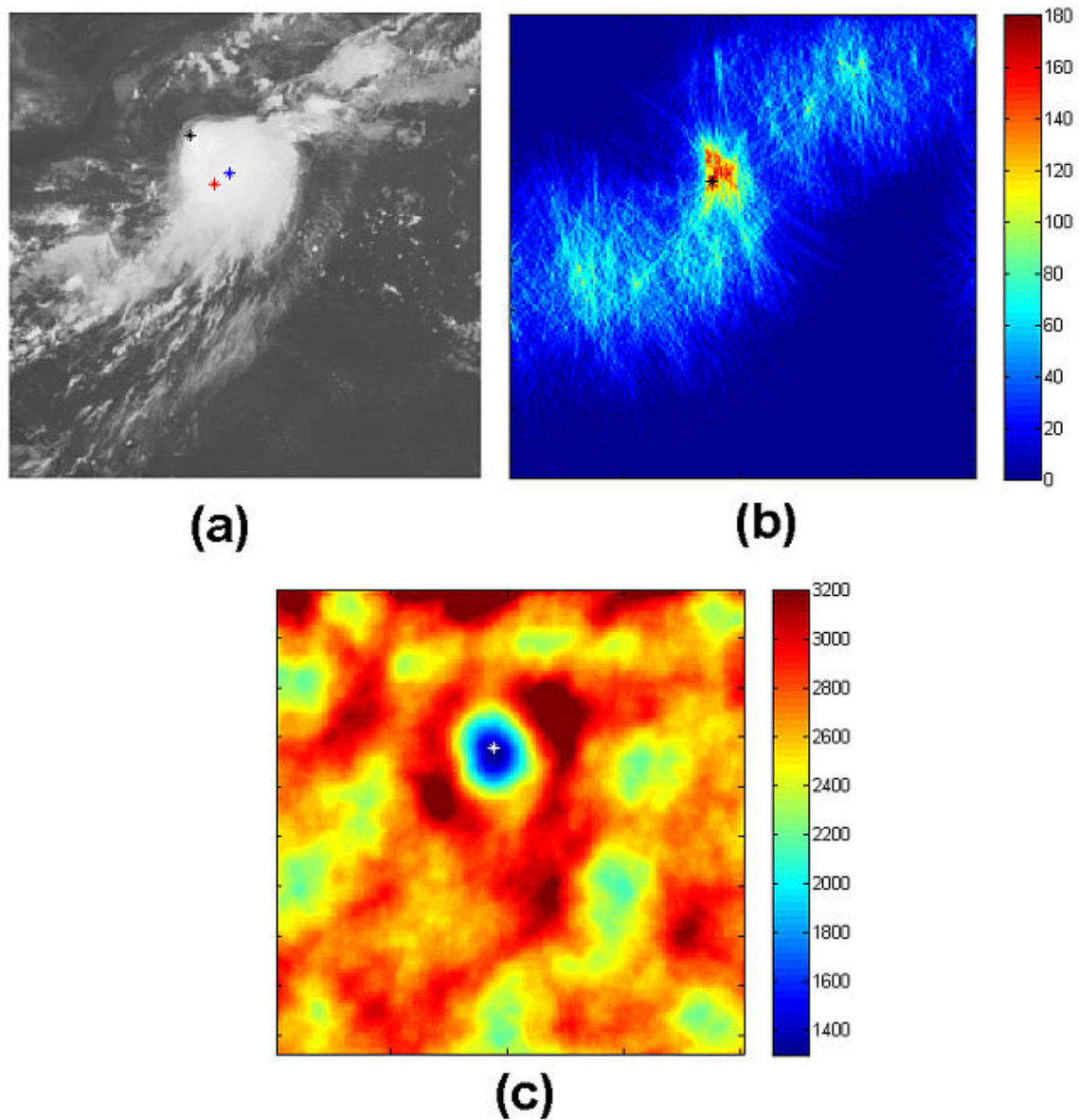


Figure 6.4. Image of Tropical Storm Franklin at 1800 UTC 24 July 2005. Intensity 45 kt, 1000 hPa. a) Infrared image, the black star corresponds to the best-track center position at 31.1°N , 71.2°W , the red star indicates the accumulator matrix center at 29.6°N , 70.3°W , and the blue star indicates the map of variances center at 30.1°N , 70°W ; b) Accumulator matrix, the location of the maximum value is indicated by the star; c) Map of variances, the location of the minimum value is indicated by the star.

For intense tropical cyclones, the error is reduced to less than 90 kilometers, typically the center is within the eye as shown in Figure 6.5. Recall that the diameter of the eye is typically between 30 and 60 km. However, centers calculated for hurricanes characterized by small convective areas and large tails can be shifted out of the eye. This is because those gradient vectors in the tail of the hurricane, which is within the radius of analysis (350 km) from the eye, can impact the calculation of the axisymmetry at the inner ring of the hurricane. One potential method to improve this difficulty is to utilize a near infrared channel as well as the 11 μ m channel employed in this study. The difference between the 11 μ m and the 3 μ m channels can potentially highlight low-level clouds, which are better indicators of the near-surface circulation in a tropical cyclone than high clouds. However, the methodology for doing this is beyond the scope of the work.

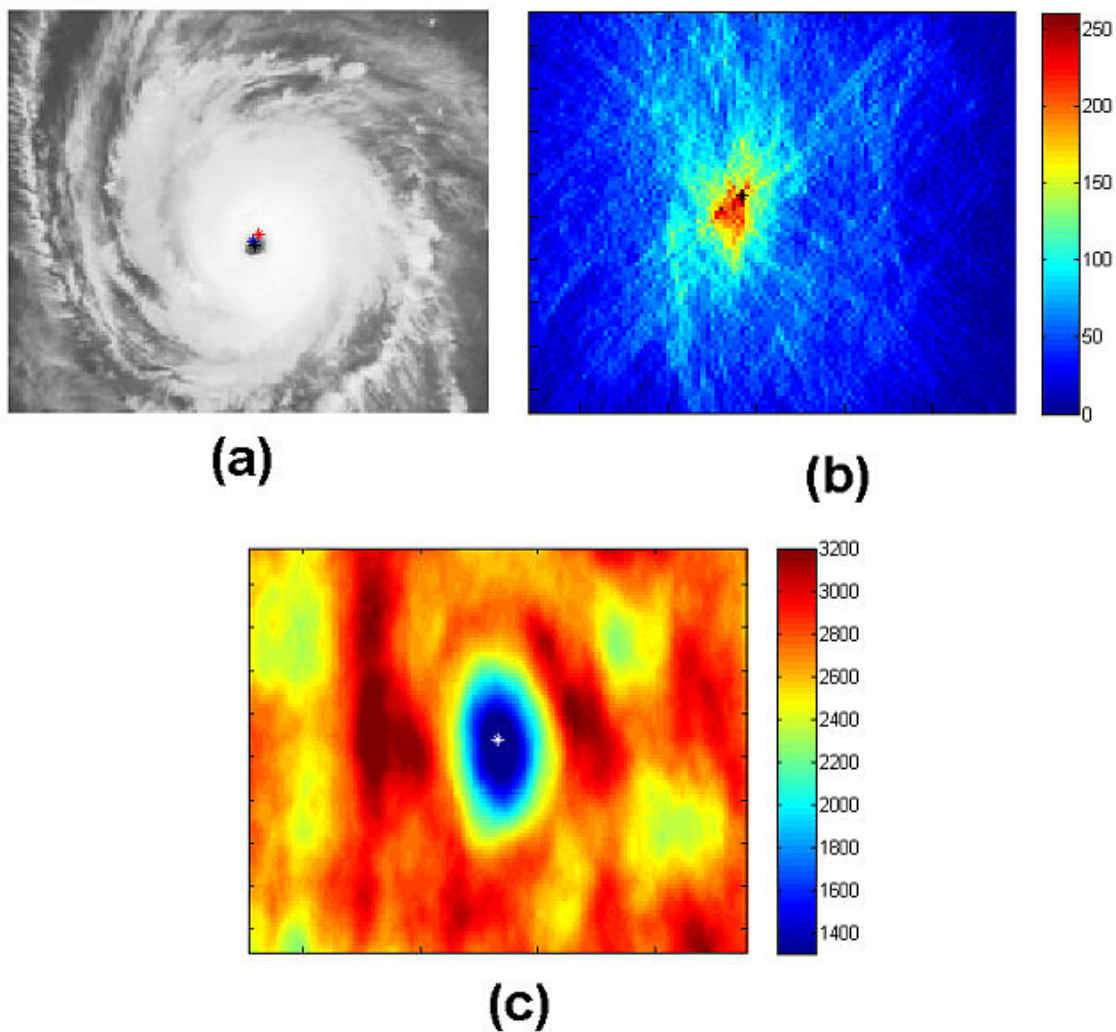


Figure 6.5. Image of Hurricane Frances at 0000 UTC 01 September 2004. Intensity 120 kt, 941 hPa. a) Infrared image, the black star corresponds to the best-track center position at 20.6°N , 66.4°W , the red star indicates the accumulator matrix center at 20.9°N , 66.3°W , and the blue star indicates the map of variances center at 20.8°N , 66.5°W ; b) Accumulator matrix, the location of the maximum value is indicated by the star; c) Map of variances, the location of the minimum value is indicated by the star.

The results of applying both techniques are summarized in Figure 6.6 and Table 6.1. The technique based on the map of variances is slightly more accurate than the accumulator matrix. The RMS distance error for the whole subset of samples is 49 pixels (245 km) and 55 pixels (275 km) respectively. The average distance error is 35 pixels (175 km) for the map of variances and 40 pixels (200 km) for the accumulator matrix technique. Note that the accuracy of both techniques increase as tropical cyclones intensify because of the increasing axisymmetry of the cloud system. Figure 6.7 shows an example of the center positions calculated with both techniques for Hurricane Rita (2005), Table 6.2 summarized these results. Note the large differences between the curves at the initial part of the trajectory when Rita had low intensity. The primary reason why the errors are high at early stages of the lifecycle of a tropical cyclone is that both techniques are designed to locate organized cloud structures around a point, but at early stages not only are the clouds highly asymmetric, but also the circulation is not strong enough to organize the clouds around it. In contrast, the best-track center of circulation indicates the location of minimum winds or minimum atmospheric pressure.

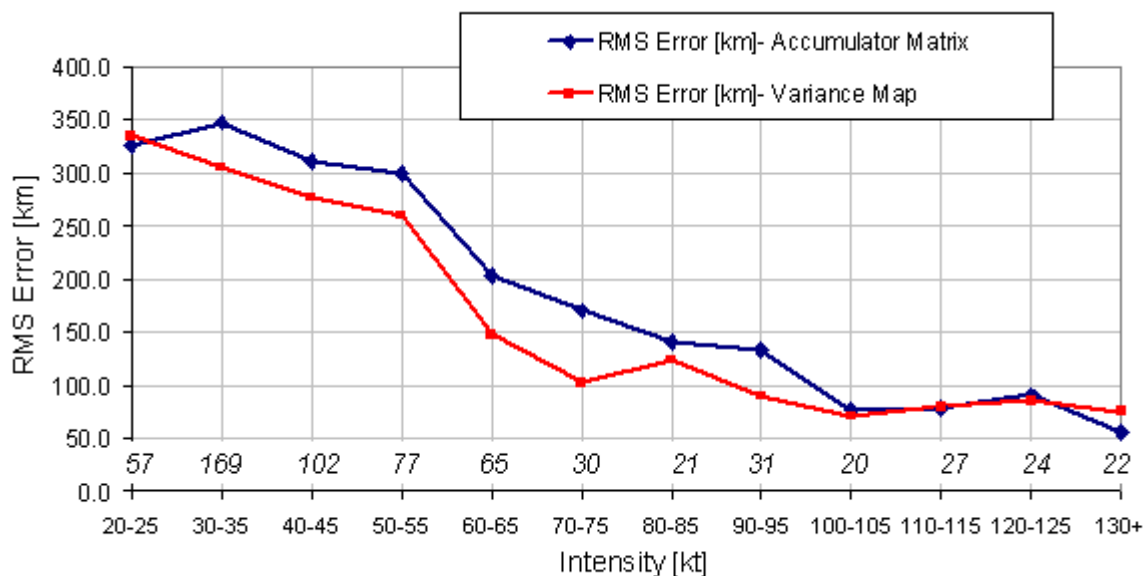


Figure 6.6. RMS distance error [km] vs intensity [kt] results of applying the accumulator matrix and the variance map techniques to locate the center of a tropical cyclone, the results are contrasted to the NHC best-track center database. The number of samples is indicated in italics.

6.1 Summary

Two objective techniques to locate the center of a tropical cyclone were compared to the NHC best-track center database: the accumulator matrix (section 3.4) and the map of variances (Chapter 5). These techniques are based on the axisymmetry of cloud structures, which is related to the intensity of the tropical cyclone. The accuracy of both techniques increase as the tropical cyclone intensifies because of the increasing axisymmetry. At early stages, cloud structures are not characterized by common patterns, in these cases the point of the highest axisymmetry does not necessarily coincide with the

best-track center estimates. Results are shown that the accuracy of the map of variances is slightly higher than the accumulator matrix technique. The average RMS distance error is 49 (245 km) and 55 pixels (275 km) for the map of variances and the accumulator matrix technique respectively.

| Intensity [kt] | Accumulator Matrix | | Map of Variances | | No. Samples |
|----------------|-----------------------------|-------------------------|-----------------------------|-------------------------|-------------|
| | RMS Distance Error [Pixels] | RMS Distance Error [km] | RMS Distance Error [Pixels] | RMS Distance Error [km] | |
| 20-25 | 65.2 | 326.1 | 66.9 | 334.7 | 57 |
| 30-35 | 69.6 | 347.9 | 61.0 | 304.9 | 169 |
| 40-45 | 62.2 | 310.9 | 55.4 | 277.2 | 102 |
| 50-55 | 59.9 | 299.6 | 51.8 | 259.1 | 77 |
| 60-65 | 40.6 | 202.9 | 29.6 | 148.2 | 65 |
| 70-75 | 33.9 | 169.5 | 20.5 | 102.5 | 30 |
| 80-85 | 28.2 | 141.0 | 24.7 | 123.5 | 21 |
| 90-95 | 26.7 | 133.3 | 17.9 | 89.3 | 31 |
| 100-105 | 15.3 | 76.3 | 14.1 | 70.5 | 20 |
| 110-115 | 15.7 | 78.4 | 15.9 | 79.6 | 27 |
| 120-125 | 18.1 | 90.4 | 17.1 | 85.6 | 24 |
| >130 | 11.2 | 56.0 | 15.1 | 75.5 | 22 |
| Total | 55 | 275 | 49 | 245 | 645 |

Table 6.1. RMS distance error vs intensity results of applying the accumulator matrix and the variance map techniques to locate the center of a tropical cyclone, the results are contrasted to the NHC best-track center database.

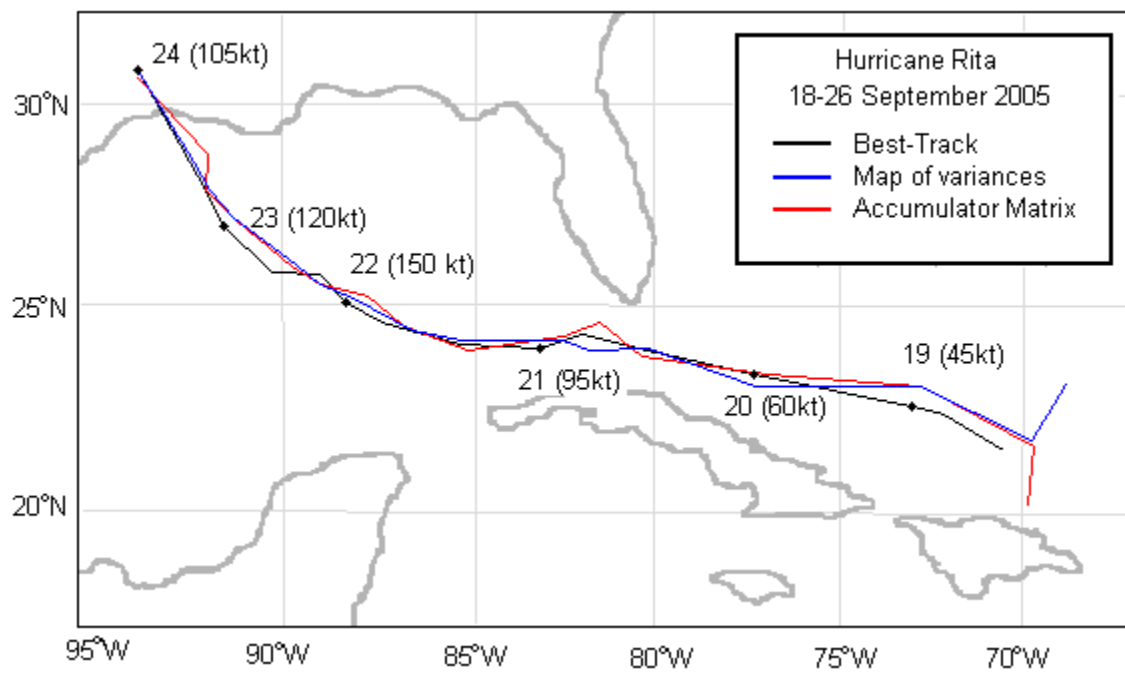


Figure 6.7. Trajectory of Hurricane Rita, 18-26 September 2005.

| Date-Time UTC | Intensity [kt] | Best-Track | | Accumulator Matrix | | Error [km] | Map of Variances | | Error [km] |
|------------------|-------------------|-------------|-------------|-----------------------|-------------|---------------|---------------------|-------------|---------------|
| | | Lat [°N] | Lon [°W] | Lat [°N] | Lon [°W] | | Lat [°N] | Lon [°W] | |
| 18-0000 | 25 | 21.3 | 69.9 | 20.3 | 70 | 111.2 | 23.3 | 69.9 | 221.4 |
| 18-1200 | 30 | 21.9 | 71.5 | 21.7 | 69.7 | 189.6 | 21.9 | 69.8 | 177.8 |
| 19-0000 | 45 | 22.4 | 73 | 23.1 | 72.8 | 80.3 | 23.2 | 72.8 | 91.0 |
| 20-0000 | 60 | 23.3 | 77.2 | 23.5 | 77 | 30.5 | 23.1 | 77.3 | 24.5 |
| 20-1200 | 75 | 23.7 | 80.3 | 24 | 77.4 | 305.2 | 24.1 | 80.2 | 45.5 |
| 20-1800 | 85 | 23.9 | 81.6 | 24.8 | 81.6 | 99.6 | 24 | 81.9 | 33.3 |
| 21-0000 | 95 | 24.1 | 82.7 | 24.5 | 82.6 | 45.5 | 24.3 | 82.6 | 24.5 |
| 21-1200 | 120 | 24.2 | 85.2 | 24.1 | 85.1 | 15.2 | 24.4 | 85.3 | 24.5 |
| 21-1800 | 145 | 24.3 | 86.2 | 24.1 | 85.1 | 117.2 | 24.4 | 86.2 | 11.1 |
| 22-0000 | 150 | 24.5 | 86.9 | 24.7 | 87 | 24.5 | 24.7 | 86.7 | 30.5 |
| 22-1200 | 140 | 25.2 | 88.3 | 25.5 | 87.8 | 62.0 | 25.4 | 88.3 | 22.1 |
| 22-1800 | 125 | 25.6 | 89.1 | 25.8 | 89.2 | 24.5 | 25.7 | 89 | 15.2 |
| 23-0000 | 120 | 26 | 89.9 | 26.1 | 90 | 15.2 | 26.1 | 89.8 | 15.2 |
| 23-1200 | 115 | 27.1 | 91.5 | 27.3 | 91.6 | 24.5 | 27.3 | 91.6 | 24.5 |
| 23-1800 | 110 | 27.8 | 92.3 | 28 | 92.4 | 24.5 | 28 | 92.1 | 30.5 |
| 24-0000 | 105 | 28.6 | 93 | 28.9 | 92.3 | 80.4 | 28.8 | 92.6 | 47.3 |
| 24-1200 | 65 | 30.5 | 94.1 | 30.7 | 94.1 | 22.1 | 30.8 | 94.1 | 33.2 |
| Average | | | | | | 74.8 | | | 51.8 |
| RMS | | | | | | 105.2 | | | 77.0 |

Table 6.2. Trajectories comparison for Hurricane Rita, 18-26 September 2005.

7 DISCUSSION, CONCLUSIONS AND FUTURE WORK

Tropical cyclones are important atmospheric events because of the impact on the environment that they can produce along their path. The estimation of the intensity and trajectory of tropical cyclones is perhaps the most important task performed by forecast centers around the world, which rely on satellite-based measurements as a primary source of data. In particular, the Dvorak technique has been successfully utilized for more than 30 years as the main procedure to estimate the intensity of a tropical cyclone. However, this technique is subjective and its accuracy depends on the expertise of the user. In addition, the variability in the ways tropical cyclones develop makes it difficult to estimate their intensity. Thus, an objective technique that can detect the formation and subsequent evolution of a tropical cyclone throughout its lifecycle would help the forecasters to predict its behavior with some confidence.

This document describes an objective technique for characterizing features associated with the shape and the dynamics of structures embedded in tropical cyclones. The technique can also be extended to predict the formation of tropical cyclones by detecting the presence of vortices in early stages of their lifecycle. Using a single infrared channel of geostationary satellite-based remotely-sensed imagery, development of the tropical cyclone from an unstructured cloud cluster to a more axisymmetric organization about an identified reference point is characterized. The technique calculates the gradient of the infrared brightness temperatures to measure the level of symmetry of tropical cyclone, which in turn reflects its intensity. When the cloud system is a disorganized tropical

depression, the calculated deviation-angle variance is large. As the storm system increases in intensity and organization, the variance decreases.

For the purposes of this research, the deviation-angle variance, which characterizes structure, is compared to the NHC best-track intensity estimate as a measure of how successful the technique is. Although the two measures should not be identical (small-scale convective structure change does not necessarily translate to changes in the overall surface intensity of the tropical cyclone), the deviation-angle variance measure does demonstrate a high magnitude correlation to the best-track intensity estimate. For the 2005 Atlantic hurricane season, the mean filtered correlation magnitude is 0.74 (0.55 for the unfiltered time series), the median correlation is 0.83, and well over 50% of the cases have a correlation of 0.8 and higher (Figure 4.4). The RMS intensity error of the deviation-angle variance technique with respect to best-track record is 19.45 kt for the 2004 season when utilizing 2005 as the training set, which is a little higher than the error of the Dvorak technique for intensification periods (10 - 15 kt). However, the technique is objective and easy to implement. The accuracy of the technique is reduced because the reference metric used as a comparison is developed specifically to provide a smoothly varying intensity estimate and does not capture the variations of the tropical cyclone's intensity, i.e., diurnal and semidiurnal frequency components, these oscillations may provide valuable information about the dynamics of the tropical cyclone but reduce the accuracy of the intensity estimation compared to the best track value. Furthermore, this technique shows potential to characterize the entire lifecycle of individual tropical cyclones. The results shown in chapters 3 and 4, are an encouraging indication of the

ability of this technique to analyze organized structures within cloud features in infrared imagery.

Future work includes the analysis of the deviation-angle variances time series using synthetic data from numerical weather models. From these models, the intensity and center of a tropical cyclone can be obtained at high temporal resolution and used to adjust the technique without using the best-track records. Other future work consists of the study of tropical cyclones in other ocean basins and the analysis of the physical meaning of the frequency components observed in the deviation-angle variance signal. In addition, these components may provide new descriptors in the study of the dynamics and evolution of tropical cyclones according to the geographic location, ocean basin, time of the year, and trajectory. These descriptors may help to classify tropical cyclones, and perhaps, by analyzing them in real time, provide information about the final intensity. Furthermore, the time series of the deviation-angle variance may be used to automatically detect the extratropical transition [35] of some tropical cyclones as a disruption of the axisymmetry.

The deviation-angle variance technique is extended to avoid the initial center calculation of a tropical cyclone. The result is a map of variances that indicates the regions where the cloud structures with high axisymmetry are. The early detection of those structures pinpoints the potential formation of a tropical cyclone. The technique produces an excellent performance in detecting potential tropical cyclones. 85% of the tropical cyclones of 2004 and 2005 were detected 27h on average before they reached tropical storm intensity, and only 22% of false alarms.

Based on the results from 2004 and 2005, this technique has the potential to improve tropical cyclogenesis prediction. The technique performs exceptionally well in spite of there being many unusual developments during these seasons (e.g. 2004 included several tropical cyclones that made landfall in Florida, and 2005 was the most active season on record with 26 cases in a season that extended into 2006) demonstrating that the fundamental concept behind the technique is robust. Currently the system is designed to highlight a cloud cluster when it reaches a certain level of organization based on the deviation-angle variance threshold and the results described earlier testify to its success. While the technique can be applied by forecasters right now, there are some obvious next steps that will: 1) decrease the false alarm rate by combining more features in the classification; 2) modify the way the output is produced such that a probability of development of a particular cloud cluster within a certain period (e.g., 48 hours) is calculated; and 3) further test the robustness of the results by adding more years of data. Future work also can incorporate other types of remotely-sensed data such as water vapor imagery into the technique particularly for use in identifying the early stages of tropical cyclone development. Other future work includes adjusting the technique for other tropical cyclone basins, and turning the system into a real-time forecast tool or protocol, and developing a procedure to decrease the number of false alarms.

Two new procedures are compared to locate the center of a tropical cyclone based on its axisymmetry: accumulator matrix; and the map of variances technique. Results show that the accuracy of both techniques with respect the best-track records increase as the tropical cyclone intensifies. At early stages, the structure of a tropical cyclone presents a

large variety of patterns makes it difficult to consistently locate the center by quantifying the axisymmetry of the cloud system.

Finding the center of a tropical cyclone is a difficult task because it identifies the center of circulation (minimum winds). In contrast, centering procedures that use visible and infrared imagery such as those applied in the Dvorak technique [7][8], the technique described in [18], and the techniques proposed in this document, generally utilizes features of cloud clusters to find the center.

The accuracy of the map of variances technique is slightly higher than the accumulator matrix. The overall RMS distance error calculated is 49 pixels (245 km) and 55 pixels (275 km) respectively. However, for intensities higher than 30 kt, the RMS distance error decreases to 39 pixels (195 km) for the map of variances, and 45 pixels (225 km) for the accumulator matrix technique. In addition, the error is only 21 pixels (105 km) and 25 pixels (125 km) for intensities higher than 60 kt. These results show that both techniques have the potential to locate consistently the center of circulation of tropical cyclones by using indirect measurements. Future work includes adding new information from other remotely-sensed imagery such as water vapor. This data may reduce the error of both centering techniques because low-level currents of humid air are visible, which is important for those cases where the best-track center is located outside the cloud structure in the infrared image. Other future work consists in determining the conditions in which the accuracy of the map of variances technique is higher than the accumulator matrix. The combination of both techniques may provide better results than using only one when

applying the deviation-angle variance procedure. In addition, both techniques may be incorporated into the Advanced Dvorak Technique that is being developed.

APPENDIX A: TROPICAL CYCLONES IN 2004-2005

The following table summarizes the tropical cyclones analyzed during 2004 and 2005. Hurricane Vince (2005) and Danielle (2004) were removed of the analysis because relevant periods of their lifecycle occurred in regions out of scope of the images. In the table, the best track columns indicate the time and position when the tropical cyclone reached 35 kt for first time according to the NHC. The detection columns correspond to the time and position when the tropical cyclone was detected in the map of variances by using the variance threshold value of 1700. The last column indicates the difference of time with respect to the best-track time column. Note that a negative time corresponds to a early detection of the tropical cyclone. The table does not include the cases shown in Table 5.2.

| Tropical Cyclone | Best Track | | | Detection (1700 variance threshold) | | | Detection Time [h] |
|-----------------------|---------------------------|-------------------|-------------------|-------------------------------------|----------|----------|--------------------|
| | Date (MMDDYY) /Time (UTC) | Lon (°W) at 35 kt | Lat (°N) at 35 kt | Date (MMDDYY) /Time (UTC) | Lon (°W) | Lat (°N) | |
| Hurricane Alex | 080104/1800 | 79.2 | 31.6 | 073004/1015 | 67.2 | 22.5 | -55.75 |
| Tropical Storm Bonnie | 080904/1200 | 87.6 | 22.5 | 080504/1515 | 69 | 14.8 | -92.75 |
| H. Charlie | 081004/0600 | 65.3 | 12.9 | 081104/0045 | 71.8 | 15.7 | 18.75 |
| TS. Earl | 081404/1800 | 53.5 | 10.5 | 081204/0745 | 32.8 | 10 | -58.25 |
| H. Frances | 082504/1800 | 39.8 | 11.5 | 082404/0615 | 31 | 10.1 | -35.75 |
| H. Gaston | 082804/0600 | 78.2 | 31.1 | 082704/1645 | 77.7 | 33.5 | -13.25 |
| TS. Hermine | 082904/1200 | 69.8 | 31.1 | Not Detected | | | |
| H. Ivan | 090304/0600 | 30.3 | 9.7 | 090304/0645 | 30.8 | 7.5 | 0.75 |
| H. Jeanne | 091404/1200 | 62.6 | 16.4 | 091404/1445 | 62 | 15.9 | 2.75 |
| H. Karl | 091604/1800 | 32.1 | 11.2 | 091704/0315 | 31.5 | 11.2 | -3.75 |

| Tropical Cyclone | Best Track | | | Detection (1700 variance threshold) | | | Detection Time [h] |
|------------------------------------|---------------------------|-------------------|-------------------|-------------------------------------|----------|----------|--------------------|
| | Date (MMDDYY) /Time (UTC) | Lon (°W) at 35 kt | Lat (°N) at 35 kt | Date (MMDDYY) /Time (UTC) | Lon (°W) | Lat (°N) | |
| H. Lisa | 092004/1200 | 35.4 | 13.5 | Not Detected | | | |
| TS. Matthew | 100804/1800 | 94.2 | 24.1 | 100804/0745 | 93.5 | 24.5 | -10.25 |
| TS. Nicole | 101004/0000 | 65.2 | 30 | Not Detected | | | |
| TS. Otto | 112604/0600 | 41 | 27.3 | 112604/0945 | 36.1 | 30.1 | -20.25 |
| TS. Arlene | 060905/0600 | 83.9 | 18.2 | 060905/0415 | 84 | 14.8 | -1.75 |
| TS. Bret | 062905/0000 | 95.8 | 20 | Not Detected | | | |
| H. Cindy | 070505/0600 | 90.2 | 25.1 | 070105/0245 | 74 | 13.5 | -99.25 |
| H. Denis | 070505/1200 | 65.9 | 13 | 070505/0645 | 65.1 | 13.3 | -5.25 |
| H. Emily | 071205/0000 | 46.8 | 11 | 071105/2215 | 46.8 | 11.3 | -1.75 |
| TS. Frankin | 072205/0000 | 75.9 | 25.7 | 072105/1045 | 73.3 | 23.6 | -13.25 |
| TS. Gert | 072405/0600 | 95 | 20.8 | 072105/1045 | 81.1 | 14.8 | -67.25 |
| TS. Harvey | 080305/0600 | 68.6 | 29.5 | 080205/1345 | 67.8 | 18.2 | -16.25 |
| H. Irene | 080705/1200 | 45 | 20.2 | 080605/1515 | 40 | 7.1 | -20.75 |
| H. Katrina | 082405/1200 | 76.5 | 24.5 | 082405/1445 | 75.5 | 24.6 | 2.75 |
| TS. Jose | 082205/1800 | 95 | 19.6 | 082205/1045 | 94.2 | 19.3 | -7.25 |
| TS. Lee | 083105/1200 | 50.4 | 29 | 082905/0315 | 52.8 | 15.1 | -56.75 |
| H. Maria | 090205/1200 | 49.4 | 21.1 | 090105/1515 | 46.9 | 21.9 | -20.75 |
| H. Nate | 090605/0000 | 66.6 | 28.4 | 090605/0645 | 65.3 | 18.4 | 6.75 |
| H. Ophelia | 090705/0600 | 78.8 | 27.9 | 090705/0645 | 78.5 | 29 | 0.75 |
| H. Phillipe | 090705/1800 | 54.9 | 13.5 | 091405/0645 | 35.2 | 12.1 | -83.25 |
| H. Rita | 091705/1800 | 72.3 | 22.2 | 091805/0645 | 72.8 | 21.1 | 5.75 |
| H. Stan | 100205/0600 | 87.2 | 19.5 | 093005/0645 | 79 | 19.6 | -47.25 |
| Subtropical Depression Twenty Two. | | | | | | | |
| | 100205/1200 | 73 | 38.9 | Not Detected | | | |
| TS. Tammy | 100505/0600 | 79.7 | 27.3 | 100505/0315 | 77 | 27.5 | -2.75 |
| H. Wilma | 101705/0600 | 79.7 | 16.3 | 101505/1345 | 79.1 | 17 | -40.25 |
| TS. Alpha | 102205/0600 | 68.5 | 16.5 | 102205/1645 | 66.1 | 15 | -1.25 |
| H. Beta | 102705/0600 | 81.3 | 11 | 102705/1745 | 81.3 | 11.5 | 11.75 |
| TS. Gamma | 111105/0600 | 66 | 14.3 | 111505/0145 | 59.4 | 18.2 | -100.25 |
| TS. Delta | 112005/1800 | 43.5 | 28 | 111705/1045 | 47 | 25.5 | -79.25 |
| H. Epsilon | 112905/0600 | 49.2 | 31.5 | 112705//1245 | 44.8 | 23 | -41.25 |
| TS. Zeta | 123005/0600 | 36.1 | 24.2 | Not Detected | | | |

APPENDIX B: FALSE ALARMS

The following table summarizes the time and date of the false alarms obtained when applying the threshold value of 1700 in the map of variances. These cases are divided into African Easterly waves and regular cloud clusters:

I. African Easterly Waves

| Date (MMDDYY) /Time (UTC) | Longitude (°W) | Latitude (°N) |
|------------------------------|----------------|---------------|
| 090904/1315 | 45 | 25 |
| 091305/2015 | 25.8 | 37 |
| 100305/2145 | 37.1 | 18 |
| 071505/0645 | 43.5 | 18.7 |
| 091705/2215 | 33.5 | 10.3 |
| 091905/0215 | 35.3 | 22 |
| 100105/1145 | 49.1 | 10.6 |
| 100305/0645 | 55.6 | 11.8 |
| 100505/1215 | 36.7 | 23 |
| 100605/0645 | 40.8 | 8 |
| 101605/0715 | 34 | 19.7 |
| 102705/0615 | 35.3 | 11.8 |
| 111705/1345 | 40.7 | 13.7 |

II. Regular Clouds

| Date (MMDDYY) /Time (UTC) | Longitude (°W) | Latitude (°N) |
|------------------------------|----------------|---------------|
| 073104/1115 | 60.2 | 30.2 |
| 080504/1015 | 63.8 | 22.5 |
| 080704/0115 | 68.5 | 26.3 |
| 080704/1315 | 52.5 | 23.5 |
| 082104/0845 | 66.8 | 14 |
| 091104/1345 | 54.3 | 28.5 |
| 091104/2245 | 54 | 27 |
| 100104/2245 | 76 | 17.8 |
| 112404/1715 | 84 | 30.5 |
| 120104/1745 | 38.2 | 5.8 |
| 071105/1015 | 77.8 | 8 |
| 083105/0715 | 92.9 | 18.7 |
| 100905/1145 | 71 | 19.8 |
| 102605/0815 | 73.5 | 21.1 |
| 103005/2115 | 58.5 | 16.5 |
| 112905/1445 | 82 | 16 |

REFERENCES

1. W.M. Gray, "Hurricanes: Their formation, structure and likely role in the tropical circulation," in *Meteorology Over Tropical Oceans*, D. B. Shaw, Ed. Roy. Meteor. Soc., James Glaisher House, Grenville Place, Bracknell, Berkshire, RG12 1BX, 1979, pp.155-218.
2. C. S. Velden, B. Harper, F. Wells, J. L. Beven II, R. Zehr, T. Olander, M. Mayfield, C. Guard, M. Lander, R. Edson, L. Avila, A. Burton, M. Turk, A. Kikuchi, A. Christian, P. Caroff, and P. McCrone, "The Dvorak Tropical Cyclone Intensity Estimation Technique: A Satellite-Based Method that Has Endured for over 30 Years," *Bulletin of the American Meteorological Society*, vol. 87, 2006, pp. 1195–1210.
3. C. S. Velden, B. Harper, F. Wells, J. L. Beven II, R. Zehr, T. Olander, M. Mayfield, C. Guard, M. Lander, R. Edson, L. Avila, A. Burton, M. Turk, A. Kikuchi, A. Christian, P. Caroff, and P. McCrone, "Supplement To: The Dvorak Tropical Cyclone Intensity Estimation Technique: A Satellite-Based Method that Has Endured for over 30 Years," *Bulletin of the American Meteorological Society*, vol. 87, 2006, pp S6–S9.
4. M. D. Powell, E. W. Ulhorn, J. D. Kepert, "Estimating Maximum Surface Winds from Hurricane Reconnaissance Measurements", *Weather and Forecasting*, vol. 24, 2009, pp. 868-883.
5. E. A. Ritchie, J. Simpson, T. Liu, J. Halverson, C. Velden, K. Brueske, and H. Pierce, "Present day satellite technology for hurricane research: A closer look at formation and intensification," in *Hurricane! Coping with disaster*, R. Simpson, Ed, AGU Publications, 2003, pp 249-289 .
6. S. Fritz, "Satellite pictures and the origin of hurricane Anna," *Monthly Weather Review*, vol. 90, 1962, pp. 507–513.
7. L. Hubert, and A. Timchalk, "Estimating hurricane wind speeds from satellite pictures," *Monthly Weather Review*, vol. 97, 1969, pp. 382–383.
8. F. Dvorak, "Tropical Cyclone Intensity Analysis and Forecasting from Satellite Imagery," *Monthly Weather Review*, vol. 103, 1975, pp. 420–430.

9. V. F. Dvorak, *Tropical Cyclone Intensity Analysis Using Satellite Data*, NOAA Technical Report, NESDIS 11, 1984, pp. 3, 6-25.
10. V. F. Dvorak, *A Workbook on Tropical clouds and cloud systems observed in satellite imagery: Tropical cyclones*, NOAA/NESDIS, 5200 Auth Rd., Washington, DC, 20333, 1995, vol. 2., pp 2-1 – 2-11, 5-20, 8-8.
11. C. Velden, T. Olander, R. Zehr, “Development of an Objective Scheme to Estimate Tropical Cyclone Intensity from Digital Geostationary Satellite Infrared Imagery,” *Weather and Forecasting*, vol. 13, 1998, pp. 172-186.
12. R. Gonzalez and R. Woods, *Digital Image Processing*, 2nd Ed., Prentice Hall, 2002, pp 701-703, pp 587, pp134.
13. B. K. P. Horn, B. G. Schunck, “Determining Optical Flow”, *Artificial Intelligence*, 1981, pp 185- 203.
14. W. Bresky, J. Daniels, “The Feasibility of an Optical Flow Algorithm for Estimating Atmospheric Motion,” presented at the 8th International Winds Workshop, Beijing, China, April 24-28, 2006.
15. S. Bow, *Pattern Recognition and Image Preprocessing*, 2nd Ed., Marcel Dekker, 2002, pp 346, pp 311-312.
16. S. Sheu, C. Jung-Hua. “Automatic Recognition of Two-Dimensional Vortices by Digital Image Processing,” *Journal of Flow Visualization & Image Processing*, vol. 11, 2004, pp 269-279.
17. S. Q. Kidder, T. H. V. Haar, *Satellite Meteorology an Introduction*, Academic Press, 1995, pp 55.
18. D. B.Brow, J.L. Franklin. “Accuracy of Pressure-wind Relationships and Dvorak Satellite Intensity Estimates for Tropical Cyclones Determined from Recent Reconnaissance-based best-track data,” presented at the 25th Conference on Hurricanes and Tropical Meteorology, San Diego, CA. American Meteorology Society. April 29 - May 3, 2002.
19. T. Olander, C. Velden, “The Advanced Objective Dvorak Technique (AODT) – Continuing the Journey,” presented at the 26th Conference on Hurricanes and Tropical Meteorology, Miami, FL, May 2-7, 2004.

20. A. Wimmers, C. Velden, "Satellite-Based Center-Fixing of Tropical Cyclones: New Automated Approaches," presented at the 26th Conference on Hurricanes and Tropical Meteorology, Miami, FL, May 2-7, 2004.
21. T. Olander, C. Velden, "The Advanced Dvorak Technique: Continued Development of an Objective Scheme to Estimate Tropical Cyclone Intensity Using Geostationary Infrared Satellite Imagery," *Weather and Forecasting*, vol. 22, 2007, pp. 287-298.
22. T. Olander, C. Velden, "ADT – Advanced Dvorak Technique USERS' GUIDE (McIDAS 7.23)," University of Wisconsin-Madison. 2008. Available: <http://cimss.ssec.wisc.edu/tropic2/misc/adt/info.html>
23. T. Olander, C. Velden, "Update on the UW-CIMSS Advanced Dvorak technique (ADT)." Presented at the Meteorological Satellite and Tropical Cyclone Conference, Pearl Harbor, HI, April 27-May 1, 2009.
24. Space Systems-Loral, USA, 1996. *GOES I-M DataBook*. Available: <http://goes.gsfc.nasa.gov/text/goes.databook.html>
25. Tropical Cyclone Reports. National Hurricane Center. Available: <http://www.nhc.noaa.gov/pastall.shtml>
26. Jet Propulsion Laboratory, USA, 2006, QuikSCAT Science Data Product User's Manual. Available: http://podaac.jpl.nasa.gov/DATA_PRODUCT/OVW/index.html#quikscat
27. New AREA Format Information, University of Wisconsin-Madison. 1996. Available: http://www.ssec.wisc.edu/mcidas/doc/misc_doc/area2.html
28. McIDAS Introduction, University of Wisconsin-Madison. 1996. Available: http://www.ssec.wisc.edu/mcidas/software/about_mcidas.html
29. A. V. Oppenheim, R. W. Schaffer, *Digital Signal Processing*, Prentice-Hall, 1975, pp 211-212

30. T. Muramatsu, "Diurnal variations of satellite-measured TBB areal distribution and eye diameter of mature typhoons," *J. Meteor. Soc. Japan*, vol. 61, 1983, pp 77–89.
31. J.S. Hobgood, "A possible mechanism for the diurnal oscillation of tropical cyclones," *Journal of the Atmospheric Sciences*, vol. 43, 1983, pp. 2901–2922.
32. J.P. Kossin, "Daily Hurricane Variability Inferred from GOES Infrared Imagery," *Monthly Weather Review*, vol. 130, 2002, pp. 2260-2270.
33. M. F. Pineros, E.A. Ritchie, J. S. Tyo, "Objective Measures of Tropical Cyclone Structure and Intensity Change From Remotely Sensed Infrared Image Data," *IEEE transactions on Geoscience and Remote Sensing*, vol 46, part 1, Nov 2008, pp 3574-3580.
34. W. M. Frank, E. A. Ritchie, "Effects of Vertical Wind Shear on Hurricane Intensity and Structure," *Monthly Weather Review*, vol 129, 2001, pp 2249-2269.
35. P. M. Klein, P. A. Harr, R. L. Elsberry, "Extratropical Transition of Western North Pacific Tropical Cyclones: An Overview and Conceptual Model of the Transformation Stage," *Weather and Forecasting*, vol 15, 2000, pp 375-395.